Department of Geography and Atmospheric Science
University of Kansas
1475 Jayhawk Boulevard
Lawrence, KS 66045
Email: bpu@ku.edu

Dr. Yves Balkanski
Institut Pascal et
IPSL/LSCE (Laboratoire des Sciences du Climat et de l'Environnement)
CEA-CNRS-UVSQ-UPSaclay UMR 8212
L'Orme des Merisiers - Bat 714, pce 1012
91191 Gif sur Yvette Cedex, FRANCE

October 27th, 2019

Dear Editor Balkanski,

We have submitted a revised paper entitled "Retrieving the global distribution of threshold of wind erosion from satellite data and implementing it into the GFDL AM4.0/LM4.0 model" by B. Pu, P. Ginoux and co-authors for consideration for *Atmospheric Chemistry and Physics*. The helpful comments from two anonymous reviewers are sincerely appreciated. Our replies to each reviewer's comments are attached. We also made some edits in the manuscript.

We gratefully appreciate your time and consideration!

Sincerely,

Bing Pu

Review of the ACPD manuscript "Retrieving the global distribution of threshold of wind erosion from satellite data and implementing it into the GFDL AM4.0/LM4.0 model" by Pu et al.

We thank the reviewer for very helpful comments. We reply to your comment (in Italic) below.

The article by Pu et al. describes a new data set for the threshold wind velocity for dust emission and shows the impact on dust aerosol simulated with the GFDL model. The authors used a comprehensive collection of observational data to approach the problem. In principle, the contribution is relevant to the field, since modeling dust aerosol is fraught by uncertainty. I have, however, concerns that should be address prior to publication of the article. These are the unclear description of the method, the lack of an uncertainty assessment for the retrieval, as well as the need for a comparison to independent data and citing of relevant literature. In the following, I provide more details.

In addition to reply each of the following comments, we also edited the manuscript to better address your comments and suggestions.

Main comments:

1) The description and uncertainties of the method are unclear. The article suffers from an unclear description and partly missing information on the retrieval technique. Moreover, the value of the article would be substantially improved when the uncertainty in the retrieval would be quantitatively assessed. The many threshold criteria in the retrieval currently cast some doubt on the robustness of the retrieval when these values would be slightly changed.

We modified lines 335-393 to improve the clarity of the retrieval method and added section 2.3 and Tables 2-3 to discuss and quantify the uncertainties associated with slight changes of retrieval criteria and selection of surface wind datasets. We found small changes in soil moisture, LAI, and snow coverage do not change the derived $V_{threshold}$ much, within 1 m s^{-1} over most regions. The results are more sensitive to DOD_{thresh} and the selection of surface winds from reanalysis products (Tables 2-3). The uncertainty of DOD frequency distribution and $V_{threshold}$ associated with transported dust is also discussed over North Africa (lines 414-426, 432-438). Global $V_{threshold}$ using DOD_{thresh} =0.2 (or 0.02) and 0.5 (or 0.05) are further compared and discussed in section 3.1.

2) The article needs more comparisons to existing works. The current article does not acknowledge other existing treatments of the threshold of wind erosion for global models. For instance, Cheng et al. (2008), Jones et al. (2011) and Rieger et al. (2017) do not prescribe globally constant threshold wind speeds for dust emission, but parameterize it with dependencies on other variables. These are the global models ECHAM-HAM, HadGEM2-ES, and ICON-ART. Such studies should be cited and used for comparison of the new development in the GFDL model.

Thanks a lot for your suggestions. We added lines 64-68 to better address this question: "On the other hand, some models, such as the ECHAM-HAM, HadGEM2-ES, and ICON-ART, parameterize the constant dry threshold friction velocity (usually a function of soil particle size, soil and air density) or threshold wind velocity with dependencies on soil moisture, surface roughness length, and vegetation coverage (e.g., Takemura et al. 2000; Ginoux et al. 2001; Zender et al. 2003; Cheng et al. 2008; Jones et al. 2011; Rieger et al. 2017)."

While Cheng et al. (2008), Jones et al. (2011) and Rieger et al. (2017) all parameterize the threshold friction velocity in different models with dependencies on other variables, such as soil moisture, surface roughness length, and vegetation coverage, the dry friction velocities used in the models are largely based on constant values such as air and soil density and soil particle size (e.g., Eq. 3 of Rieger et al. 2017; Eq. 1 of Cheng et al. 2008; Eq. 3 of Woodward 2011).

Specific comments:

P1. L.37: "enhancing net radiant energy loading" Use a physically better phrase.

We changed "enhancing net radiant energy loading" to "enhancing net radiation".

P1. L46: "the life cycle of dust" -> "the life cycle of dust aerosols"

Done.

P.6 L124-126: "We require that the single scattering albedo at 470 nm to be less than 1 for dust due to its absorption of solar radiation. This separates dust from scattering aerosols, such as sea salt." The single scattering albedo is by definition smaller than 1. So it will not separate dust and sea-salt aerosol. This statement leaves me puzzled about the adopted method for obtaining dust aerosol optical depth from MODIS. The method needs to be revised and the description clarified. The remaining sentences of the paragraph give more details, but it is not obvious how the method works without reading all the other publications. My recommendation is giving a more concrete and easier to follow description of the method here*. For instance, how is dust separated from other aerosols and how are dust sources identified. Also provide important numbers, e.g., for the separation of fine-mode vs. dust aerosols and the definition of high-resolution.*

Lines 136-146 are modified to better address the comment. We used single-scattering albedo at 470 nm to be less than 0.99 for dust, as the single-scattering albedo of sea salt is close to 1. The resolution of the MODIS products is 0.1° by 0.1°. The retrieval method is summarized in Eq. 1.

P.6 L.134-137: What does a flag of QA=1 and QA=3 imply for the quality of the data?

We modified lines 151-153 to clarify this. For MODIS Deep Blue AOD products, quality assurance flag (QA) equals 0, 1, 2, or 3 (Hsu et al. 2013). QA=0 indicates no retrieval, while QA=1 indicates lowest quality of retrieved AOD, and QA=3 implies the highest quality.

P.6 L.139-143: I understand combining the morning and afternoon measurements is the best we can do, but the text should acknowledge that the location and amount of dust emission typically changes between the morning and afternoon. Peak contributions from convective storms would be missed due to the temporal resolution. A relatively large number of literature assesses the diurnal cycle of dust emission and some of those studies could be cited here. My point is that the strengths and weaknesses of the method need to *be named as far as it is currently known. This also applies to the other satellite products (soil moisture, snow cover, LAI) introduced in the next paragraphs.*

We added lines 162-165 to better address this issue: "Note that due to the temporal coverage of MODIS products, the diurnal variations in dust (e.g., Orgill and Sehmel 1976; Mbourou et al. 1997; Knippertz et al. 2008; Schepanski et al. 2009) are not included in current study." Later in lines 772-773, we mentioned: "Diurnal variability of dust emission and short-duration events such as haboobs are also not included. " Lines 184-185, 207-208 are also added to discuss the uncertainties associated with soil moisture and LAI products.

P.8 L.177: "Vegetation can protect soil (...)" -> Vegetation protects soils (...)

Done.

P.8 L. 182-184: The description of the data set is not published. At least a short description of the retrieval is needed and also a statement on where one can access or request that data.

We modified lines 204-205 to address this point. Details about LAI retrieval can be found from Yan et al. 2016a, b. We mentioned that the data was obtained via personal communication with Ranga Myneni and Taejin Park in Boston University in 2016 in text. In the Acknowledgement we added "MODIS LAI data may be requested by contacting Dr. Ranga Myneni at Boston University".

P. 9 L. 186-187: A six hourly resolution of the winds does not sufficiently resolve their diurnal cycle and hence their effect on dust emission. Again, the diurnal cycle of dust emission is an issue here, but for the model data we could fix it.

We mentioned in lines 162-165 and 772-773 that diurnal cycles are not included in the analysis. 6-hourly winds from the NCEP are selected because surface winds in the model are nudged toward NCEP winds, and we would like to use a reanalysis that is close to the climatology of the model. Similar methods can be applied to other reanalyses with higher temporal resolutions, e.g., hourly surface winds from the ERA5 as discussed in section 2.3. On the other hand, whether model can faithfully capture the diurnal cycle of dust also depends on the dust emission scheme and model's capability to simulate high-speed winds and mesoscale convective system, which are beyond the scope of this study.

Section 2.1.2: Why did you choose two different re-analyses? Did you also consider using MERRA?

As we mentioned above, the NCEP reanalysis is chosen because surface winds are nudged toward it. For soil temperature at the first layer, we use the ERA-Interim, which has higher spatial resolution. The horizontal resolution of ERA-Interim is about 0.7° and is comparable with that of MERRA (Rienecker et al. 2011) or MERRA-Land (Reichle 2012) on a 1/2° by 2/3° grid. While MERRA surface temperature is found have a relatively large bias (>3°C) in comparison with AMSR-E temperature in desert region (Yi et al. 2011), MERRA-Land surface soil moisture is found to have slightly lower skill than the ERA-Interim when comparing with SCAN in situ surface moisture (Reichle et al. 2011). Later, we also used surface winds from the ERA-Interim and ERA5 to examine the sensitivity of $V_{threshold}$ to the selection of reanalysis products.

P.9 L. 192: "closet" -> closest

Done.

P.9 L. 205: "coarse mode AOD" What is the radius for separating coarse and fine-mode AOD in your work?

Based on O'Neill et al. (2003) coarse-mode AOD has a radius greater than 0.6 μm. We added this to line 240.

P.10 L. 209-210: Three years is a very short time period for a climatology, especially in light of the strong year-to-year variability in dust aerosol burden. I agree that as little data as possible should be removed. However, I recommend giving an estimate of the uncertainty, e.g., try a stricter criterion and compare the climatologies.

Thanks for you suggestion. We found a stricter criterion will result a smaller sample size and the results won't change much. For instance, if a minimum record length of five years is used, there will be 225 sites for SDA COD and 263 sites for AOT (instead of 313 and 351 stations as shown in Fig. 5). If seven-year is used as a requirement, there will be 156 SDA COD sites and 195 AOT sites. The climatologies of using five or seven years records as a criterion are shown in Figures R1 and R2, respectively. Results are very similar the climatology using three years as a criterion (Fig. 4).

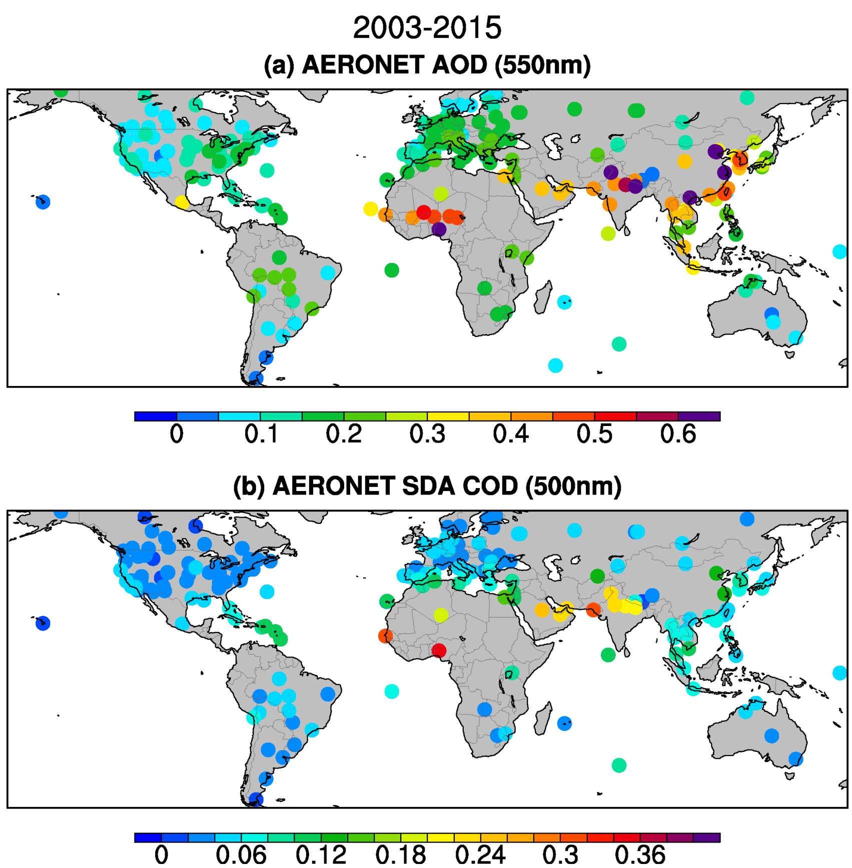

Figure R1. Same as Fig. 4 but using stations with at least five years of records.

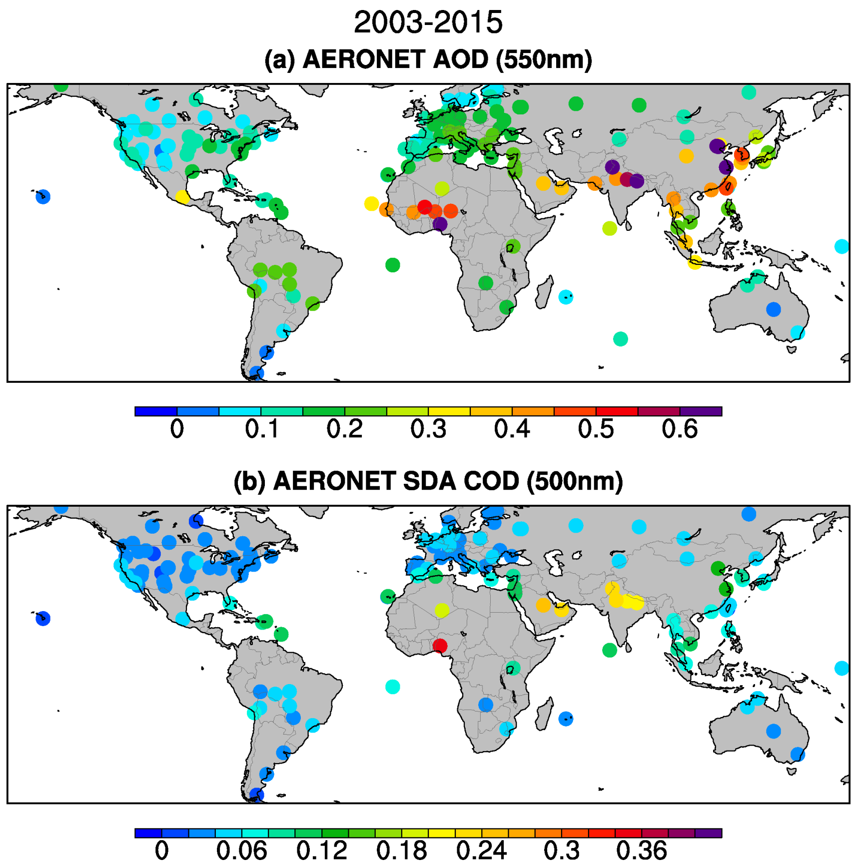

Figure R2. Same as Fig. 4 but using stations with at least seven years of records.

P.10 L.227: Refer to the section of the article.

We removed lines 259-262 in the revision (lines 224-227 in the previous version of the manuscript).

Section 2.1.3: Consider showing a map with the location of the different stations used for this research. You could use color to indicate the record length of the stations.

We added the length of records of the RSMAS stations to Table S1 in the Supplement, where the latitude/longitude of each station is also shown. The record length of AERONET AOT and SDA data are now added to Figure S6 in the Supplement. The location and length of records from the IMPROVE can be found from Pu and Ginoux (2018; Fig. S1), while the location of three LISA sites can be found in Fig. S7 in the Supplement of this paper. All available hourly LISA station data from 2006 to 2014 are used to calculate daily mean and then monthly mean as mentioned in lines 324-325.

P.12 L. 254-255: " (...) assume that the climatology of the surface dust concentrations do not change greatly from the 1980s to the 2000s" Why is this a reasonable assumption?

I agree this is not necessarily a good assumption. Lines 288-292 are modified to better address this point: "Note that since most station records end earlier than 1998, the dataset largely represents the climatology during the 1980s and 1990s. Thus the discrepancies between model output and the RSMAS data include both model biases and the difference in surface dust concentration from the 1980s to the 2000s." Despite the uncertainties, the RSMAS dataset has been widely used for model validation. For instance, Huneeus et al. (2011) used the climatology of the data to validate AeroCom model simulations in 2000.

P.14 L.303-307: Why did you choose these thresholds? For instance, why not a snow cover of 0% and an LAI of 0? I can imagine this is due to fractional difference within a grid box, but it is unclear whether a slight change in the thresholds would have a big effect on the results. Maybe you could test it for obtaining more confidence in the results.

As mentioned in lines 347-353, similar criteria have been used to detect or confine dust source regions by different studies. For instance, "LAI less than 0.3 has been used as a threshold for dust emission in the Community Land Model (Mahowald et al., 2010; Kok et al., 2014a)". We also added sensitivity tests in section 2.3 better quantify how the small variations in the retrieval criteria may affect the retrieved $V_{threshold}$.

P.15 L.321-333: I understand that you choose different background dust AODs per region, but where does 0.2 and 0.02 come from? Could you use the minimum in dust AOD from daily values in your MODIS climatology to accurately compute the background values?

MODIS DOD has small values near zero (see Fig. S1 form Pu and Ginoux 2017), so it is difficulty to use the minimum value in DOD to compute background aerosol values. DOD_{thresh}=0.2 was used by Ginoux et al. (2012) to distinguish dust events from background aerosols. We used DOD_{thresh}=0.02 for less dusty regions, such as North America, South Africa, South America, and Australia, largely because dust emission in these regions are at least ten times smaller than that from dusty regions such as North Africa (Huneeus et al. 2011). As shown in Fig. 15, in these less dusty regions, the averaged frequency distribution of DOD peak over much smaller values than dusty regions (lines 748-751). While the selection of DOD_{thresh}=0.2 (or 0.02) is empirical, we also tested DOD_{thresh}=0.5 (or 0.05), and results are discussed in section 3.1.

P.15 L. 339-343: I appreciate the general acknowledgement of potential uncertainty in the thresholds. I think a quantitative assessment of the uncertainty would substantially strengthen your work. You could easily do so by varying the threshold criteria within bounds you perceive reasonable (justified by physical arguments) and show the associated changes in your results.

Thanks for your advice. We added section 2.3, Tables 2-3 and modified later discussion in section 3.1 (lines 505-569) to better quantify the uncertainties associated with the varying threshold retrieval criteria.

P.16 L.365: How was the scaling factor determined?

The scaling factor *C* in the standard version of the AM4.0/LM4.0 was determined by matching the modeled surface dust concentrations with the RSMAS station data. We did not change it in the simulations in order to compare the differences associated with different $V_{threshold}$.

P.18 L.399: "differences in simulated dynamic vegetation by LM4.0 among the three simulations are actually very small and can be ignored" add that this is the case because of the short simulation when the land use does not change as much as over longer time periods.

Done.

P.18 L.412: What primarily controls the threshold differences between North Africa and Eurasia? A threshold of 3 m s^{-1} is very low and needs an explanation.

These lines are removed and Tables 2-3 are added to better quantify the regional difference of $V_{threshold}$. The magnitude of threshold wind erosion is determined by matching the cumulative frequency of DOD at certain DOD_{thresh} level with the frequency distribution of surface wind speed. Therefore, regions with higher DOD frequency (e.g., high FoO in Figs. 1a-e) generally have lower threshold of wind erosion. As discussed in sections 2.3 and 3.1, value of $V_{threshold}$ in North Africa is lower in comparison with previous station based estimations, and this is largely associated with lower surface wind speed in the NCEP1 reanalysis and the ignorance of the contribution of transported dust to total DOD. Increasing DOD_{thresh} to 0.5 can increase annual mean $V_{threshold}$ over North Africa to 4.9 ~7.6 m s^{-1} (Table 2). However, despite the relatively low value of $V_{threshold}$ in North Africa, we found the spatial and temporal varying $V_{threshold}$ largely improve the simulation of DOD spatial pattern and seasonal cycle over North Africa in the AM4.0/LM4.0 model.

P.19 L.435: "weed" -> wind

Done.

P.19 L.423- 439: A discussion is useful, but the results keep me thinking of the potential impact of the threshold choices in the retrieval. This is not picked up in the discussion of your lower threshold velocities than in previous studies.

We added section 2.3 and Tables 2-3 to quantify the uncertainties associated with slight changes of retrieval criteria, and modified lines 538-540, 544-545, 562-569 in section 3.1 to discuss these uncertainties when comparing with previous studies.

P.25 L.572: Harmattan winds are important in winter and spring. Fiedler et al. (2015) provide a complete climatology of dust aerosol associated with the Harmattan.

We modified line 697: "...are associated with the dry northerly Harmattan wind in boreal winter and spring..." and added the citation of Findler et al. (2015).

P.27 L. 608: "storm centers a bit" -> storm center is located

Done.

Section 3.3: It would be useful to compare against independent data sets already published since both the model and the observational estimates have been newly developed in the current article. Relevant works are for instance Schepanski et al. (2007) and Evan et al. (2015).

Since section 3.3 and Fig. 15 only show regional averaged frequency distribution of DOD instead of spatial pattern, we add discussion in lines 387-393 to compare the FoO in Fig. 1 with dust emission frequency over North Africa from Evans et al. (2015) and frequencies of dust source activation from Schepanski et al. (2007).

Figure 8: Refine the color scale for the surface concentration in the dust belt. The same red shading does not allow a comparison of the results in the dust regions.

Done.

Figure 10: Except for India, US and South America, the difference in the annual cycles in Vthres12mn and VthresAnn is very small. It suggests that the month-to-month variation in threshold wind velocities does not have a large impact on the climatological mean dust aerosol optical depth in main dust sources. Is this primarily so because the variations in soil moisture of deserts are small or what explains the similarity?

We agree that in Fig. 10 (now Fig. 11) expect India, U.S. and South America the differences between V_{thresh}Ann and V_{thresh}12mn are small. The small season variations in soil moisture in dust source regions (largely arid or semi-arid regions) may play a role. On the other hand, the differences between V_{thresh}Ann and V_{thresh}12mn simulations are larger when comparing surface dust concentration (Figs. 9, 10,13a-c).

Figure 14: Add VthresAnn.

We show results form V_{thresh}Ann here in Figure R3. The regional mean DOD frequency distribution from the V_{thresh}Ann simulation (yellow) is largely similar to that from the V_{thresh}12mn (orange), except over the U.S., India, and South America, where DOD peaks at higher values, i.e., slightly closer to the peaks in MODIS. This is consistent with higher DOD in these regions (Fig. 11) in comparison with the V_{thresh}12mn simulation. Since results from V_{thresh}12mn generally show better agreement with station observations and MODIS DOD (e.g., Figs. 8-13), we chose to focus on the results form the V_{thresh}12mn in section 3.2.4 and 3.3 (Figs. 14-15).

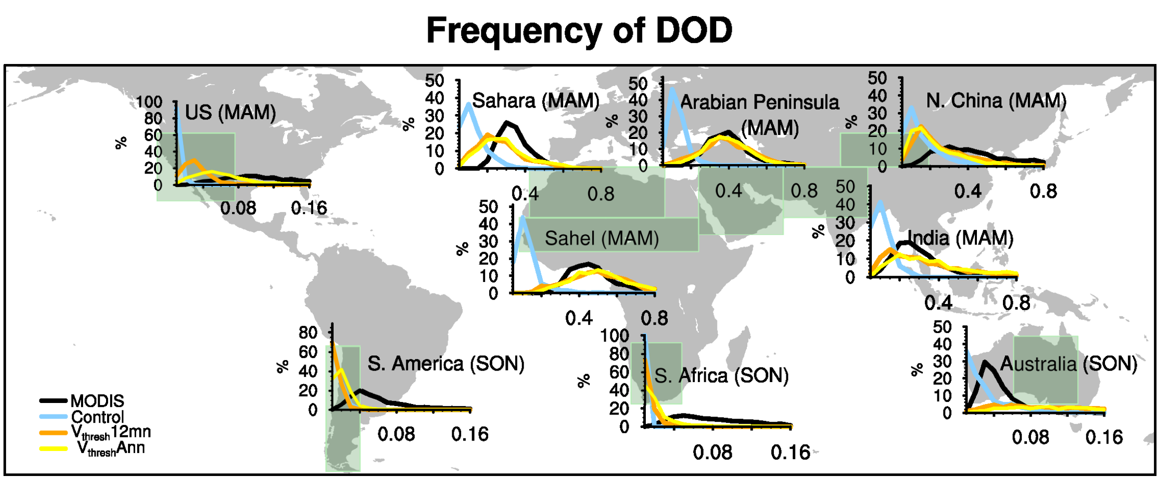

Figure R3. Same as Fig. 15 but also include the DOD distribution frequency from the V_{thresh}Ann simulation (yellow line).

References:

Cheng, T., Peng, Y., Feichter, J., and Tegen, I.: An improvement on the dust emission scheme in the global aerosol-climate model ECHAM5-HAM, Atmos. Chem. Phys., 8, 1105-1117, https://doi.org/10.5194/acp-8-1105-2008, 2008.

Evan, A. T., Fiedler, S., Zhao, C., Menut, L., Schepanski, K., Flamant, C., & Doherty, O.: Derivation of an observation-based map of North African dust emission. Aeolian Research, 16, 153-162, 2015.

Fiedler, S., Kaplan, M. L., and Knippertz, P. (2015), The importance of Harmattan surges for the emission of North African dust aerosol, Geophys. Res. Lett., 42, 9495–9504, doi: 10.1002/2015GL065925.

Jones, C. D., Hughes, J. K., Bellouin, N., Hardiman, S. C., Jones, G. S., Knight, J., Liddicoat, S., O'Connor, F. M., Andres, R. J., Bell, C., Boo, K.-O., Bozzo, A., Butchart, N., Cadule, P., Corbin, K. D., Doutriaux-Boucher, M., Friedlingstein, P., Gornall, J., Gray, L., Halloran, P. R., Hurtt, G., Ingram, W. J., Lamarque, J.-F., Law, R. M., Meinshausen, M., Osprey, S., Palin, E. J., Parsons Chini, L., Raddatz, T., Sanderson, M. G., Sellar, A. A., Schurer, A., Valdes, P., Wood, N., Woodward, S., Yoshioka, M., and Zerroukat, M.: The HadGEM2-ES implementation of CMIP5 centennial simulations, Geosci. Model Dev., 4,543-570, https://doi.org/10.5194/gmd-4-543-2011, 2011.

Rieger, D., Steiner, A., Bachmann, V., Gasch, P., Förstner, J., Deetz, K., Vogel, B., and Vogel, H.: Impact of the 4 April 2014 Saharan dust outbreak on the photovoltaic power generation in Germany, Atmos. Chem. Phys., 17, 13391-13415, https://doi.org/10.5194/acp-17-13391-2017, 2017.

Schepanski, K., Tegen, I., Laurent, B., Heinold, B., and Macke, A.: A new Saharan dust source activation frequency map derived from MSG-SEVIRI IR-channels, Geophys. Res. Lett., 34, L18803, doi:10.1029/2007GL030168, 2007.

References:

Reichle, R., R. Koster, G. De Lannoy, B. Forman, Q. Liu, S. Mahanama, A. Touré, 2011: Assessment and Enhancement of MERRA Land Surface Hydrology Estimates, J. Climate, 24, 6322-6338, DOI: 10.1175/JCLI-D-10-05033.1.

Rienecker, M. M., and Coauthors, 2011: MERRA: NASA's Modern-Era Retrospective Analysis for Research and Applications. J. Climate, 24, 3624–3648.

Reichle, R. H., 2012: The MERRA-Land Data Product. GMAO Office Note No. 3 (Version 1.2), 38 pp, available from http://gmao.gsfc.nasa.gov/pubs/office_notes.

Yan, K. and co-authors, 2016a: Evaluation of MODIS LAI/FPAR product collection 6. Part 1: Consistency and Improvements, Remote Sensing, 8, 359, doi:10.3390/rs8050359.

Yan, K. and co-authors, 2016b: Evaluation of MODIS LAI/FPAR product collection 6. Part 2: Validation and intercomparison, Remote Sensing, 8, 460, doi:10.3390/rs8060460.

Yi, Y., J. Kimball, and L. Jones, 2011: Evaluation of MERRA Land Surface Estimates in Preparation for the Soil Moisture Active Passive Mission, J. Climate, 24, 3797-3816, DOI: 10.1175/2011JCLI4034.1.

Interactive comment on "Retrieving the global distribution of threshold of wind erosion from satellite data and implementing it into the GFDL AM4.0/LM4.0 model" by Bing Pu et al.

We thank the reviewer for very helpful comments. We reply to your comment (in Italic) below.

This is an interesting paper that produces the first estimation of the global distribution of threshold wind speeds for wind erosion (dust aerosol emission). They do so by combining a calculation of the frequency of dust events per grid box with a probability distribution of wind speeds per grid box from a reanalysis product (NCEP/NCAR). They then implement their estimation of threshold wind speeds into a global model and study the results relative to a control run with a globally-constant threshold wind speed. The paper is overall well-written and easy to follow, and the results could be important because they could help advance dust models beyond the use of a globally constant threshold friction velocity. However, I think there are some important issues with the methodology, the interpretation of the retrieved threshold wind speeds, and with interpreting the results from the global model. The paper would need substantial revisions. Comments follow below.

In addition to reply each of the following comments, we also edited the manuscript to better address your comments and suggestions.

Main comments:

- A major weakness of the methodology is that it equates high dust AOD in a gridbox with the occurrence of dust emission. This causes problems in their methodology because it causes advected dust to be interpreted as emitted dust, and thus results in an underestimation of the dust emission threshold. Since there are large differences in advected dust between regions – for instance areas in major dust regions are bound to be more affected by advected dust – this problem could cause potential biases in the retrieved threshold wind speed. Although the authors commendably acknowledge the problem (e.g., on line 340-2), the magnitude of this bias is not investigated. And unfortunately, without a reasonable analysis of the magnitude of this bias, I do not think the authors can conclude that the threshold wind speed in the Sahel is actually lower than in Northern Africa. And similarly, it is not clear that the lower threshold in the major source regions (e.g., the Sahara) than in the more marginal regions (e.g., the US) is real, or is a result of this bias. In fact, both these results are consistent with the anticipated effect of this bias, as the authors acknowledge for the Sahel. Therefore, the authors need to add an analysis that reasonably bounds the effect of this bias. Perhaps the authors could analyze the wind speed threshold in different regions, conditional on the DOD in the surrounding regions, in order to try to quantify and bound this bias?

Thanks for your suggestion. We roughly estimated the influence of transported dust on wind erosion threshold ($V_{threshold}$) in North Africa using a surface DOD (sDOD) data retrieved by combining lidar vertical profiles from CALIOP and MODIS Dust Optical Depth in section 2.3 (lines 414-426). As shown in Table 2, $V_{threshold}$ over the Sahel (6.05 vs. 3.21 m s^{-1}) and Sahara (7.66 vs. 4.61 m s^{-1}) from sDOD are higher than that from DOD directly. Here $V_{threshold}$ in the Sahara is still higher than that in the Sahel.

This is consistent with the findings of Chomette and Legrand (1999) and Cowie et al. (2014), who also showed wind erosion threshold was higher in most part of the Sahara than the Sahel.

We also quantify and discuss the uncertainties of $V_{threshold}$ associated with slight variations in retrieval criteria including levels of soil moisture, LAI, snow coverage, DOD_{thresh}, and surface wind speed from different reanalyses in section 2.3 and added Tables 2-3 to better display the regional difference of retrieved $V_{threshold}$. In most case, we notice the $V_{threshold}$ in the Sahara is lower than in the U.S., except using sDOD in North Africa and when we used DOD_{thresh} =0.5 (and 0.05 for less dusty regions).

- I also think the interpretation of the differences between threshold wind speed must be improved. Of relevance here is that wind speed itself is not the main explanatory variable for dust fluxes. Rather, this is the wind stress on the surface as quantified by the friction velocity, which is linked to the 10m wind speed through the aerodynamic surface roughness. There are strong experimental constraints on the threshold friction velocity above which surface particles become mobile and dust emission starts (e.g., Shao, 2008). It is therefore very relevant what the NCEP/NCAR surface roughness in the different source regions is: do differences in the roughness between source regions explain the differences in the threshold wind speed? Are threshold wind speed variables substantially correlated with the roughness values used in NCEP/NCAR for each grid box? The authors can also use the surface roughness to determine the distribution of threshold friction velocities for the different regions, which is more fundamental and thus more useful to the community. Another important consideration that follows from this above concern is that, since it's the friction velocity (and wind stress) that drives dust fluxes, the roughness used in GFDL should match the roughness used in the NCEP/NCAR reanalysis. Is this the case?

The reviewer is wondering if the differences in surface roughness in the NCEP/NCAR reanalysis can explain the differences in the threshold wind speed between source regions. The distribution of threshold wind is determined by matching the frequency distribution of DOD at certain level of DOD_{thresh} with the frequency distribution of surface wind speed from the NCEP/NCAR reanalysis. The roughness length (z_0) in the NCEP/NCAR reanalysis came from the Simple Biosphere Model (Kalnay et al. 1996). It is calculated based on height of the top and base of the canopy, the height of the maximum leaf area density, leaf drag coefficients, time-varying leaf area index, and ground roughness length for each vegetation table (Table 3 and Fig. 7 from Dorman and Sellers, 1989). The spatial pattern shows dependence on vegetation type (Fig. 7 of Dorman and Sellers, 1989), and has little variation over bare ground. While roughness length plays an important role in the calculation of surface momentum transfer and friction velocity, it does not directly related to the spatial pattern of the $V_{threshold}$ we derived.

The reviewer also suggested calculating the distribution of threshold friction velocity (u_t^*) based on surface roughness. While friction velocity has been used in a lot of dust emission schemes and can be approximated with surface roughness, developing a global distribution of u_t^* and compare with available observations is beyond the scope of this study. Also, instead of using $V_{threshold}$ and surface roughness, it is probably better to use the frequency distribution of u^* and DOD to derive the u_t^*, i.e., using a similar method as proposed here.

The dust emission scheme (Ginoux et al. 2001) in the GFDL AM4.0/LM4.0 uses surface wind speed, rather than friction velocity. We did not tune surface roughness in the GFDL model toward that in the NCEP/NCAR reanalysis, which is calculated by the turbulent transfer model in the Simple Biosphere Model (Dorman and Sellers, 1989; Sellers et al. 1989). However, in our simulations, surface wind speeds are nudged toward the surface wind of the NCEP/NCAR reanalysis with a relaxation timescale of 6 hours.

- Similarly, the authors should investigate differences in other parameters that determine the threshold friction velocity (and 10m wind speed), namely soil moisture, vegetation, and soil texture. If the authors can provide plausible physical reasons for the variations between the threshold wind speed between the regions, that would also help alleviate the concern that their results might be primarily driven by biases arising from using high DOD as a proxy for dust emission (previous comment).

We added section 2.3 and Tables 2-3 to better discuss the sensitivity of $V_{threshold}$ to retrieval method, reanalysis products, and also the possible biases of using DOD frequency distribution to approximate dust emission in North Africa. We found small changes in soil moisture, LAI, and snow coverage do not change the derived $V_{threshold}$ much, within 1 m s^{-1} over most regions. The results are more sensitive to DOD_{thresh} and the selection of surface winds from reanalysis products (Tables 2-3). The uncertainty of DOD frequency distribution and $V_{threshold}$ associated with transported dust is also discussed over North Africa (lines 414-426, 432-438). Global $V_{threshold}$ using DOD_{thresh} =0.2 (or 0.02) and 0.5 (or 0.05) are further compared and discussed in section 3.1.

Regional differences of $V_{threshold}$ are also better quantified in the Tables 2-3. The spatial and temporal differences of the threshold of wind erosion ($V_{threshold}$) are largely determined by frequency distribution of DOD and surface wind speeds. Therefore, for areas with high dust frequency of occurrence (FoO), e.g., North Africa and the eastern Arabian Peninsula, $V_{threshold}$ is generally lower (Figs. 1e and j). We added discussion in lines 387-393 and modified lines 505-513 to better address this.

Although the overall magnitude of retrieved $V_{threshod}$ using surface winds from the NCEP1 reanalysis is lower than previous station based studies over North Africa. We found the spatial pattern of $V_{threshold}$ —with lower values over the Sahel and slightly higher values over the Sahara —are consistent with results from Chomette and Legrand (1999) and Cowie et al. (2014). The magnitude of retrieved $V_{threshold}$ over northern China is largely consistent with previous studies (Kurosaki and Mikami 2007; Ginoux and Beroubaix 2017).

- The rationale for implementing the retrieved threshold wind speed into the GFDL model is not made very clear in the paper, but I assume it is to try and show that using the retrieved threshold wind speed improves GCM simulations of the dust cycle. If so, although the analysis presented is interesting and draws on a commendably wide variety of data, it has some important problems that need to be addressed. First, the proportionality constant in the dust emission equation (Eq. 3) is not constrained by physics (i.e., there's no reason it should be 0.75e-9 ug/s2/m5 instead of 1e-9 or 0.1e-9 ug/s2/m5), and presumably C was set at an earlier stage by maximizing agreement

against observational data. Therefore, the fact that using the retrieved threshold wind speeds reduces the underestimation of DOD and dust concentration is not an indication that the retrieved threshold wind speeds actually improve the realism of the model simulation. You would get the same effect simply by increasing the (unconstrained) value of C. The authors should therefore compare apples to apples by tuning the simulations to the same global loading or DOD, and then compare against the AERONET and other data. This is especially important because using the retrieved threshold wind speeds results in a very large (and again, arbitrary, because C is unconstrained) increase in emissions by a factor of 4 (Table S2).

We added lines 441-442, 570-574 to better explain the purpose of implementing the retrieved threshold wind speed into the GFDL model.

The reviewer found C in Eq. 4 is not constrained by physics. Here C is a global tuning factor to adjust the magnitude of dust emission. In the model, surface winds are modulated by the model resolution as well as the model physics parameterizations, which make necessary to use a global tuning factor, assuming that the biases are constant globally. In the default version of the AM4.0/LM4.0, $C = 0.75\times10^{-9}$ is obtained by matching modeled dust surface concentrations with RSMAS station records.

We agree with the reviewer that increasing C will increase the magnitude of dust emission and also DOD, which can reduce the bias of underestimation in the Control run. However, as mentioned in lines 476-480: "Here we choose not to retune the dust emission scheme but instead test the usage of $V_{threshold}$, which theoretically provides a more physics-based way to improve dust simulation. We also choose to keep the tuning factor C (Eq. 4) the same in all simulations to better examine the effects of implementing the newly developed $V_{threshold}$. " While tuning C can increase overall dust emission and DOD magnitude, it cannot improve the spatial pattern and seasonal cycle of DOD or surface dust concentrations. We added lines 812-817 to better clarify this point: "The major benefit of using the spatial and temporal varying $V_{threshold}$ is that it improves the simulation of DOD spatial pattern (Figs. 6-7), seasonal cycle (Figs. 11-13), and frequency distribution (Fig. 15) as well as the spatial pattern of surface dust concentrations (Figs. 9-10), which cannot be achieved by simply modifying the global tuning factor (C in Eq. 4) to fit the observations such as surface concentrations or optical depth."

We also conducted a test run to increase dust emission in the Control run (namely, Control II) to about 1232 Tg yr^{-1}, which is close the to a previous estimation based on MODIS DOD (1223 Tg yr^{-1}; Ginoux et al. 2012) or the AeroCom multi-model median (1123 Tg yr$^{-1;}$ Huneeus et al. 2011). We found the magnitude of DOD slightly increases, e.g., over the Sahel annual mean increases from 0.07 to 0.09, however, there's no improvement in terms of seasonal cycle or spatial pattern, as expected (see discussion in lines 818-825).

We also follow the comments of the reviewer to conduct two other simulations using this enlarged C and 12-month and annual mean $V_{threshold}$ (using DOD_{thresh}= 0.5 or 0.05), i.e., V_{thresh}12mn II and V_{thresh}Ann II simulations, to compare with Control II (see lines 826-837 for details). We choose to use the same C instead of tuning all the simulations to a similar magnitude of global dust emission or DOD. This will help us better attribute the differences among simulations, and also help us quantify the modification on global dust emission/DOD due to the implementation of the $V_{threshold.}$ We found similar improvement in DOD seasonal cycle and weaker improvement in DOD spatial pattern and frequency distribution and surface dust concentrations in V_{thresh}12mn II and V_{thresh}Ann II simulations. This is largely because higher $V_{threshold}$ results in lower global dust emissions in the V_{thresh}Ann II (1961 Tg yr^{-1}) and V_{thresh}12mn II simulations (1705 Tg yr^{-1}) and overall lower DOD globally. Over Mediterranean coast, Europe, and northern Asia, DOD spatial pattern is not as well captured in the V_{thresh}12mn II run as in the V_{thresh}12mn run, likely due to relatively high $V_{threshold}$ in these regions.

- Another problem with the model comparisons against data is that its interpretation requires more rigorous statistics. Keeping in mind the previous comment that the absolute values of DOD and concentration are arbitrary because the emission proportionality constant is unconstrained, the authors would need to show statistically significantly increased correlations between the model and data in order to conclude that the retrieved threshold wind speeds improve the model realism. Otherwise, I do not think the conclusion in the abstract and the paper that the retrieved threshold wind speed improve the simulation can be supported. Correlations are reported in Figs. 4 and 5, and I'm guessing that the improvement is large enough that it's statistically significant, but this ought to be shown. Correlations are not currently reported for the varied results in Figs. 8 – 14, so should be added.

As we mentioned above, the default *C* in the model is not an "arbitrary" value. It is obtained by matching modeled dust surface concentrations with RSMAS station records.

Following the comments from the reviewer, we show in Table R1 here to demonstration whether the correlations between the V_{thresh}12mn simulations and observational data in comparison with correlations between the Control and observational data are significantly different (or increased) for Figs. 5, 6, 9, 10.

Table R1 Correlations between model output and observational datasets for Fig. 5, 6, 9, and 10.

Correlations	**Figure #**	**Correlation coefficient (r)**	**95% confidence intervals**	**Significantly different?**
Control COD vs. AERONET COD	Fig. 5	0.68	0.62~ 0.74	Y
V_{thresh}12mn vs. AERONET COD	Fig. 6	0.84	0.80~ 0.87	
Control surface dust vs. RSMAS	Fig. 9	0.76	0.42~ 0.91	N
V_{thresh}12mn vs. RSMAS	Fig. 9	0.72	0.35~ 0.90	
Pattern correlation of Control vs. IMPROVE	Fig. 10	0.41	0.38~ 0.43	Y
Pattern correlation of V_{thresh}12mn vs. IMPROVE	Fig. 10	0.55	0.53~ 0.57	

As shown in Table R1, when the 95% confidence intervals of the correlation between the Control and observation (e.g., r1) is not overlapped with the confidence intervals of the of the correlation between the V_{thresh}12mn and observation (e.g., r2), it is considered the two correlations (r1 and r2) are significantly different. So the correlations for COD (Figs. 5 and 6) and fine dust concentration (Figs. 10) are significantly increased in the V_{thresh}12mn simulation. In Fig. 9, although the correlation for the 16 RSMAS sites in the V_{thresh}12mn actually decreases in comparison with that in the Control run (0.72 vs. 0.76), the differences with the observations are largely reduced (more white triangles, indicating more stations have the model to observation ratio between 0.5 and 2).

Seasonal cycles are shown in Figs. 11-13. Since the sample size is quite small, only 12 (months), the correlation can be less reliable; consequently the corresponding confidence intervals are quite large. We thus choose not to display correlations in plots but just list the correlations for each region/site in Table R2 here. As shown in Table R2, over most regions/sites correlations with the output from the V_{thresh}12mn simulations increase in comparison with the correlations with the Control run.

Table R2 Correlations between the Control output and the observations (column 3) and between the V_{thresh}12mn output with the observations (column 4) for Figs. 11-13. Correlation coefficients not significant at the 95% level are list in Italic.

Figure #	**Regions/sites**	**Correlation with Control**	**Correlation with V_{thresh}12mn**
Fig. 11	Sahel	0.90	0.86
	Sahara	0.81	0.94
	Arabian Peninsula	0.97	0.98
	N. China	0.44	0.58
	India	0.91	0.96
	US	0.91	0.90
	S. Africa	*0.11*	*0.36*
	S. America	*0.40*	*0.54*
	Australia	0.89	0.87
Fig. 12	Site 1	0.91	0.94
	Site 2	0.88	0.65
	Site 3	0.91	0.94
	Site 4	0.99	0.98
	Site 5	0.91	0.85
	Site 6	0.90	0.93
	Site 7	0.69	0.92
	Site 8	0.82	0.95
	Site 9	0.60	0.88
	Site 10	0.67	0.83
	Site 11	0.64	0.84
	Site 12	0.73	0.80
Fig. 13	Banizoum	0.72	0.90
	Cinzana	0.79	0.92
	M’Bour	*0.14*	0.92

Fig. 14 shows the case study, we choose not to apply correlation analysis, and the correlations for Fig. 15 are listed in Table R3. Over the Sahel, Arabian Peninsula, and

India the correlations are significantly higher than that between MODIS and the Control run.

Table R3 Correlations between model output and MODIS dust event frequency distribution as shown in Fig. 15. Correlation coefficients significant at the 95% confidence level are listed in bold. Whether the correlation between MODIS and the V_{thresh}12mn simulation is significantly different from that between MODIS and the Control is indicated in the last column.

Regions	**Correlation with Control**	**Correlation with V_{thresh}12mn**	**Significant?**
Sahara	-0.17	**0.62**	N
Sahel	-0.36	**0.89**	Y
Arabian Peninsula	-0.28	**0.96**	Y
N. China	-0.17	0.35	N
US	-0.37	-0.42	N
India	0.05	**0.84**	Y
S. Africa	-0.30	-0.33	N
S. America	-0.13	-0.15	N
Australia	0.35	0.42	N

Other comments:
- Line 2: I'd suggest saying "many" instead of "most", as I believe most models at least account for the effect of soil moisture on the threshold wind speed.

Done.

- Do you have a sense of how sensitive your results are to the particular reanalysis product used?

We tested the sensitivities of our method to surface winds in different reanalysis products in Table 3. Discussion is added in section 2.3.

- Line 304: it seems hard to imagine that snow cover of 0.2% would prevent or substantially reduce the occurrence of wind erosion. Please provide support for this assumption.

We added in line 342-343: "since snow cover percentage is round-up to integer in MODIS product, this criterion actually requires no snow cover". We also test the sensitivities of the results to the criteria of snow cover and found it only slightly affect the magnitude of the threshold wind speed in a few regions (Table 2), such as northern China, U.S., and South America, by up to 0.3 m s^{-1} if changing from no snow cover to 10%.

- Line 311-2: "soil moisture ranging from 1.01 to 11.2 kg kg-3"; the units here are incorrect, and I think the number is much too high if the intended unit was kg of water per kg of soil.

Thanks for pointing this out. The numbers are from Table 1 in (Fećan et al. 1999), and the unit is %.

- Line 317: I don't think it makes sense to only pick out the daily maximum surface wind speed when you have wind speeds at 6-hours resolution. You could either argue that the DOD is a product of emission that occurs over a longer time period and thus use winds at all time steps, or you could argue that you are using DOD as a proxy for emissions in the moment and thus use the wind speed closest to your DOD observation (presumably noon since overpasses are at 10:30 am and 1:30 pm). But using the daily maximum does not make sense to me.

We use daily maximum wind speed largely because wind erosion occurs when the wind speed is relatively high, so we want to focus on the maximum of 6-hourly wind speed. Ginoux and Deroubaix (2017) also used daily maximum surface wind speed from the EAR-Interim to retrieve threshold of wind erosion over northern China. We added line 361-365 to better clarify this point: "Following Ginoux and Deroubaix (2017), we use maximum daily wind speed instead of daily mean wind speed, largely because dust emission only occur when wind speed is strong enough, and the emission magnitude is roughly proportional to the third power of surface wind speed in empirical estimations."

- The authors use a threshold DOD of 0.2 over the major source regions of North Africa, the Middle East, etc, which is consistent with previous work in Ginoux et al. (2012). But they use a threshold DOD of only 0.02 in lesser source regions such the US, South America, etc. This is a very large difference of a factor of 10, and seems rather arbitrary. Could the authors either provide an analysis of the sensitivity of their results to this choice or use the actual frequency distribution of DOD in the different source regions to inform these thresholds?

As shown in Fig. 15 and also mentioned in lines 376-378 and 748-751, the regional mean DOD frequency distribution in less dusty regions, such as the U.S., South America, South Africa, Australia, peaks at a much lower value. We chose to use a DOD threshold ten times smaller for these less dusty regions also because the magnitude of dust emission in these regions are at least ten times smaller than major dust source regions such as North Africa and the Middle East. In Table 2 (also see discussion in section 2.3), we tested the sensitivity of using DOD_{thresh} of 0.5 and 0.05. In the U.S., South Africa, South America, and Australia, changing DOD_{thresh} from 0.02 to 0.05 will increase annual mean threshold of wind erosion by about 1.27, 1.05, 1.74 and 1.30 m s^{-1}, respectively.

- Section 3.2.3: How are you obtaining AERONET data as a gridded product since data density is so sparse in most dust source regions?

In this section, we shows regional averaged DOD from model output along with MODIS DOD and grided AERONET COD (interpolating from station data to a 0.5° by 0.5° grid) in Fig. 11, while in Figs. 12-13, only AERONET station data are shown. AERONET station data are quite sparse in some regions, e.g., the Sahel, thus the interpolated COD has a large difference with MODIS. So when discussing Fig. 11 we mentioned in lines 665-668: "Since the gridded COD may have large uncertainties over regions with only a few stations, such as the Sahel, Sahara, northern China, and South Africa, MODIS DOD is used as the main reference in the comparison."

- It's not clear to me whether the control run accounts for the effects of soil moisture on the threshold wind speed or whether it truly uses a constant threshold wind speed, regardless even of soil moisture content. Could you clarify?

The default setting in the AM4.0/LM4.0, or the Control run, does not include soil moisture in dust emission. The dust emission scheme follows Eq. 4. So a constant threshold of wind erosion is used.

Editorial comments:

- Line 57: Since wind speeds are a function of height, please note what these wind speeds refer to.

We added "for surface 10 m wind" in line 57.

- Since the methodology is quite involved and lengthy, I recommend you provide an overview of your methodology in a paragraph at the beginning of section 2 to make the paper easier to read.

Thanks for your suggestion. We added lines 124-129 to better introduce this section.

- 182-184: Please provide more info or a citation to a peer-reviewed paper here for the reader to understand how LAI is calculated.

We added reference in text (Yan et al. 2016a, b).

- Line 254-5: This is a common assumption in using the dust concentration data, so you could support this by citing precedent in previous studies.

We modified lines 289-292 to better clarify this point. We cited Ginoux et al. (2001) and Huneeus et al. (2011) who also used the data to validate model output in different periods in lines 281-283.

- Section 3.3: I think this section would be placed more logically before the case study.

We'd like to keep the original order because section 3.2.4 is a case study about the DOD simulation in one region at a particular time (a few days), while section 3.4 examined global frequency distribution of DOD in the model, an aspect largely ignored by previous studies. So we'd like to keep it in a separate section. Also, in section 3.3, DOD frequency distributions in MODIS, the Control and V_{thresh}12mn simulations are discussed and summarized for individual regions.

- Figure 8: since the data here span 3 orders of magnitude, providing statistics in linear space is not very meaningful as it weighed heavily toward the large concentration data. Please provide statistics in logarithmic space.

We updated Fig. 9 (previously Fig. 8) to change the statistics in logarithmic space.

- Fig. 14: What is the bin spacing on the horizontal axis? The reader needs that to interpret the percentage given on the vertical axis.

We added the information in figure caption. The bin spacing for dusty regions is 0.05 while for less dusty regions is 0.01.

References:

Dorman, J. L., and P. J. Sellers, 1989: A global climatology of albedo, roughness length and stomatal resistance for atmospheric general circulation models as represented by the Simple Biosphere Model (SiB), J. of Applied Meteorology, 28, 833-855.

Sellers, P., W. Shuttleworth, J. Dorman, A. Dalcher, J. Roberts, 1989: Calibrating the Simple Biosphere Model for Amazonian tropical forest using filed and remote sensing data. Part I: Average calibration with field data, Journal of Applied Meterology, 28, 727-759.

Yan, K. and co-authors, 2016a: Evaluation of MODIS LAI/FPAR product collection 6. Part 1: Consistency and Improvements, Remote Sensing, 8, 359, doi:10.3390/rs8050359.

Yan, K. and co-authors, 2016b: Evaluation of MODIS LAI/FPAR product collection 6. Part 2: Validation and intercomparison, Remote Sensing, 8, 460, doi:10.3390/rs8060460.

Retrieving the global distribution of threshold of wind erosion from satellite data and implementing it into the GFDL AM4.0/LM4.0 model

Bing Pu[1, 2, *], Paul Ginoux[2], Huan Guo[2, 3], N. Christine Hsu[4], John Kimball[5], Beatrice Marticorena[6], Sergey Malyshev[2], Vaishali Naik[2], Norman T. O'Neill[7], Carlos Pérez García-Pando[8], Joseph M. Prospero[9], Elena Shevliakova[2], Ming Zhao[2]

[1]Atmospheric and Oceanic Sciences Program, Princeton University, Princeton, New Jersey 08544

[2] NOAA Geophysical Fluid Dynamics Laboratory, Princeton, New Jersey 08540

[3] Cooperative Programs for the Advancement of Earth System Science, University Corporation for Atmospheric Research, Boulder, Colorado, 80301

[4] NASA Goddard Space Flight Center, Greenbelt, Maryland, 20771

[5] Department of Ecosystem and Conservation Sciences, University of Montana, Missoula, Montana 59812

[6]LISA, Universités Paris Est-Paris Diderot-Paris

[7] Département de géomatique appliquée , Université de Sherbrooke

[8] Barcelona Supercomputing Center, Barcelona, Spain, 08034

[9] Rosenstiel School of Marine and Atmospheric Sciences, University of Miami, Miami, Florida, 33149

[*] Current affiliation: Department of Geographical and Atmospheric Science, the University of Kansas, Lawrence, Kansas, 66045

Abstract. Dust emission is initiated when surface wind velocities exceed the threshold of wind erosion. ~~Most~~ Many dust models used constant threshold values globally. Here we use satellite products to characterize the frequency of dust events and land surface properties. By matching this frequency derived from Moderate Resolution Imaging Spectroradiometer (MODIS) Deep Blue aerosol products with surface winds, we are able to retrieve a climatological monthly global distribution of wind erosion threshold ($V_{threshold}$) over dry and sparsely-vegetated surface. This monthly two-dimensional threshold velocity is then implemented into the Geophysical Fluid Dynamics Laboratory coupled land-atmosphere model (AM4.0/LM4.0). It is found that the climatology of dust optical depth (DOD) and total aerosol optical depth, surface PM_{10} dust concentrations, and seasonal cycle of DOD are better captured over the "dust belt" (i.e. North Africa and the Middle East) by simulations with the new wind erosion threshold than those using the default globally constant threshold. The most significant improvement is the frequency distribution of dust events, which is generally ignored in model evaluation. By using monthly rather than annual mean $V_{threshold}$, all comparisons with observations are further improved. The monthly global threshold of wind erosion can be retrieved under different spatial resolutions to match the resolution of dust models and thus can help improve the simulations of dust climatology and seasonal cycle as well as dust forecasting.

1. Introduction

Mineral dust is one of the most abundant aerosols by mass and plays an important role in the climate system. Dust particles absorb and scatter solar and terrestrial radiation, thus modifying local energy budget and consequently atmospheric circulation patterns. Studies have shown that the radiative effect of dust can affect a wide range of environmental processes. Dust is shown to modulate West African (e.g., Miller and Tegen, 1998; Miller et al., 2004; Mahowald et al., 2010; Strong et al., 2015) and Indian (e.g., Jin et al., 2014; Vinoj et al., 2014; Jin et al., 2015; Jin et al., 2016; Solmon et al., 2015; Kim et al., 2016; Sharma and Miller, 2017) monsoonal precipitation. During severe droughts in North America, there is a positive feedback between dust and the hydrological cycle (Cook et al., 2008, 2009; 2013). African dust is also found to affect Atlantic tropical cyclone activities (e.g., Dunion and Velden, 2004; Wong and Dessler, 2005; Evan et al., 2006; Strong et al., 2018). When deposited on snow and ice, dust reduces the surface reflectivity, enhancing ~~net radiant energy loading~~net radiation and accelerating snow and ice melting, and consequently affecting runoff (e.g., Painter et al., 2010; 2018; Dumont et al., 2014). Dust can serve as ice nuclei and affect the formation, lifetime, and characteristic of clouds (e.g., Levin et al., 1996; Rosenfield et al., 1997; Wurzler et al., 2000; Nakajima et al., 2001; Bangert et al., 2012), perturbing the hydrological cycle. Iron and phosphorus enriched dust is also an important nutrient for the marine and terrestrial ecosystems and thus interacts with the ocean and land biogeochemical cycles (e.g., Fung et al., 2000; Jickells et al., 2005; Shao et al., 2011; Bristow et al., 2010; Yu et al., 2015).

Given the importance of mineral dust, many climate models incorporate dust emission schemes to simulate the life cycle of dust aerosols (e.g., Donner et al., 2011; Collins et al., 2011; Watanabe et al., 2011; Bentsen et al., 2013). Mineral dust particles are lifted from dry and bare soils into the atmosphere by saltation and sandblasting. This process is initiated when surface winds reach a threshold velocity of wind erosion. The value of this wind erosion threshold depends on soil and surface characteristics, including soil moisture, soil texture and particle size, and presence of pebbles, rocks, and vegetation residue (e.g., Gillette et al., 1980; Gillette and Passi, 1988; Raupach et al., 1993; Fécan et al., 1999; Zender et al., 2003; Mahowald et al., 2005), and thus varies spatially and temporally (Helgren and Prospero, 1987). Due to a lack of in-situ data at global scale and uncertainties on these dependencies, most dust and climate models prescribe a spatially and temporally constant threshold of wind erosion for surface 10 m wind (e.g., around 6 to 6.5 m s^{-1}) over dry surface for simplicity ~~. Globally uniform values (e.g., around 6 to 6.5 m s^{-1}) are either directly used over dry surfaces~~ (e.g., Tegen and Fung, 1994; Takemura et al., 2000; Uno et al., 2001; Donner et al., 2011). ~~or with modulations related to other factors, such as soil moisture (e.g., Takemura et al., 2000; Ginoux et al. 2001; Zender et al., 2003; Kok et al., 2014a).~~ For instance, in the Geophysical Fluid Dynamics Laboratory coupled land-atmosphere model AM4.0/LM4.0 (Zhao et al., 2018a, b), a constant threshold of 6 m s^{-1} is used. On the other hand, some models, such as the ECHAM-HAM, HadGEM2-ES, and ICON-ART, parameterize the constant dry threshold friction velocity (usually a function of soil particle size, soil and air density) or threshold wind velocity with dependencies on soil moisture, surface roughness length, and vegetation coverage (e.g., Takemura et al. 2000; Ginoux et al. 2001; Zender et al. 2003; Cheng et al., 2008; Jones et al., 2011; Rieger et al., 2017).

The threshold of wind erosion may be approximately inferred using observations. For instance, Chomette et al. (1999) used the Infrared Difference Dust Index (IDDI) and 10 m winds reanalysis from the European Centre for Medium-Range Weather Forecasts (ECMWF) between 1990 and 1992 to calculate the threshold of wind erosion over seven sites over the Sahel and Sahara. The IDDI was used to determine whether there was a dust event for subsequently calculating an emission index defined as the number of dust events to the total number of potential events. The distribution of surface wind speed was matched with the emission index, and the threshold of wind erosion was determined when the emission index was around 0.9. The resulting average threshold of wind erosion ranged from 6.63 m s^{-1} at a Sahelian site to about 9.08 m s^{-1} at a Niger site, consistent with the model results by Marticorena et al. (1997).

Later, Kurosaki and Mikami (2007) used World Meteorological Organization (WMO) station data from March 1998 to June 2005 to examine the threshold wind speed in East Asia. Using the distribution of surface wind speed and associated weather conditions (i.e., with or without dust emission events), they approximated a dust emission frequency by dividing number of dust events to the total number of observations for each wind bin, and then determined threshold wind speeds at the 5% and 50% levels, corresponding to the most favorable and normal land surface conditions for dust emission, respectively. They found that the derived threshold wind speed varied in space and time, with a larger seasonal cycle in grassland regions, such as northern Mongolia, and smaller seasonal variations in desert regions, such as the Taklimakan and Gobi

Deserts and the Loess Plateau. Cowie et al. (2014) applied a similar method over northern Africa, using wind data observed between 1984 and 2012, and focused on threshold winds at the 25%, 50%, and 75% levels.

Draxler et al. (2010) derived the distribution of threshold of wind erosion over the U.S. by matching the frequency of occurrence (FoO) of Moderate Resolution Imaging Spectroradiometer (MODIS) Deep Blue (Hsu et al., 2004) aerosol optical depth (AOD) above 0.75 with the FoO of friction velocities extracted from the North American Mesoscale (NAM) forecast model at each grid point. This new threshold and a soil characteristics factor was then incorporated into the Hybrid Single-Particle Lagrangian Integrated Trajectory (HYSPLIT) model (Draxier and Hess, 1998) to forecast dust surface concentrations. It was found that major observed dust plume events in June and July 2007 were successfully captured by the model. Later, Ginoux and Deroubaix (2017) used FoO derived from the MODIS Deep Blue dust optical depth (DOD) record to retrieve the wind erosion threshold of surface 10 m winds over East Asia.

For individual dust events, the threshold of friction velocity can also be determined by fitting a second-order Taylor series to dust saltation flux measurements (Barchyn and Hugenholtz, 2011; Kok et al., 2014b).

Nonetheless, a global distribution of threshold of wind erosion ~~based on observation~~with observational constraints that may be implemented in climate models is still lacking. In this study, we propose a method to retrieve monthly global threshold of wind erosion (hereafter, $V_{threshold}$) for dry and sparsely-vegetated surface (i.e., under favorable conditions for dust emission) using high-resolution satellite products and reanalysis datasets. ~~-~~This two-dimensional threshold of surface 10 m winds is then implemented into the Geophysical Fluid Dynamics Laboratory (GFDL) coupled land-atmosphere model, AM4.0/LM4.0 (Zhao et al., 2018a, b). The benefits of using this spatial and temporal varying threshold in simulating present-day climatology and seasonal cycles of dust are analyzed by comparing the model results with observations.

The data and method used to retrieve the threshold of wind erosion are detailed in section 2. The distribution of the derived $V_{threshold}$ and its implication in the climate model is presented in section 3. Section 4 discusses the uncertainties associated with this method, and major conclusions are summarized in section 5.

2. Data and Methodology

In this section we first introduce the satellite products, observational data, and reanalyses used to retrieve the threshold of wind erosion and validate model output (section 2.1). The processes to retrieve the threshold of wind erosion are detailed in section 2.2. The uncertainties of $V_{threshold}$ associated with the retrieval criteria and selection of surface wind datasets are discussed in section 2.3. Section 2.4 introduces GFDL AM4.0/LM4.0 model, its dust emission scheme, and simulation designs.

2.1 Data

2.1.1 Satellite products

1) MODIS Aqua and Terra dust optical depth

DOD is column-integrated extinction by mineral particles. Here daily DOD is retrieved from MODIS Deep Blue aerosol products (collection 6, level 2; Hsu et al., 2013; Sayer et al., 2013): aerosol optical depth (AOD), single-scattering albedo (ω), and the Ångström exponent (α). All the daily variables are first interpolated to a 0.1° by 0.1° grid using the algorithm described by Ginoux et al. (2010). We require that the single-scattering albedo at 470 nm to be less than 0.99~~1~~ for dust due to its absorption of solar radiation. This separates dust from scattering aerosols, such as sea salt. Then a continuous function relating the Ångström exponent, which is highly sensitive to particle size (Eck et al., 1999), to fine-mode AOD established by Anderson et al. (2005; their Eq. 5) is used to separate dust from fine particles. In short, DOD is retrieved using the following equation:

$$DOD = AOD \times (0.98 - 0.5089\alpha + 0.0512\alpha^2) \quad . \qquad (1)$$

Details about the retrieval process and estimated errors are summarized by Pu and Ginoux (2018b). High-resolution MODIS DOD products (0.1° by 0.1°) have been used to identify and characterize dust sources (Ginoux et al., 2012; Baddock et al., 2016) and examine the variations in~~of~~ dustiness in different regions (e.g., Pu and Ginoux, 2016, 2017, 2018b).

Following the recommendation from Baddock et al. (2016), who found the dust sources are better detected using DOD with a low-quality flag (i.e., quality assurance flag, QA, equals =1, following the category of retrieval quality flags in MODIS Deep Blue products; Hsu et al., 2013) than that with a high-quality flag (i.e., QA=3) as retrieved aerosol products were poorly flagged over dust source regions, we also use DOD with the flag of QA=1. Both daily DOD retrieved from Aqua and Terra platforms are used by averaging the two when both products are available or using either one when only one product is available. Since Terra passes the equator from north to south around 10:30 am local time (LT) and Aqua passes the Equator from south to north around 13:30 pm LT, an average of the two combines the information from both morning and afternoon hours. This process also largely reduces missing data (Pu and Ginoux, 2018b). This combined daily DOD, hereafter MODIS DOD, is available from January 2003 to December 2015 at a resolution of 0.1° by 0.1° grid. Note that due to the temporal coverage of MODIS products, the diurnal variations in dust (e.g., O'rgill and Sehmel, 1976; Mbourou et al., 1997; Knippertz, 2008; Schepanski et al., 2009) are not included in current study.

2) Soil moisture

Soil moisture is an important factor that affects dust emission (Fécan et al., 1999). Daily surface volumetric soil moisture (VSM) retrievals derived from similar calibrated microwave (10.7 GHz) brightness temperature observations from the Advanced Microwave Scanning Radiometer-Earth Observing System (AMSR-E) onboard the NASA Aqua satellite (from June 2002 to October 2011) and the Advanced Microwave Scanning Radiometer 2 (AMSR2) sensor onboard the JAXA GCOM-W1 satellite (from July 2012 to June 2017) from the University of Montana (Du et al., 2017a; Du et al., 2017b) was used to retrieve wind erosion threshold. Both AMSR-E and AMSR2 sensors provide global measurements of polarized microwave emissions at six channels, with ascending and descending orbits crossing the equator at around 1:30 pm and 1:30 am LT, respectively. The VSM retrievals are derived from an iterative retrieval algorithm that exploits the variable sensitivity of different microwave frequencies and polarizations, and minimizes the potential influence of atmosphere, vegetation, and surface water cover on the soil signal. The VSM record represents surface (top ~2 cm) soil conditions and shows favorable global accuracy and consistent performance (Du et al. 2017b), particularly over areas with low to moderate vegetation cover that are also more susceptible to wind erosion, although cautions are needed when examining long-term trends due to the small biases between AMSR-E and AMSR2. The horizontal resolution of the product is about 25 km by 25 km, and the daily product from January 2003 to December 2015 is used. The ascending and descending obit VSM retrievals are averaged to get the mean VSM for each day.

3) Snow cover

Snow cover may affect dust emission in the mid-latitudes during spring, for instance, over northern China (Ginoux and Deroubaix, 2017). The interannual variation of snow cover is also found to affect dust emission in regions, such as Mongolia (Kurosaki and Mikami, 2004). Here monthly snow cover data from MODIS/Terra level 3 data (Hall and Riggs, 2015) with a resolution of 0.05° by 0.05° from 2003 to 2015 is used. The high spatial resolution of the product is very suitable for this study.

4) Leaf area index (LAI)

Vegetation ~~can~~ protects soil from the effects of wind and thus modulates dust emission (e.g., Marticorena and Bergametti, 1995; Zender et al., 2003). While dense vegetation coverage can increase surface roughness and reduce near surface wind speed, the roots of vegetation can increase soil cohesion and further reduce wind erosion. LAI describes the coverage of vegetation with a unit of m^2/m^2, i.e., leaf area per ground area. Here monthly LAI retrieved by Boston University from MODIS onboard Aqua (Yan et al., 2016a; Yan et al., 2016b; via personal communication with Ranga Myneni and Taejin

Park; Boston University, 2016) with a resolution of 0.1° by 0.1° from 2003 to 2015 is used. The root mean square error of the product is 0.66, with some overestimation of LAI in sparsely vegetated regions (Yan et al. 2016b; Garrigues et al., 2008).

2.1.2 Reanalysis

Surface wind speed is a critical factor that affects wind erosion. Here 6 hourly 10 m wind speed from the NCEP/NCAR reanalysis (Kalnay et al., 1996, hereafter NCEP1) on a T62 Gaussian grid (i.e., 192 longitude grids equally spaced and 94 latitude grids unequally spaced) is used. The NCEP1 is a global reanalysis with relatively long temporal coverage, from 1948 to the present. We chose to use the NCEP1 reanalysis ~~also~~ mainly because surface winds in the GFDL AM4.0 model are nudged toward the NCEP1, and we preferred to use the reanalysis surface wind that is closests~~set~~ to the model climatology.

ERA-Interim (Dee et al., 2011) is ~~another~~ a global reanalysis produced from ECMWF. It provides high spatial resolution (about 0.75° or 80 km) 6-hourly, daily, and monthly reanalysis from 1979 to present day. ~~Here we use soil~~Soil temperature from the ERA-Interim is used to determine the regions where wind erosion may be prohibited by the frozen surface. Monthly temperature of the first soil layer (0 to 0.07 m) from 2003 to 2015 is used.

In order to quantify the uncertainties of the retrieved threshold wind erosion in association with the selection of reanalysis products, surface 10 m winds from 6-hourly ERA-Interim and hourly ERA5 (Hersbach and Dee, 2016) are both examined. The ERA5 is the latest reanalysis product from the ECMWF, with a horizontal resolution of about 31 km and hourly temporal resolution.

2.1.3 Station data

Multiple ground-based datasets are used to validate AM4.0/LM4.0 simulated aerosol and dust optical depth and surface dust concentrations.

1) AERONET

The AErosol RObotic NETwork (AERONET; Holben et al., 1998) provides quality assured cloud-screened (level 2) aerosol measurements from sunphotometer records. In this paper we used the data products of the version 3.0 AERONET processing routine. To examine model simulated DOD, we used coarse mode AOD (COD; i.e., radius > 0.6 μm) at 500 nm processed by the Spectral Deconvolution Algorithm (O'Neill et al., 2003; hereafter SDA). SDA COD monthly data is first screened to remove those months with less than five days of records. To get the annual means, years with less than five months of records were removed. Only stations with records of at least three years during the period were used to calculate the 2003-2015 climatology (the same time period when MODIS DOD is available). Overall, records from 313 stations were obtained.

AERONET monthly aerosol optical thickness (AOT) data around 550 nm (e.g., 500 nm, 551 nm, 531 nm, 440 nm, 675 nm, 490 nm, 870 nm, etc.) and the Ångström exponents across the dual wavelength of 440-675 nm, 440-870 nm, and 500-870 nm are used to calculate AOD at 550 nm (τ_{550}). If AOT for 551 nm, 555 nm, 531 nm or 532 nm exist, then these values are directly used as AOD 550 nm. Otherwise, the AOT at wavelength λ_A (less than 550 nm), i.e., τ_A , AOT at wavelength λ_B (larger than 550 nm), i.e., τ_B, and Ångström exponent between wavelengths λ_A and λ_B (α) are used to derive AOD 550 nm using the following equations:

$$\tau_{550} = \tau_A \left(\frac{550}{\lambda_A}\right)^{-\alpha} \qquad \text{if } \tau_A \text{ is available ,}$$ (2~~1~~)

$$\tau_{550} = \tau_B \left(\frac{550}{\lambda_B}\right)^{-\alpha} \qquad \text{if } \tau_B \text{ is available.}$$ (3~~2~~)

~~While this process of extrapolating to 550 nm using a classical Ångström exponent is a bit incoherent with the higher order spectral approach of the SDA, errors due to the choice of spectral order will be negligible in comparison with the types of model versus measurement differences that we will be evaluating in this paper.~~

In a manner similar to the process of screening SDA COD data, monthly AOD 550 nm data with less than three days of records in a given month are removed. When calculating the annual means we excluded years having less than five months of records. Finally, to calculate the climatology of 2003-2015, only stations with at least three years of records during this period are used totaling to 351.

We also developed a method to derive DOD at 550 nm from AOD at 550 nm based on the relationship between Ångström exponent and fine-mode AOD established by Anderson et al. (2005; their Eq. 5). This adds a few more sites over the Sahel than the SDA COD stations. DOD is calculated by subtracting the fine-mode AOD from the total AOD. Due to the large uncertainties of single scattering albedo in AERONET records over regions where AOD is lower than 0.4 (e.g., Dubovik and King, 2000; Holben et al., 2006; Andrews et al., 2017), we did not use single scattering albedo to screen AOD to further separate dust from scattering aerosols. Therefore, the derived AERONET DOD over coastal stations may be contaminated by sea salt.

2) RSMAS surface dust concentration

The Rosenstiel School of Marine and Atmospheric Science (hereafter RSMAS dataset) at University of Miami collected mass concentration of dust, sea salt, and sulfate over stations globally, with most of stations on islands (Savoie and Prospero, 1989). The dataset has been widely used for model evaluation (e.g., Ginoux et al., 2001; Huneeus et al., 2011).

Only stations with records longer than four years were used and of those stations only those years with at least eight months of data are used for calculating climatological annual means. So, totally 16 stations are used. Station names, ~~and~~ locations, and record length are listed in Table S1 of the Supplement. We compare the climatology of annual mean surface dust concentration with model output during 2000-2015. Note that since m~~M~~ost station records end earlier than 1998, the dataset largely represents the climatology during the 1980s and 1990s. Thus the discrepancies between model output and the RSMAS data include both model biases and the difference in surface dust concentration from the 1980s to the 2000s. ~~So here we also assume that the climatology of the surface dust concentrations do not change greatly from the 1980s to the 2000s.~~

3) IMPROVE surface fine dust concentration

The Interagency Monitoring of Protected Visual Environments (IMPROVE) network has collected near-surface particulate matter 2.5 ($PM_{2.5}$) samples in the U.S. since 1988 (Malm et al., 1994; Hand et al., 2011). IMPROVE stations are located in national parks and wilderness areas, and $PM_{2.5}$ sampling is performed twice weekly (Wednesday and Saturday; Malm et al., 1994) prior to 2000 and every third day afterwards. Fine dust (with aerodynamic diameter less than 2.5 μm) concentration is calculated using the concentrations of aluminum (Al), silicon (Si), calcium (Ca), iron (Fe), and titanium (Ti) by assuming oxide norms associated with predominant soil species (Malm et al., 1994; their Eq. 5). This dataset has been widely used to study variations in surface fine dust in the U.S. (e.g., Hand et al., 2016; Hand et al., 2017, Tong et al., 2017; Pu and Ginoux, 2018a). Here only monthly data with at least 50% of daily data available in a month (i.e., at least 5 records) are used. Since station coverage over the central U.S. increases after 2002 (e.g., Pu and Ginoux, 2018a), monthly station data from 2002 to 2015 are used and interpolated to a 0.5° by 0.5° grid using inverse distance weighting interpolation. The gridded data are used to evaluate modeled surface fine dust concentrations.

4) LISA PM_{10} surface concentration

Surface PM_{10} concentration from stations from the Sahelian Dust Transect, which was deployed in 2006 under the framework of African Monsoon Multidisciplinary Analysis International Program (Marticorena et al., 2010), were used to examine the surface dust concentration over the Sahelian region. The data are maintained by Laboratoire Interuniversitaire des Systèmes Atmosphériques (LISA) in the framework of the International Network to study Deposition and Atmospheric composition in Africa (INDAAF; Service National d'Observation de l'Institut National des Sciences de l'Univers, France) ~~network~~. Three stations are located within the pathway of Saharan and Sahelian dust plumes moving towards the Atlantic Ocean. Here hourly PM_{10} concentrations from these stations, Banizoumbou (Niger, 13.54° N, 2.66° E), Cinzana (Mali, 13.28° N, 5.93° W), and M'Bour (Senegal, 14.39° N, 16.96° W), from 2006 to 2014 are used. The hourly station data are averaged to obtain daily and monthly mean records to compare with model output.

2.1.4 Other data

Soil depth from the Food and Agriculture Organization of the United Nations (FAO/IIASA/ISRIC/ISS-CAS/JRC, 2009) on a 0.08° by 0.08° resolution is used to examine whether the soil depth is too shallow (i.e. less than 15 cm) for wind erosion.

2.2 Retrieving threshold of wind erosion

The monthly climatological threshold of wind erosion is retrieved by matching the frequency distribution of the MODIS DOD at certain level, namely, DOD_{thresh}, with the frequency distribution of surface 10 m winds from the NCEP1 reanalysis over the period from 2003 to 2015. The process can be summarized by the following steps:

Step1: Since dust is emitted from the dry and sparsely-vegetated surface, the daily DOD data is first masked out to remove the influences of non-erodible factors and unfavorable environmental conditions that are known to prevent dust emission using criteria as follows: daily VSM less than 0.1 $cm^3\ cm^{-3}$; monthly LAI less than 0.3;

monthly snow cover less than 0.2% (since snow cover percentage is round-up to integer in MODIS product, this criterion actually requires no snow cover); monthly top-layer soil temperature higher than 273.15 K, i.e., over unfrozen surface; and soil depth thicker than 15 cm. These criteria approximate the most favorable land surface conditions for wind erosion.

Similar criteria have been used in previous studies to detect or confine dust source regions. For instance, Kim et al. (2013) used NDVI less than 0.15, soil depth greater than 10 cm, surface temperature greater than 260 K, and without snow cover to mask topography based dust source function. LAI less than 0.3 has been used as a threshold for dust emission in the Community Land Model (Mahowald et al., 2010; Kok et al., 2014a), while gravimetric soil moisture ranging from 1.01 to 11.2 ~~kg kg^{-3}~~% depending on soil clay content is recommended to constrain dust emission (Fécan et al., 1999). The uncertainties associated with small variations in the retrieval criteria are further quantified and discussed in section 2.3.

Step 2: Masked daily DOD from Step 1 is then interpolated to a 0.5° by 0.5° grid using bilinear interpolation. This is close to the horizontal resolution of the GFDL AM4.0/LM4.0 model used in this study. Then the cumulative frequency distribution of daily DOD from 2003 to 2015 is derived at each grid point for each month.

Step 3: Daily maximum surface wind speed is first derived from 6-hourly NCEP1 surface winds and then interpolated to a 0.5° by 0.5° grid. Following Ginoux and Deroubaix (2017), we use maximum daily wind speed instead of daily mean wind speed, largely because dust emission only occur when wind speed is strong enough, and the emission magnitude is roughly proportional to the third power of surface wind speed in empirical estimations. The cumulative frequency distribution of daily maximum surface wind from 2003 to 2015 is then calculated at each grid point for each month.

Step 4: A minimum value of DOD (i.e., DOD_{thresh}) is used to separate dust events from background dust. The cumulative frequency (in %) of dust events passing this threshold is compared to the cumulative frequency of surface winds. The minimum surface winds with the same frequency correspond to the threshold of wind erosion, $V_{threshold}$ (see a schematic diagram in Figure S1 in the Supplement). This operation is performed for all grid points for each month. Ginoux et al. (2012) used $DOD_{thresh} = 0.2$ to separate dust events from background dust and quantify the FoO of local dust events. Similarly, $DOD_{thresh} = 0.2$ is used here in major dusty regions (North Africa, Middle East, India, northern China), while for less dusty regions, such as the U.S., South America, South Africa, and Australia, $DOD_{thresh} = 0.02$ is used. The reason to use a lower DOD_{thresh} for less dusty regions is because: i) the overall dust emission in these regions are at least ten times smaller than major dusty regions, such as North Africa (e.g., Huneeus et al., 2011); ii) the frequency distribution of DOD in these regions also peaks at a much lower DOD band (see discussion in section 3.3). We also tested the $DOD_{thresh} = 0.5$ for dusty regions and $DOD_{thresh} = 0.05$ for less dusty regions, and results are discussed in sections 2.3 and 3.1.

Figures 1a-e show the seasonal and annual mean FoO (days when DOD is greater than DOD_{thresh}) using ~~the~~ $DOD_{thresh} = 0.2$ or 0.02 ~~defined here~~. The shaded area covers major dust sources, and the pattern is very similar to that obtained by Ginoux et al. (2012; their Fig. 5), although there are some differences, largely due to the masked DOD (i.e., from Step 1) used in this study and a lower threshold in less dusty regions. The higher

FoO in North Africa during summer in comparison with other seasons is consistent with the summer peak of the frequency of dust source activation derived from the Meteosat Second Generation (MSG) images (Schepanski et al., 2007; their Fig. 1). The relatively high value of FoO over the northern Sahel to southern Sahara is also consistent with dust emission frequency derived from the Meteosat Second Generation Spinning Enhanced Visible and InfraRed Imager (Evan et al., 2015; their Fig. 1).

Note that the selections of masking criteria in Step 1 and DOD_{thresh} in Step 4 are empirical and can add uncertainties to this method. Also, we approximate dust emission using cumulative frequency of DOD, which may overestimate dust emission in regions where the contribution of transported dust is significant and thus underestimate the $V_{threshold}$ in those regions. These uncertainties are further discussed in the following section.

2.3 Sensitivities of $V_{threshold}$ associated with retrieval criteria and the selection of reanalysis surface winds

Table 2 shows variations in derived annual mean $V_{threshold}$ averaged in nine dust source regions (see Table 1 for locations) following slight changes of retrieval criteria: soil moisture, LAI, snow coverage, and DOD_{thresh}. When the soil moisture threshold is changed from 0.1 to 0.15 cm^3 cm^{-3} or without the soil moisture constraint, the variations in $V_{threshold}$ are quite small, ranging from 0.01 to about 0.73 m s^{-1} (Table 2). Similarly, changes of LAI criteria from 0.15 to 0.5 m^2 m^{-2} or snow coverage from 0.2% to 10% slightly change $V_{threshold}$ — within 1 m s^{-1} over most regions. On the other hand, $V_{threshold}$ is quite sensitive to the selection of the DOD_{thresh}. $V_{threshold}$ would increase about 1 to 3 m

s^{-1} if using DOD_{thresh}= 0.5 for dusty regions (0.05 for less dusty regions) instead of DOD_{thresh}= 0.2 (or 0.02). For instance, using DOD_{thresh}=0.5 increases the averaged annual mean $V_{threshold}$ over the Sahara from 4.6 m s^{-1} (using DOD_{thresh}=0.2) to about 7.6 m s^{-1}.

As mentioned earlier, dust event frequency can be overestimated in regions with high ratio of transported dust and consequently $V_{threshold}$ would be underestimated. Here we provide a rough estimation about the influence of transported dust on $V_{threshold}$ over North Africa. It is hard to separate local dust emission and transported dust in the column integrated DOD, so we use surface DOD data (sDOD; personal communication with Juliette Paireau), i.e., DOD form surface to about 400 m, to approximate the component of DOD due to local emission. sDOD is derived by using DOD vertical profile from the Cloud-Aerosol Lidar with Orthogonal Polarization (CALIOP; Winker et al., 2004; Winker et al., 2007) to first calculate a ratio of near surface DOD (0~400 m) to total DOD (0~12km) and then multiplying the ratio to daily MODIS Aqua DOD over North Africa from 2003-2014. Using sDOD, $V_{threshold}$ over the Sahel would increase from 3.2 to 6.0 m s^{-1}, while over the Sahara, $V_{threshold}$ would increase from 4.6 to 7.7 m s^{-1} (Table 2, last column).

How $V_{threshold}$ would change when using surface winds from different reanalyses are examined in Table 3. Surface winds from the ERA-Interim produce higher $V_{threshold}$ than the NCEP1 by 0.2 to 2.2 m s^{-1}. Using surface winds from the ERA5 also would increase $V_{threshold}$ by 1 to 1.6 m s^{-1} over North Africa and about 1.5 m s^{-1} over Australia but create smaller differences in other regions.

In short, $V_{threshold}$ are less sensitive to small changes in the criteria to define a favorable, dry, and sparsely vegetated land surface condition for wind erosion than the choices of DOD_{thresh} or surface wind speeds from different reanalysis products. Over North Africa, not separating transported dust from total DOD may lead to an underestimation of $V_{threshold}$ up to 3 m s^{-1} based on a rough estimation. However, due to the large uncertainties in quantifying transported dust and the regional converge of sDOD dataset, we chose not to incorporate the results from sDOD to the global $V_{threshold}$.

2.4~~3~~ Simulation design

We will examine if the observation-constrained, spatial and temporal varying $V_{threshold}$ would improve dust simulation in the GFDL AM4.0/LM4.0. The AM4.0/LM4.0 is a coupled land-atmosphere model newly developed at GFDL (Zhao et al., 2018a,b). It uses the recent version of the GFDL Finite-Volume Cubed-Sphere dynamical core (FV^3; Putman and Lin, 2007), which is developed for weather and climate applications with both hydrostatic and non-hydrostatic options. Some substantial updates have been incorporated into the AM4.0, such as an updated version of the model radiation transfer code, an alternate topographic gravity wave drag formulation, a double-plume model representing shallow and deep convection, a "light" chemistry mechanism, and modulation on aerosol wet removal by convection and frozen precipitation (Zhao et al., 2018a,b). Here we used a model version with 33 vertical levels (with model top at 1hPa) and cube-sphere with 192×192 grid boxes per cube face (approximately 50 km grid size).

The aerosol physics is based in large part on that of the GFDL AM3.0 (Donner et al., 2011), but with a simplified chemistry where ozone climatology from AM3.0 simulation (Naik et al., 2013) is prescribed. AM4.0 simulates the mass distribution of five aerosols: sulfate, black carbon, organic carbon, dust, and sea salt. Dust is partitioned into five size bins based on radius: 0.1~1 μm (bin 1), 1~2 μm (bin 2), 2~3 μm (bin 3), 3~6 μm (bin 4), and 6~10 μm (bin 5). The dust emission scheme follows the parameterization of Ginoux et al. (2001), as shown in the following equation:

$$F_p = C \times S \times s_p \times V_{10m}^2 (V_{10m} - V_t) \qquad (\text{if } V_{10m} > V_t), \qquad (4\cancel{3})$$

where F_p is flux of dust of particle size class p, C is a scaling factor with a unit of μg s^2 m^{-5}, here C is set to 0.75×10^{-9}. S is the source function based on topographic depressions (Ginoux et al., 2001), s_p is fraction of each size class, and V_{10m} is surface 10 m wind speed, and V_t = 6 m s^{-1} is the threshold of wind erosion.

Three simulations with prescribed sea surface temperature (SST) and sea ice (Table 4~~2~~) were conducted from 1999 to 2015, with the first year discarded for spin up. The Atmospheric Model Intercomparison Project (AMIP)-style SST and sea ice data (Taylor et al., 2000) are from the Program for Climate Model Diagnosis and Intercomparison (PCMDI), which combined HadISST (Rayner et al., 2003) from UK Met Office before 1981 and NCEP Optimum Interpolation (OI) v2 SST (Reynolds et al., 2002) afterwards. The surface winds in the simulations are nudged toward the NCEP1 reanalysis with a relaxation timescale of 6 hours (Moorthi and Suarez, 1992). Note that the nudged surface winds are actually weaker than the surface wind speed simulated by the standard version of AM4.0/LM4.0 without nudging, so the overall magnitude of dust emission is lower than the standard version. Here we choose not to retune the dust emission scheme but instead test the usage of $V_{threshold}$, which theoretically provides a more physics-based way to improve dust simulation. We also choose to keep the tuning factor C (Eq. 4) the same in all simulations to better examine the effects of implementing the newly developed $V_{threshold}$.

In the Control run, the default model setting is used for dust emission, with a prescribed 6 m s^{-1} threshold of wind erosion (cf. Ginoux et al., 2019). In the V_{thresh}12mn simulation, the observation based climatological monthly $V_{threshold}$ is used to replace the constant wind erosion threshold. The default source function S in Eq. 4~~3~~ only allows dust emission over bare ground by masking out regions with vegetation cover. Since LAI masking is already applied in the retrieval of $V_{threshold}$ (i.e., LAI<0.3), we choose to use a source function that is the same as the default source function S but without vegetation masking, i.e., S' (Figure S2 in the supplement). This allows the influence of the spatial and temporal variations in~~of~~ $V_{threshold}$ to be fully examined. The combination of source function S' and $V_{threshold}$ also extends dust source from bare ground to sparsely vegetated area as outlined by $V_{threshold}$, e.g., over central North America, central India, and part of Australia, and can increase dust emission in these regions. The pattern of extended dust source area largely resembles the vegetated dust source identified by Ginoux et al. (2012; their Fig. 15b) and Kim et al. (2013; their Fig. 9). All the other settings are the same as the Control run. The V_{thresh}Ann simulation is the same as the V_{thresh}12mn but uses the annual mean ~~of~~ $V_{threshold}$ for each month. Since the same SST and sea ice are prescribed for all simulations and land use dose not change much during the short duration of simulation, the differences in simulated dynamic vegetation by LM4.0 among the three simulations are actually very small and can be ignored (see Figures S3-4 in the Supplement).

3. Results

3.1 Thresholds of wind erosion with DOD_{thresh} = 0.2 (or 0.02) and DOD_{thresh} = 0.5 (or 0.05)

Figures 1f-j show the derived threshold of wind erosion for each season and annual mean using DOD_{thresh} =0.2 (or 0.02). The seasonal variations in~~of~~ wind erosion threshold are largely due to the variations in DOD and surface wind frequency distributions that are in turn associated with ~~of~~ variations in land surface features ~~examined here~~, such as soil moisture, soil temperature, snow cover, and vegetation coverage in each month. $V_{threshold}$ is generally lower in MAM and JJA (SON and DJF) for Northern (Southern) Hemisphere dusty regions than in other seasons, consistent with higher FoO in these seasons. $V_{threshold}$ values are also lower in ~~major dust source regions (i.e.,~~ regions with a high FoO (~~in~~ Figs. 1a-e). ~~Globally, the lowest $V_{threshold}$ values (~3-5 m s^{-1}) are located over North Africa and the Middle East, while the highest values (>10 m s^{-1}) occur over northern Eurasia.~~

~~Figure 2a shows the cumulative frequency of $V_{threshold}$ over the global land area for each season and annual mean. The globally constant threshold 6 m s^{-1} used in the GFDL AM4.0/LM4.0 is actually above the 50% level for all seasons and annual mean, indicating the default setting in model likely overestimates the threshold of wind erosion. In fact, the 50% level of $V_{threshold}$ is around 4.5 m s^{-1} for the annual mean and ranges from 4 m s^{-1} in JJA to about 5 m s^{-1} in SON and DJF.~~

The distributions of $V_{threshold}$ for annual mean (black bars) and dusty seasons (color lines; MAM and JJA for the Northern Hemisphere and SON and DJF for the Southern Hemisphere) for each dust source~~y~~ region (see Fig. 1f and Table 1 for locations) are shown in Figs. 2a~~b~~-i~~j~~. In the Sahel and Sahara, the annual mean $V_{threshold}$ peaks around 4 and 4.5-5.5 m s^{-1}, respectively (Figs. 2a-b~~b~~). This magnitude is lower than indicated from previous studies based on station observations in the region, e.g., Helgren and Prospero (1987) found the threshold velocity over eight stations in Northwest Africa ranged from 6.5 to 13 m s^{-1} during summer in 1974. Chomette et al. (1999) and Marsham et al. (2013) also reported higher wind erosion thresholds around 6-9 m s^{-1} at individual stations. On the other hand, Cowie et al. (2014) found that the annual threshold of wind erosion at the 25% level, i.e., when surface condition is favorable for dust emission, can be lower than 6 m s^{-1} at some sites in the Sahel (their Fig. 5). Several factors may contribute to the discrepancies. Firstly, studies suggest that reanalysis datasets may underestimate surface wind speed in spring and for monsoon days in Africa (e.g., Largeron et al., 2015), and therefore could lead to a lower value of $V_{threshold}$ than that derived from station observations. In fact, Bergametti et al. (2017) found even 3-hourly wind speed record at stations may miss short events with high wind~~weed~~ speed. As shown in Table 3, among the reanalysis wind products tested here, the NCEP1 actually produced a lower $V_{threshold}$ in North Africa than the other two reanalyses. ~~As mentioned earlier,~~Secondly, using DOD frequency to approximate dust emission may lead to an overestimation of dust emission over regions such as the southern Sahel where transported dust is a large component and consequently an underestimation of $V_{threshold}$. Based on our rough estimation, $V_{threshold}$ in North Africa can be underestimated by up to 3 m s^{-1} (section 2.3). In addition, d~~D~~ifferent analysis time periods or methods to retrieve the wind erosion threshold may also contribute to the differences.

The annual mean $V_{threshold}$ in ~~the Sahara and~~ Arabian Peninsula is a bit higher, with mean values at ~~4.5 and~~ 5.2 m s^{-1}~~, respectively~~ (Fig~~s~~. 2~~c-~~c~~d~~). The $V_{threshold}$ over northern China is even higher, with an annual mean of 7.8~~9~~ m s^{-1}. This is consistent with the results of Kurosaki and Mikami (2007), who found that under favorable land surface conditions the threshold wind speed ranges from 4.4± 0.6 m s^{-1} in Taklimakan Desert to 6.9± 1.2 m s^{-1} over the Loess Plateau and around 9.8± 1.6 m s^{-1} in the Gobi Desert. These values are also consistent with Ginoux and Deroubaix (2017) who found that regional mean wind erosion threshold over northern China ranges from 6.5 to 9.1 m s^{-1}. In India, the $V_{threshold}$ peaks at about 4.5 m s^{-1} and 6.5 m s^{-1}, respectively (Fig. 2e~~f~~). The second peak is probably related to anthropogenic dust sources over the central Indian subcontinent (Ginoux et al., 2012). We also note that in the Northern Hemisphere, the $V_{threshold}$ in dusty seasons is shifted towards lower values than the annual mean (blue and green lines in Figs. 2a~~b~~-f~~g~~), but is similar to the annual mean in the Southern Hemisphere (especially South America and Australia), indicating stronger influences of surface variability in the Northern Hemisphere.

Fig. 3 shows the seasonal mean and annual mean global $V_{threshold}$ using DOD_{thresh} =0.5 (or 0.05). The corresponding distribution of annual mean $V_{threshold}$ in each region is shown in Figure S5 in the Supplement. The derived $V_{threshold}$ is generally higher than using DOD_{thresh} =0.2 (or 0.02), especially over North Africa, the Arabian Peninsula, India, and Asia (Fig. 3 and Table 2). The results are thus closer to previous station based studies over North Africa. On the other hand, over northern China, $V_{threshold}$ is around or greater than 8 m s^{-1} (Fig. 3e), slighter higher than previous estimates (e.g., Kurosaki and Mikami 2007; Ginoux and Deroubaix 2017).

In the following section, we will exam if the spatial and temporal varying $V_{threshold}$ would improve model simulation of DOD spatial pattern, seasonal variations, frequency distribution and surface dust concentrations in the GFDL AM4.0/LM4.0. Results using $V_{threshold}$ with DOD_{thresh} =0.2 (or 0.02) are shown in sections 3.2 to 3.3 and results using $V_{threshold}$ with DOD_{thresh} =0.5 (or 0.05) are briefly discussed in section 4.

3.2 $V_{threshold}$ in the GFDL AM4.0/LM4.0 model

~~The derived $V_{threshold}$ is then implemented into the GFDL AM4.0/LM4.0 models.~~ In this section we analyze the model output using the default setting (Control; Table 4), 12-month (V_{thresh}12mn), and annual mean $V_{threshold}$ (V_{thresh}Ann) by comparing model results with multiple observational datasets and MODIS DOD. ~~to see how $V_{threshold}$ may affect the simulation of DOD, surface dust concentration, and dust event frequency in the model~~.

3.2.1 Climatology of AOD and DOD

In order to compare the model results with observations, we first show the climatology of AERONET AOD and COD from 2003 to 2015. The length of records for each station is shown in Figure S6 in the Supplement. As shown in Figure 4~~3~~, annual mean global AOD is highest over Africa, the Arabian Peninsula, Indian subcontinent, and Southeast Asia. In the latter two regions, high sulfate concentrations (e.g., Ginoux et al., 2006) and organic carbon from biomass burning in Southeast Asia (e.g., Lin et al., 2014) contribute substantially to the total AOD. The SDA COD shows the optical depth due to coarse aerosols, which includes both dust and sea salt, and sea salt over coastal regions or islands can be a major contributor. Here, high values (>0.2) are largely located over dusty regions such as North Africa, the Arabian Peninsula, and northern India (Fig. 4~~3~~b).

Figures 5~~4~~a-b show the scatter plots of modeled AOD and COD in the Control run versus AERONET AOD and COD, respectively. Here column-integrated extinction from both dust and sea salt is used to calculated COD in the model. The relative differences (%) between AM4.0 output and AERONET station data are also shown (Figs. 5~~4~~c-d). The percentage of DOD to total COD in the model is displayed at the bottom (Fig. 5~~4~~e). The simulated AOD is lower than that from the AERONET over North Africa, the Middle East, and western India, largely due to low values of COD simulated in these regions (Fig. 5~~4~~d). Besides these regions, the COD over North America, South America, South Africa, and northern Eurasia is also, for the most part, underestimated by the model. Dust is the dominant contributor to the COD value over most of these low COD regions, except over the central to eastern North America and central South America (Fig. 5e).

~~The underestimation of~~ COD (and effectively DOD given its dominance in most regions) was ~~improved~~ better simulated in the subsequent model run using a prescribed 12-month $V_{threshold}$ in terms of both magnitude and spatial pattern. Figure 6~~5~~ shows the results from the V_{thresh}12mn simulation. COD is better captured while the AOD effectively moves from a negative to a slightly positive bias (Figs. 6~~5~~a-d). Most sites over North Africa and the Middle East show a relatively small difference with AERONET COD (Fig. 6~~5~~d). Over the Indian subcontinent, COD is overestimated, while over North America excluding the east coast, northern Eurasia, and part of South America, COD is also better captured than in the Control run.

These improvements are largely associated with a better simulation of DOD in the "dust belt" (i.e., North Africa and the Middle East). Figure 7~~6~~ shows the DOD at 550 nm derived from AERONET AOD (see methodology for details) versus that from the V_{thresh}12mn simulation. Over most stations in the Sahel, Mediterranean coasts, and central Middle East, the relative differences between modeled and observed DOD is within ± 25%.

Figure 8~~7~~ shows the regional averaged annual mean DOD over nine dusty regions from MODIS and three simulations. The Control run largely underestimates DOD in all regions, while the magnitude of DOD is better captured in the V_{thresh}12mn and V_{thresh}Ann simulations, although slightly overestimated in the Sahel and greatly overestimated over Australia. In general, DOD simulated by the V_{thresh}Ann run using a constant annual mean $V_{threshold}$ is higher than that simulated by the V_{thresh}12mn run, consistent with the higher dust emission in the V_{thresh}Ann run (Table S2 in the Supplement). Lack of soil moisture constraint in the model, which is a very important element in capturing the variation of DOD in Australia (Evans et al., 2016), may contribute to the large overestimation of DOD in Australia.

3.2.2 Climatology of surface dust concentration

While DOD is a key parameter associated with the climate impact of dust, surface dust concentration is an important factor affecting local air quality. Here we compare the modeled surface dust concentration with RSMAS station observations. Model output is averaged from 2000 to 2015 to form the annual climatology. Consistent with the DOD output, the Control run largely underestimates surface dust concentrations at almost all of the sites (except sites 9 and 15; Figure 9~~8~~ top panel). The underestimation ~~bias~~ is reduced in the V_{thresh}Ann simulation (Fig. 9~~8~~, middle panel), with seven stations having model/observation ratios between 0.5 and 2 (white triangles). Over the coastal U.S. (e.g., sites 16 and 13), dust concentrations are overestimated, consistent with the overestimation of DOD over the U.S. and the Sahel (Fig. 8~~7~~). Dust concentrations in Australia and the east coast of China are also overestimated by more than five-folds. Surface dust concentration is further improved in the V_{thresh}12mn simulation (Fig. 9~~8~~, bottom), with eight stations showing a model/observation ratio between 0.5 and 2 and only four stations overestimating or underestimating dust concentrations by more than five times.

Simulated surface fine dust concentration (calculated as dust bin 1+0.25×dust bin 2) in the U.S. is compared with gridded IMPROVE data (Figure 10~~9~~). While the Control run largely underestimates surface fine dust concentration, the simulated concentration is overall too high in the V_{thresh}Ann run. The spatial pattern of fine dust concentration is better captured in the V_{thresh}12mn run, with higher values over the southwestern U.S., but the magnitude is still overestimated, and additional dust hot spots are simulated over the northern Great plains and the Midwest, which are not shown in the IMPROVE data. Such an overall overestimation may be attributed to lack of soil moisture modulation in the dust emission scheme. The way in which dust bins are partitioned in the model can add uncertainties to model's representation of surface fine dust concentrations as well. On the other hand, the relatively low spatial coverage of IMPROVE sites over the northern Great Plains and Midwest (e.g., Pu and Ginoux, 2018a) may also add uncertainties to the data itself.

3.2.3 Seasonal cycles

Figure 11~~0~~ compares the seasonal cycle of DOD from three simulations with MODIS DOD in nine dusty regions. The seasonal cycle of gridded AERONET COD (as an approximation to DOD; on a 0.5° by 0.5° grid) is also shown. Since the gridded COD may have large uncertainties over regions with only a few stations, such as the Sahel, Sahara, northern China, and South Africa, MODIS DOD is used as the main reference in the comparison. Seasonal cycles are better captured by the V_{thresh}12mn simulation in the Sahel, the Sahara, and the Arabian Peninsula (Figs. 11~~0~~a-c), although the spring and summer peak in the Sahel is overestimated and winter minimum in the Sahara is underestimated. The MAM peak of MODIS DOD in northern China is missed by both V_{thresh}12mn and V_{thresh}Ann simulations (Fig. 11~~0~~d), while the JJA peak over India is largely overestimated (Fig. 11~~0~~e). Over the U.S. dusty region, the seasonal cycle in the V_{thresh}12mn simulation is slightly underestimated compared to MODIS DOD but overestimated from May to August in the V_{thresh}Ann simulation (Fig. 11~~0~~f). DOD is underestimated in South Africa in all three simulations (Fig. 11~~0~~g). Over South America, the peak from October to February is roughly captured by the V_{thresh}12mn run but is overestimated by the V_{thresh}Ann run (Fig. 11~~0~~h). The seasonal cycles of DOD in Australia are very similar in all three simulations and largely resemble that in the MODIS, although both the V_{thresh}12mn and V_{thresh}Ann simulations overestimate the DOD by about an order of magnitude.

Figure 12~~1~~ shows the seasonal cycle of COD from 12 AERONET SDA sites over North Africa and nearby islands (see Figure S7~~5~~ in the Supplement for site locations) along with MODIS DOD and DOD simulated in three runs. The magnitude of

AERONET COD and MODIS DOD in these sites are very similar, despite missing values at sites 1, 4, 5, 8, 11, and a smaller value at site 2 in MODIS. Over most of the sites, the seasonal cycle is better captured in the V_{thresh}12mn and V_{thresh}Ann simulations than the Control run, although the peak over Cairo_EMA_2 (site 12) is slightly underestimated, which is consistent with the underestimation of annual mean DOD in the area (Fig. 7~~6~~).

We also examined the seasonal cycle of PM_{10} surface concentration at three Sahelian INDAAF stations (see Figure S7~~5~~ in the Supplement for site locations) from the LISA project. Figures 13~~2~~a-c show PM_{10} surface dust concentration (here dust dominates total PM_{10} concentration) from the Control, V_{thresh}12mn, and V_{thresh}Ann simulations versus observed PM_{10} concentration from three LISA sites. PM_{10} concentrations in these sites peak during boreal winter and spring and reach minima from July to September. These seasonal variations are associated with the dry northerly Harmattan wind in boreal winter and spring that transports Saharan dust southward to the Guinean coast and the scavenging effect of monsoonal rainfall in boreal summer that removes surface dust (Marticorena et al., 2010; Fiedler et al., 2015). While the Control run does not capture the seasonal cycles in these sites, the V_{thresh}12mn run largely captures the spring peak and summer minimum, although the magnitude is overestimated. In all three sites, the simulated concentration in the V_{thresh}Ann run is larger than that in the V_{thresh}12mn run, especially in boreal fall to early spring. Such an overestimation is probably due to the prescribed constant annual mean $V_{threshold}$, which is lower than it would be during the less dusty season (i.e., boreal fall to winter) and thus increases dust emission and surface concentration.

Figs. 13~~2~~d-f show the seasonal cycle of DOD from three AERONET sites co-located with LISA INDAAF stations and from three simulations. The V_{thresh}12mn and V_{thresh}Ann simulations largely captured the seasonal cycle of DOD at these sites. The overestimation of near surface PM_{10} dust concentration (Figs. 13~~2~~a-c) and the generally well-captured column integrated DOD (Figs. 13~~2~~d-f) indicate that model likely underestimates dust concentration in the atmospheric column above the surface, which needs further investigation in future studies.

3.2.4 A dust storm over U.S. northern Great Plains on October 18th, 2012

Can the AM4.0/LM4.0 with prescribed $V_{threshold}$ better represent individual dust events? Here we examine a major dust storm captured by MODIS Aqua true color-image on Oct. 18th, 2012 (https://earthobservatory.nasa.gov/images/79459/dust-storm-in-the-great-plains) over the U.S. northern Great Plains. There was a severe drought in 2012 with anomalously low precipitation centered over the central U.S. (e.g., Hoerling et al., 2014). The dry conditions favored dust storm development when there were intensified surface winds. However, this storm was not predicted by the forecast models, such as the Goddard Earth Observing System version 5 (GEOS-5; Rienecker et al., 2008) and Navy Aerosol Analysis Prediction System (NAAPS; Witek et al., 2007; Reid et al., 2009; Westphal et al., 2009).

As shown in Figure 14~~3~~, MODIS DOD also captures this event, with a peak value above 0.5 over southwest Nebraska and northern Kansas on Oct. 18th, 2012. The V_{thresh}12mn run also largely captures this event (Fig. 14~~3~~ bottom panel), although the Control run totally misses it (not shown). In the model, the dust storm appears in South

Dakota and Nebraska on Oct. 17th, 2012, along with the anomalous southwesterly winds. It reaches a maximum on Oct. 18th, in association with intensified anomalous southwesterly winds at the surface and an anomalous low-pressure system at 850 hPa (Figure S8~~6~~ in the Supplement). Note that the modeled dust storm center~~s~~ is located a bit northeastward compared to the MODIS DOD pattern and it also has greater magnitude and covers a larger area. On Oct. 19th, both the anomalous low-pressure system and surface wind speeds weaken and the dust storm dissipates, with slightly elevated DOD levels over a region extending over the lower Mississippi River basin and the Midwest. This is somewhat consistent with MODIS records, which also shows slightly higher DOD levels over Tennessee and northern Alabama on Oct. 19th, regardless of large area of missing values.

3.3 Frequency distribution of DOD in the model versus that from MODIS

Figure 15~~4~~ shows the frequency distribution of regional mean DOD during one dusty season (MAM in the Northern Hemisphere and SON in the Southern Hemisphere) for nine regions. Results from MODIS, the Control, and V_{thresh}12mn runs are shown in black, blue, and orange lines, respectively. In most dusty regions, such as the Sahara, Sahel, Arabian Peninsula, India, and northern China, MODIS DOD frequency largely peaks between 0.2 to 0.4, while DOD frequency peaks at a much lower level between 0.02 to 0.08 in less dusty regions, such as the U.S., South America, South Africa and Australia. This also justifies our selection of DOD_{thresh} of 0.02 (instead of 0.2) in the less dusty regions. The DOD distribution in the Control run is biased low and peaks around 0.05 in those dusty regions and between 0 and 0.01 in less dusty regions. The frequency is much better captured in the V_{thresh}12mn run over the Arabian Peninsula and the Sahel, slightly improved but still biased low over the Sahara, northern China, India, and the U.S. The modeled frequency in the V_{thresh}12mn run is biased high in Australia (peaks outside the maximum of x-axis, not shown) and shows little improvement over South Africa and South America. The overall improvement of DOD frequency using the time-varying 2D $V_{threshold}$ occurs mostly over major dusty regions, which is consistent with the improvements in DOD climatology and seasonal cycle in the model simulations.

4. Discussion

A global distribution of the threshold of wind erosion is retrieved using high resolution MODIS DOD and land surface constraints from relatively high–resolution satellite products and reanalyses. While this climatological monthly $V_{threshold}$ provides useful information about the spatial and temporal variations in~~of~~ wind erosion threshold, there are some uncertainties associated with it. Here DOD frequency is derived using MODIS and other satellite products, thus the uncertainties in the satellite products are inherited in the derived DOD frequency distribution. Due to the cloud screening processes of MODIS products, dust activities over cloud-covered regions may be underestimated. Also, DOD frequency is derived based on daily observations over a 13-year record, so that some variability of dust emission associated with alluvial sediments deposited by seasonal flooding may be not captured. Diurnal variability of dust emission and short-duration events such as haboobs are also not included. Since DOD is a column integrated variable, it includes both local emitted and remotely transported dust. When using DOD frequency distribution to approximate dust emission, it may overestimate dust emission in regions where transported dust is dominated~~, e.g., over the southern Sahel,~~ and lead to an underestimation of $V_{threshold}$. Future studies to better quantify the influences of transported dust would further improve quantitative retrieval of $V_{threshold}$.

Previous study found that over regions such as North Africa, reanalysis products may underestimate surface wind speed in spring and monsoon seasons but overestimate it during dry nights (e.g., Largeron et al., 2015). This is largely because mechanisms such as density current that can enhance surface wind speed are not parameterized in the atmospheric models to produce the reanalysis products, while coarse spatial and temporal sampling may also contribute to the underestimation of reanalysis wind speeds. ~~These limitations add uncertainties to the $V_{threshold}$ estimates derived here.~~ The selection of surface winds from different reanalysis products also affects the derived $V_{threshold}$. Among the three reanalyses examined here, $V_{threshold}$ derived from the NCEP1 reanalysis shows slightly lower values than others.

In addition, $V_{threshold}$ is derived by matching the frequency distribution of DOD at certain levels (~~0.2 or 0.02~~i.e., DOD_{thresh}) with the frequency distribution of daily maximum wind. ~~, and these two values are derived empirically.~~ An issue is that selecting a value of DOD_{thresh} is quite empirical. The influences of soil properties such as soil cohesion, particle size, and particle compositions on the threshold of wind erosion (e.g., Fécan et al., 1999; Alfaro and Gomes, 2001; Shao, 2001; Kok et al., 2014b) are not explicitly examined here and will need further investigation.

The influences of $V_{threshold}$ on AM4.0/LM4.0 results are twofold. On the one hand, it modifies the default constant threshold of wind erosion (V_t in Eq. 4~~3~~) by allowing spatial and temporal variations of wind erosion threshold over bare ground, i.e., within the domain of default dust source function *S* (Figs. S9~~7~~a-e in the Supplement). On the other hand, it slightly extends the potential emission area to sparsely-vegetated regions as outlined by $V_{threshold}$ (Figs. S9~~7~~f-j in the Supplement). Which effect dominates? Taking the V_{thresh}12mn simulation as an example, Figure S10~~8~~ shows the differences of dust emission with the Control run. The increase of dust emission in the V_{thresh}12mn simulation (also summarized in Table S2 in the Supplement) is largely associated with the enhanced emission over the bare ground (Figs. S10~~8~~a-e in the Supplement), mainly over the regions with reduced wind erosion threshold (Figs. S9~~7~~a-e in the Supplement). The increased emission over sparsely-vegetated area over regions such as the southern Sahel, India, and Australia plays a minor role. This is consistent with Kim et al. (2013), who found global dust emission in the Georgia Institute of Technology–Goddard Ozone Chemistry Aerosol Radiation and Transport (GOCART) model is dominated by emission from bare ground.

The major benefit of using the spatial and temporal varying $V_{threshold}$ is that it improves the simulation of DOD spatial pattern (Figs. 6-7), seasonal cycle (Figs. 11-13), and frequency distribution (Fig. 15) as well as the spatial pattern of surface dust concentrations (Figs. 9-10), which cannot be achieved by simply modifying the global tuning factor (i.e., *C* in Eq. 4) to fit the observations such as surface concentrations or optical depth.

The default setting in the Control run produced a relatively low global dust emission (978 Tg yr^{-1}) in comparison with the AeroCom multi-model median (1123 Tg yr^{-1}; Huneeus et al. 2011) or a previous estimation based on MODIS DOD (1223 Tg yr^{-1}; Ginoux et al. 2012). So we also conducted a test run (Control II) to increase global dust emission in the Control run to about 1232 Tg yr^{-1} by enlarging *C* in Eq. 4. The magnitude of DOD slightly increases, e.g., over the Sahel annual mean increases from 0.07 to 0.09, however, there's no improvement in terms of seasonal cycle or spatial pattern, as expected.

We also examined the performance of $V_{threshold}$ using DOD_{thresh}= 0.5 (or 0.05) in the AM4.0/LM4.0. Similarly, we conducted simulations with 12-month $V_{threshold}$ (V_{thresh}12mn II) and annual mean $V_{threshold}$ (V_{thresh}Ann II), all using the same tuning factor as in the Control II. We found similar improvement in DOD seasonal cycle and weaker improvement in DOD spatial pattern and frequency distribution and surface dust concentrations (except with the IMPROVE data over the U.S. and surface concentrations over the Sahel, where dust concentrations are previously overestimated). This is largely because higher $V_{threshold}$ leads to lower global dust emissions in the V_{thresh}Ann II (1961 Tg yr^{-1}) and V_{thresh}12mn II simulations (1705 Tg yr^{-1}) and overall lower DOD. Over Mediterranean coast, Europe, and northern Asia, DOD spatial pattern is not as well captured in the V_{thresh}12mn II run as in the V_{thresh}12mn run, likely due to relatively high $V_{threshold}$ in these regions.

5. Conclusion

While dust aerosols play important roles in the Earth's climate system, large uncertainties exist in modeling its lifecycle (e.g., Huneeus et al., 2011; Pu and Ginoux, 2018b). Constant thresholds of wind erosion are widely used in climate models for simplicity. Here, high-resolution MODIS Deep Blue dust optical depth (DOD) and surface wind speeds from the NCEP1 reanalysis, along with other land surface factors that affect wind erosion, such as soil moisture, vegetation cover, snow cover, soil temperature, and soil depth, were used to develop a time-varying two-dimensional climatological threshold of wind erosion, $V_{threshold}$, based on the seasonal variations of DOD and surface wind distribution frequencies. $V_{threshold}$ is generally lower in dusty seasons, i.e., MAM and JJA (SON and DJF) in the Northern (Southern) Hemisphere. ~~Globally, the lowest $V_{threshold}$ (~3-5 m s^{-1}) is located over North Africa and the Arabian Peninsula, with the highest values (>10 m s^{-1}) over northern Eurasia.~~

The climatological monthly $V_{threshold}$ was then incorporated into the GFDL AM4.0/LM4.0 model to examine the potential benefits relative to the use of a constant threshold. In comparison with the simulation using the default setting of a globally constant threshold of wind erosion (6 m s^{-1}), both the magnitude of DOD and surface dust concentrations are increased and closer to observations. However, different from modifying the global tuning factor (i.e., C in Eq. 4) to increase the overall magnitudes of DOD or surface dust concentrations, we found the spatial and temporal varying $V_{threshold}$ largely improves the simulation of the ~~frequency distribution, magnitude,~~spatial pattern, ~~and~~ seasonal cycle, and frequency distribution of DOD ~~are largely improved~~ over Northern Hemisphere dusty regions, such as North Africa and the Arabian Peninsula, and slightly improved over India, the western to central U.S., and northern China. The ~~magnitude and~~ seasonal cycle of DOD are also slightly improved in South America, although change little in South Africa. The incorporation of $V_{threshold}$ leads to an overestimation of DOD in Australia, likely in association with the absence of soil moisture constraints on dust emission in the model.

The ~~overall underestimation of~~spatial pattern of surface dust concentrations ~~under default model setting is largely reduced~~ is also improved when time-varying $V_{threshold}$ is incorporated~~, except over a central Pacific island and a Icelandic island where the concentration is still underestimated and over Australia and coastal China where dust concentration is overestimated~~. The ~~spatial pattern of surface~~ fine dust concentration in the U.S. is also better captured, with the maximum of annual mean largely located over the southwestern U.S., although the magnitude is overestimated.

A constant annual mean $V_{threshold}$ is also tested in the model, and is found to overestimate DOD over dusty seasons in the Arabian Peninsula, U.S., India, Australia, and South America. Surface PM_{10} concentrations in the Sahel during boreal fall and winter seasons are also largely overestimated with this setting. The results indicate the importance of including the seasonal cycle of $V_{threshold}$ in the model. Using time-varying $V_{threshold}$, the model was also able to capture a strong dust storm in the U.S. Great Plains in October 2012, which created deadly accidents, while some dust forecasting models failed to reproduce it.

Finally, this method to retrieve global threshold of wind erosion can be conducted under different resolutions or surface wind reanalsyses or being applied to surface fiction velocity datasets to match the resolution/scheme of dust models and may help improve their simulations and forecasting of dust distribution. As discussed in section 4, there are uncertainties associated with this method, and future studies to better quantify the influence of transported dust to overall DOD frequency distribution and incorporating station based surface wind records into the retrieval process will further improve the dataset.

Data availability. Both the monthly and annual mean $V_{threshold}$ data at a 0.5° by 0.5° resolution in NetCDF format is archived at: https://www.gfdl.noaa.gov/pag-homepage/

Author contributions. PG and BP conceived the study. PG processed the MODIS Deep Blue aerosol data and guided model simulations. HG, SM, VN, ES, and MZ assisted with model configurations, while CH, JK, BM, NO, CG, and JP provided guidance on data usage and analysis. BP conducted model simulations, analyzed data and model results, and wrote the paper with contributions from all other co-authors.

Acknowledgements.

This research is supported by NOAA and Princeton University's Cooperative Institute for Climate Science and NASA under grant NNH14ZDA001N-ACMAP and NNH16ZDA001N-MAP. The authors thank Drs. Veronica Chan and Hyeyum Shin for their helpful comments on the early version of this paper and Dr. Sophie Vandenbussche for her valuable suggestions. The helpful comments from two anonymous reviewers improved the paper. We also thank the AERONET program for establishing and maintaining the sunphotometer sites used in this study and the IMPROVE network for the data. IMPROVE is a collaborative association of state, tribal, and federal agencies and international partners. The US Environmental Protection Agency is the primary funding source, with contracting and research support from the National Park Service. The Air Quality Group at the University of California, Davis is the central analytical

laboratory, with ion analysis provided by Research Triangle Institute, and carbon analysis provided by Desert Research Institute.

The AERONET aerosol optical depth data and SDA data are downloaded from https://aeronet.gsfc.nasa.gov/new_web/download_all_v3_aod.html (last access: June 2018; Holben et al. 1998). IMPROVE fine dust data are downloaded from http://views.cira.colostate.edu/fed/DataWizard/ (last access: March 2017, Malm et al., 1994; Hand et al., 2011). MODIS LAI data may be requested by contacting Dr. Ranga Myneni at Boston University.

Reference

Alfaro, S. C., and Gomes, L.: Modeling mineral aerosol production by wind erosion: Emission intensities and aerosol size distributions in source areas, J Geophys Res-Atmos, 106, 18075-18084, Doi 10.1029/2000jd900339, 2001.

Anderson, T. L., Wu, Y. H., Chu, D. A., Schmid, B., Redemann, J., and Dubovik, O.: Testing the MODIS satellite retrieval of aerosol fine-mode fraction, J Geophys Res-Atmos, 110, 10.1029/2005jd005978, 2005.

Andrews, E., Ogren, J. A., Kinne, S., and Samset, B.: Comparison of AOD, AAOD and column single scattering albedo from AERONET retrievals and in situ profiling measurements, Atmos Chem Phys, 17, 6041-6072, 10.5194/acp-17-6041-2017, 2017.

Baddock, M. C., Ginoux, P., Bullard, J. E., and Gill, T. E.: Do MODIS-defined dust sources have a geomorphological signature?, Geophys Res Lett, 43, 2606-2613, 10.1002/2015gl067327, 2016.

Bangert, M., Nenes, A., Vogel, B., Vogel, H., Barahona, D., Karydis, V. A., Kumar, P., Kottmeier, C., and Blahak, U.: Saharan dust event impacts on cloud formation and radiation over Western Europe, Atmos Chem Phys, 12, 4045-4063, 10.5194/acp-12-4045-2012, 2012.

Barchyn, T. E., and Hugenholtz, C. H.: Comparison of four methods to calculate aeolian sediment transport threshold from field data: Implications for transport prediction and discussion of method evolution, Geomorphology, 129, 190-203, 10.1016/j.geomorph.2011.01.022, 2011.

Bentsen, M., Bethke, I., Debernard, J. B., Iversen, T., Kirkevag, A., Seland, O., Drange, H., Roelandt, C., Seierstad, I. A., Hoose, C., and Kristjansson, J. E.: The Norwegian Earth System Model, NorESM1-M - Part 1: Description and basic evaluation of the physical climate, Geosci Model Dev, 6, 687-720, 10.5194/gmd-6-687-2013, 2013.

Bristow, C. S., Hudson-Edwards, K. A., and Chappell, A.: Fertilizing the Amazon and equatorial Atlantic with West African dust, Geophys Res Lett, 37, 10.1029/2010gl043486, 2010.

Cheng, T., Peng, Y., Feichter, J., and Tegen, I.: An improvement on the dust emission scheme in the global aerosol-climate model ECHAM5-HAM, Atmos Chem Phys, 8, 1105-1117, DOI 10.5194/acp-8-1105-2008, 2008.

Chomette, O., Legrand, M., and Marticorena, B.: Determination of the wind speed threshold for the emission of desert dust using satellite remote sensing in the thermal infrared, J Geophys Res-Atmos, 104, 31207-31215, Doi 10.1029/1999jd900756, 1999.

Collins, W. J., Bellouin, N., Doutriaux-Boucher, M., Gedney, N., Halloran, P., Hinton, T., Hughes, J., Jones, C. D., Joshi, M., Liddicoat, S., Martin, G., O'Connor, F., Rae, J., Senior, C., Sitch, S., Totterdell, I., Wiltshire, A., and Woodward, S.: Development and evaluation of an Earth-System model-HadGEM2, Geosci Model Dev, 4, 1051-1075, 10.5194/gmd-4-1051-2011, 2011.

Cook, B. I., Miller, R. L., and Seager, R.: Dust and sea surface temperature forcing of the 1930s "Dust Bowl" drought, Geophys Res Lett, 35, 10.1029/2008gl033486, 2008.

Cook, B. I., Miller, R. L., and Seager, R.: Amplification of the North American "Dust Bowl" drought through human-induced land degradation, P Natl Acad Sci USA, 106, 4997-5001, 10.1073/pnas.0810200106, 2009.

Cook, B. I., Seager, R., Miller, R. L., and Mason, J. A.: Intensification of North American Megadroughts through Surface and Dust Aerosol Forcing, J Climate, 26, 4414-4430, 10.1175/Jcli-D-12-00022.1, 2013.

Cowie, S. M., Knippertz, P., and Marsham, J. H.: A climatology of dust emission events from northern Africa using long-term surface observations, Atmos Chem Phys, 14, 8579-8597, 10.5194/acp-14-8579-2014, 2014.

Dee, D. P., Uppala, S. M., Simmons, A. J., Berrisford, P., Poli, P., Kobayashi, S., Andrae, U., Balmaseda, M. A., Balsamo, G., Bauer, P., Bechtold, P., Beljaars, A. C. M., van de Berg, L., Bidlot, J., Bormann, N., Delsol, C., Dragani, R., Fuentes, M., Geer, A. J., Haimberger, L., Healy, S. B., Hersbach, H., Holm, E. V., Isaksen, L., Kallberg, P., Kohler, M., Matricardi, M., McNally, A. P., Monge-Sanz, B. M., Morcrette, J. J., Park, B. K., Peubey, C., de Rosnay, P., Tavolato, C., Thepaut, J. N., and Vitart, F.: The ERA-Interim reanalysis: configuration and performance of the data assimilation system, Q J Roy Meteor Soc, 137, 553-597, 10.1002/qj.828, 2011.

Donner, L. J., Wyman, B. L., Hemler, R. S., Horowitz, L. W., Ming, Y., Zhao, M., Golaz, J. C., Ginoux, P., Lin, S. J., Schwarzkopf, M. D., Austin, J., Alaka, G., Cooke, W. F., Delworth, T. L., Freidenreich, S. M., Gordon, C. T., Griffies, S. M., Held, I. M., Hurlin, W. J., Klein, S. A., Knutson, T. R., Langenhorst, A. R., Lee, H. C., Lin, Y. L., Magi, B. I., Malyshev, S. L., Milly, P. C. D., Naik, V., Nath, M. J., Pincus, R., Ploshay, J. J., Ramaswamy, V., Seman, C. J., Shevliakova, E., Sirutis, J. J., Stern, W. F., Stouffer, R. J., Wilson, R. J., Winton, M., Wittenberg, A. T., and Zeng, F. R.: The Dynamical Core, Physical Parameterizations, and Basic Simulation Characteristics of the Atmospheric Component AM3 of the GFDL Global Coupled Model CM3, J Climate, 24, 3484-3519, 10.1175/2011jcli3955.1, 2011.

Draxier, R. R., and Hess, G. D.: An overview of the HYSPLIT_4 modelling system for trajectories, dispersion and deposition, Aust Meteorol Mag, 47, 295-308, 1998.

Draxler, R. R., Ginoux, P., and Stein, A. F.: An empirically derived emission algorithm for wind-blown dust, J Geophys Res-Atmos, 115, 10.1029/2009jd013167, 2010.

Du, J., Jones, L. A., and Kimball, J. S.: Daily Global Land Parameters Derived from AMSR-E and AMSR2, Version 2, https://doi.org/10.5067/RF8WPYOPJKL2, 2017a.

Du, J. Y., Kimball, J. S., Jones, L. A., Kim, Y., Glassy, J., and Watts, J. D.: A global satellite environmental data record derived from AMSR-E and AMSR2 microwave Earth observations, Earth Syst Sci Data, 9, 791-808, 10.5194/essd-9-791-2017, 2017b.

Dubovik, O., and King, M. D.: A flexible inversion algorithm for retrieval of aerosol optical properties from Sun and sky radiance measurements, J Geophys Res-Atmos, 105, 20673-20696, Doi 10.1029/2000jd900282, 2000.

Dumont, M., Brun, E., Picard, G., Michou, M., Libois, Q., Petit, J. R., Geyer, M., Morin, S., and Josse, B.: Contribution of light-absorbing impurities in snow to

Greenland's darkening since 2009, Nat Geosci, 7, 509-512, 10.1038/Ngeo2180, 2014.

Dunion, J. P., and Velden, C. S.: The impact of the Saharan air layer on Atlantic tropical cyclone activity, B Am Meteorol Soc, 85, 353-+, 10.1175/Bams-85-3-353, 2004.

Eck, T. F., Holben, B. N., Reid, J. S., Dubovik, O., Smirnov, A., O'Neill, N. T., Slutsker, I., and Kinne, S.: Wavelength dependence of the optical depth of biomass burning, urban, and desert dust aerosols, J Geophys Res-Atmos, 104, 31333-31349, Doi 10.1029/1999jd900923, 1999.

Evan, A. T., Dunion, J., Foley, J. A., Heidinger, A. K., and Velden, C. S.: New evidence for a relationship between Atlantic tropical cyclone activity and African dust outbreaks, Geophys Res Lett, 33, 10.1029/2006gl026408, 2006.

Evan, A. T., Fiedler, S., Zhao, C., Menut, L., Schepanski, K., Flamant, C., and Doherty, O.: Derivation of an observation-based map of North African dust emission, Aeolian Res, 16, 153-162, 10.1016/j.aeolia.2015.01.001, 2015.

Evans, S., Ginoux, P., Malyshev, S., and Shevliakova, E.: Climate-vegetation interaction and amplification of Australian dust variability, Geophys Res Lett, 43, 11823-11830, 10.1002/2016gl071016, 2016.

Fécan, F., Marticorena, B., and Bergametti, G.: Parametrization of the increase of the aeolian erosion threshold wind friction velocity due to soil moisture for arid and semi-arid areas, Ann Geophys-Atm Hydr, 17, 149-157, DOI 10.1007/s005850050744, 1999.

Fiedler, S., Kaplan, M. L., and Knippertz, P.: The importance of Harmattan surges for the emission of North African dust aerosol, Geophys Res Lett, 42, 9495-9504, 10.1002/2015gl065925, 2015.

Fung, I. Y., Meyn, S. K., Tegen, I., Doney, S. C., John, J. G., and Bishop, J. K. B.: Iron supply and demand in the upper ocean, Global Biogeochem Cy, 14, 281-295, Doi 10.1029/1999gb900059, 2000.

Garrigues, S., Lacaze, R., Baret, F., Morisette, J. T., Weiss, M., Nickeson, J. E., Fernandes, R., Plummer, S., Shabanov, N. V., Myneni, R. B., Knyazikhin, Y., and Yang, W.: Validation and intercomparison of global Leaf Area Index products derived from remote sensing data, J Geophys Res-Biogeo, 113, 10.1029/2007jg000635, 2008.

Gillette, D. A., Adams, J., Endo, A., Smith, D., and Kihl, R.: Threshold Velocities for Input of Soil Particles into the Air by Desert Soils, J Geophys Res-Oceans, 85, 5621-5630, 10.1029/JC085iC10p05621, 1980.

Gillette, D. A., and Passi, R.: Modeling Dust Emission Caused by Wind Erosion, J Geophys Res-Atmos, 93, 14233-14242, DOI 10.1029/JD093iD11p14233, 1988.

Ginoux, P., Chin, M., Tegen, I., Prospero, J. M., Holben, B., Dubovik, O., and Lin, S. J.: Sources and distributions of dust aerosols simulated with the GOCART model, J Geophys Res-Atmos, 106, 20255-20273, Doi 10.1029/2000jd000053, 2001.

Ginoux, P., Horowitz, L. W., Ramaswamy, V., Geogdzhayev, I. V., Holben, B. N., Stenchikov, G., and Tie, X.: Evaluation of aerosol distribution and optical depth in the Geophysical Fluid Dynamics Laboratory coupled model CM2.1 for present climate, J Geophys Res-Atmos, 111, 10.1029/2005jd006707, 2006.

Ginoux, P., Garbuzov, D., and Hsu, N. C.: Identification of anthropogenic and natural dust sources using Moderate Resolution Imaging Spectroradiometer (MODIS) Deep Blue level 2 data, J Geophys Res-Atmos, 115, 10.1029/2009jd012398, 2010.

Ginoux, P., Prospero, J. M., Gill, T. E., Hsu, N. C., and Zhao, M.: Global-Scale Attribution of Anthropogenic and Natural Dust Sources and Their Emission Rates Based on MODIS Deep Blue Aerosol Products, Rev Geophys, 50, 10.1029/2012rg000388, 2012.

Ginoux, P., and Deroubaix, A.: Space observations of dust in East Asia, Air pollution in Eastern Asia: an integrated perspective, edited by: Bouarar, I., Wang, X., and Brasseur, G. P., Springer, 2017.

Ginoux, P., Malyshev, S., Shevliakova, E., Chan, H. G., Guo, H., Milly, C., Naik, V., Pascale, S., Paulot, F., Pu, B., Zhao, M., and Kapnick, S.: Distribution of absorbing aerosols in snow over high mountain ranges in GFDL AM4/LM4, in preparation, 2019.

Hand, J. L., Copeland, S. A., Day, D. E., Dillner, A. M., Indresand, H., Malm, W. C., McDade, C. E., Moore, C. T., Pitchford, M. L., Schichtel, B. A., and Watson, J. G.: IMPROVE (Interagency Monitoring of Protected Visual Environments): Spatial and seasonal patterns and temporal variability of haze and its constituents in the United States, 2011.

Hand, J. L., White, W. H., Gebhart, K. A., Hyslop, N. P., Gill, T. E., and Schichtel, B. A.: Earlier onset of the spring fine dust season in the southwestern United States, Geophys Res Lett, 43, 4001-4009, 10.1002/2016gl068519, 2016.

Hand, J. L., Gill, T. E., and Schichtel, B. A.: Spatial and seasonal variability in fine mineral dust and coarse aerosol mass at remote sites across the United States, J Geophys Res-Atmos, 122, 3080-3097, 10.1002/2016jd026290, 2017.

Helgren, D. M., and Prospero, J. M.: Wind Velocities Associated with Dust Deflation Events in the Western Sahara, J Clim Appl Meteorol, 26, 1147-1151, Doi 10.1175/1520-0450(1987)026<1147:Wvawdd>2.0.Co;2, 1987.

Hersbach, H., and Dee, D.: ERA5 reanalysis is in production, ECMWF Newsletter, No. 147, 7, 2016.

Hoerling, M., Eischeid, J., Kumar, A., Leung, R., Mariotti, A., Mo, K., Schubert, S., and Seager, R.: Causes and Predictability of the 2012 Great Plains Drought, B Am Meteorol Soc, 95, 269-282, 10.1175/Bams-D-13-00055.1, 2014.

Holben, B. N., Eck, T. F., Slutsker, I., Tanre, D., Buis, J. P., Setzer, A., Vermote, E., Reagan, J. A., Kaufman, Y. J., Nakajima, T., Lavenu, F., Jankowiak, I., and Smirnov, A.: AERONET - A federated instrument network and data archive for aerosol characterization, Remote Sens Environ, 66, 1-16, Doi 10.1016/S0034-4257(98)00031-5, 1998.

Holben, B. N., Eck, T. F., Slutsker, I., Smirnov, A., Sinyuk, A., Schafer, J., Giles, D., and Dubovik, O.: AERONET's Version 2.0 quality assurance criteria, 2006.

Hsu, N. C., Tsay, S. C., King, M. D., and Herman, J. R.: Aerosol properties over bright-reflecting source regions, Ieee T Geosci Remote, 42, 557-569, 10.1109/Tgrs.2004.824067, 2004.

Hsu, N. C., Jeong, M. J., Bettenhausen, C., Sayer, A. M., Hansell, R., Seftor, C. S., Huang, J., and Tsay, S. C.: Enhanced Deep Blue aerosol retrieval algorithm: The second generation, J Geophys Res-Atmos, 118, 9296-9315, 10.1002/jgrd.50712, 2013.

Huneeus, N., Schulz, M., Balkanski, Y., Griesfeller, J., Prospero, J., Kinne, S., Bauer, S., Boucher, O., Chin, M., Dentener, F., Diehl, T., Easter, R., Fillmore, D., Ghan, S., Ginoux, P., Grini, A., Horowitz, L., Koch, D., Krol, M. C., Landing, W., Liu, X., Mahowald, N., Miller, R., Morcrette, J. J., Myhre, G., Penner, J., Perlwitz, J., Stier, P., Takemura, T., and Zender, C. S.: Global dust model intercomparison in AeroCom phase I, Atmos Chem Phys, 11, 7781-7816, 10.5194/acp-11-7781-2011, 2011.

Jickells, T. D., An, Z. S., Andersen, K. K., Baker, A. R., Bergametti, G., Brooks, N., Cao, J. J., Boyd, P. W., Duce, R. A., Hunter, K. A., Kawahata, H., Kubilay, N., laRoche, J., Liss, P. S., Mahowald, N., Prospero, J. M., Ridgwell, A. J., Tegen, I., and Torres, R.: Global iron connections between desert dust, ocean biogeochemistry, and climate, Science, 308, 67-71, DOI 10.1126/science.1105959, 2005.

Jin, Q., Wei, J., Yang, Z. L., Pu, B., and Huang, J.: Consistent response of Indian summer monsoon to Middle East dust in observations and simulations, Atmos Chem Phys, 15, 9897-9915, 10.5194/acp-15-9897-2015, 2015.

Jin, Q. J., Wei, J. F., and Yang, Z. L.: Positive response of Indian summer rainfall to Middle East dust, Geophys Res Lett, 41, 4068-4074, 10.1002/2014gl059980, 2014.

Jin, Q. J., Yang, Z. L., and Wei, J. F.: Seasonal Responses of Indian Summer Monsoon to Dust Aerosols in the Middle East, India, and China, J Climate, 29, 6329-6349, 10.1175/Jcli-D-15-0622.1, 2016.

Jones, C. D., Hughes, J. K., Bellouin, N., Hardiman, S. C., Jones, G. S., Knight, J., Liddicoat, S., O'Connor, F. M., Andres, R. J., Bell, C., Boo, K. O., Bozzo, A., Butchart, N., Cadule, P., Corbin, K. D., Doutriaux-Boucher, M., Friedlingstein, P., Gornall, J., Gray, L., Halloran, P. R., Hurtt, G., Ingram, W. J., Lamarque, J. F., Law, R. M., Meinshausen, M., Osprey, S., Palin, E. J., Chini, L. P., Raddatz, T., Sanderson, M. G., Sellar, A. A., Schurer, A., Valdes, P., Wood, N., Woodward, S., Yoshioka, M., and Zerroukat, M.: The HadGEM2-ES implementation of CMIP5 centennial simulations, Geosci Model Dev, 4, 543-570, 10.5194/gmd-4-543-2011, 2011.

Kalnay, E., Kanamitsu, M., Kistler, R., Collins, W., Deaven, D., Gandin, L., Iredell, M., Saha, S., White, G., Woollen, J., Zhu, Y., Chelliah, M., Ebisuzaki, W., Higgins, W., Janowiak, J., Mo, K. C., Ropelewski, C., Wang, J., Leetmaa, A., Reynolds, R., Jenne, R., and Joseph, D.: The NCEP/NCAR 40-year reanalysis project, B Am Meteorol Soc, 77, 437-471, Doi 10.1175/1520-0477(1996)077<0437:Tnyrp>2.0.Co;2, 1996.

Kim, D., Chin, M. A., Bian, H. S., Tan, Q., Brown, M. E., Zheng, T., You, R. J., Diehl, T., Ginoux, P., and Kucsera, T.: The effect of the dynamic surface bareness on dust source function, emission, and distribution, J Geophys Res-Atmos, 118, 871-886, 10.1029/2012jd017907, 2013.

Kim, M. K., Lau, W. K. M., Kim, K. M., Sang, J., Kim, Y. H., and Lee, W. S.: Amplification of ENSO effects on Indian summer monsoon by absorbing aerosols, Clim Dynam, 46, 2657-2671, 10.1007/s00382-015-2722-y, 2016.

Knippertz, P.: Dust emissions in the West African heat trough - the role of the diurnal cycle and of extratropical disturbances, Meteorol Z, 17, 553-563, 10.1127/0941-2948/2008/0315, 2008.

Kok, J. F., Albani, S., Mahowald, N. M., and Ward, D. S.: An improved dust emission model - Part 2: Evaluation in the Community Earth System Model, with implications for the use of dust source functions, Atmos Chem Phys, 14, 13043-13061, 10.5194/acp-14-13043-2014, 2014a.

Kok, J. F., Mahowald, N. M., Fratini, G., Gillies, J. A., Ishizuka, M., Leys, J. F., Mikami, M., Park, M. S., Park, S. U., Van Pelt, R. S., and Zobeck, T. M.: An improved dust emission model - Part 1: Model description and comparison against measurements, Atmos Chem Phys, 14, 13023-13041, 10.5194/acp-14-13023-2014, 2014b.

Kurosaki, Y., and Mikami, M.: Effect of snow cover on threshold wind velocity of dust outbreak, Geophys Res Lett, 31, 10.1029/2003gl018632, 2004.

Kurosaki, Y., and Mikami, M.: Threshold wind speed for dust emission in east Asia and its seasonal variations, J Geophys Res-Atmos, 112, 10.1029/2006jd007988, 2007.

Largeron, Y., Guichard, F., Bouniol, D., Couvreux, F., Kergoat, L., and Marticorena, B.: Can we use surface wind fields from meteorological reanalyses for Sahelian dust emission simulations?, Geophys Res Lett, 42, 2490-2499, 10.1002/2014gl062938, 2015.

Levin, Z., Ganor, E., and Gladstein, V.: The effects of desert particles coated with sulfate on rain formation in the eastern Mediterranean, J Appl Meteorol, 35, 1511-1523, Doi 10.1175/1520-0450(1996)035<1511:Teodpc>2.0.Co;2, 1996.

Lin, C. Y., Zhao, C., Liu, X. H., Lin, N. H., and Chen, W. N.: Modelling of long-range transport of Southeast Asia biomass-burning aerosols to Taiwan and their radiative forcings over East Asia, Tellus B, 66, 10.3402/tellusb.v66.23733, 2014.

Mahowald, N. M., Baker, A. R., Bergametti, G., Brooks, N., Duce, R. A., Jickells, T. D., Kubilay, N., Prospero, J. M., and Tegen, I.: Atmospheric global dust cycle and iron inputs to the ocean, Global Biogeochem Cy, 19, 10.1029/2004gb002402, 2005.

Mahowald, N. M., Kloster, S., Engelstaedter, S., Moore, J. K., Mukhopadhyay, S., McConnell, J. R., Albani, S., Doney, S. C., Bhattacharya, A., Curran, M. A. J., Flanner, M. G., Hoffman, F. M., Lawrence, D. M., Lindsay, K., Mayewski, P. A., Neff, J., Rothenberg, D., Thomas, E., Thornton, P. E., and Zender, C. S.: Observed 20th century desert dust variability: impact on climate and biogeochemistry, Atmos Chem Phys, 10, 10875-10893, 10.5194/acp-10-10875-2010, 2010.

Malm, W. C., Sisler, J. F., Huffman, D., Eldred, R. A., and Cahill, T. A.: Spatial and Seasonal Trends in Particle Concentration and Optical Extinction in the United-States, J Geophys Res-Atmos, 99, 1347-1370, Doi 10.1029/93jd02916, 1994.

Marsham, J. H., Hobby, M., Allen, C. J. T., Banks, J. R., Bart, M., Brooks, B. J., Cavazos-Guerra, C., Engelstaedter, S., Gascoyne, M., Lima, A. R., Martins, J. V., McQuaid, J. B., O'Leary, A., Ouchene, B., Ouladichir, A., Parker, D. J., Saci, A., Salah-Ferroudj, M., Todd, M. C., and Washington, R.: Meteorology and dust in the central Sahara: Observations from Fennec supersite-1 during the June 2011 Intensive Observation Period, J Geophys Res-Atmos, 118, 4069-4089, 10.1002/jgrd.50211, 2013.

Marticorena, B., and Bergametti, G.: Modeling the Atmospheric Dust Cycle .1. Design of a Soil-Derived Dust Emission Scheme, J Geophys Res-Atmos, 100, 16415-16430, Doi 10.1029/95jd00690, 1995.

Marticorena, B., Bergametti, G., Aumont, B., Callot, Y., NDoume, C., and Legrand, M.: Modeling the atmospheric dust cycle .2. Simulation of Saharan dust sources, J Geophys Res-Atmos, 102, 4387-4404, Doi 10.1029/96jd02964, 1997.

Marticorena, B., Chatenet, B., Rajot, J. L., Traore, S., Coulibaly, M., Diallo, A., Kone, I., Maman, A., Diaye, T. N., and Zakou, A.: Temporal variability of mineral dust concentrations over West Africa: analyses of a pluriannual monitoring from the AMMA Sahelian Dust Transect, Atmos Chem Phys, 10, 8899-8915, 10.5194/acp-10-8899-2010, 2010.

Mbourou, G. N., Bertrand, J. J., and Nicholson, S. E.: The diurnal and seasonal cycles of wind-borne dust over Africa north of the equator, J Appl Meteorol, 36, 868-882, Doi 10.1175/1520-0450(1997)036<0868:Tdasco>2.0.Co;2, 1997.

Miller, R. L., and Tegen, I.: Climate response to soil dust aerosols, J Climate, 11, 3247-3267, Doi 10.1175/1520-0442(1998)011<3247:Crtsda>2.0.Co;2, 1998.

Miller, R. L., Tegen, I., and Perlwitz, J.: Surface radiative forcing by soil dust aerosols and the hydrologic cycle, J Geophys Res-Atmos, 109, 10.1029/2003jd004085, 2004.

Moorthi, S., and Suarez, M. J.: Relaxed Arakawa-Schubert - a Parameterization of Moist Convection for General-Circulation Models, Mon Weather Rev, 120, 978-1002, Doi 10.1175/1520-0493(1992)120<0978:Rasapo>2.0.Co;2, 1992.

Naik, V., Horowitz, L. W., Fiore, A. M., Ginoux, P., Mao, J. Q., Aghedo, A. M., and Levy, H.: Impact of preindustrial to present-day changes in short-lived pollutant emissions on atmospheric composition and climate forcing, J Geophys Res-Atmos, 118, 8086-8110, 10.1002/jgrd.50608, 2013.

Nakajima, T., Higurashi, A., Kawamoto, K., and Penner, J. E.: A possible correlation between satellite-derived cloud and aerosol microphysical parameters, Geophys Res Lett, 28, 1171-1174, Doi 10.1029/2000gl012186, 2001.

O'Neill, N. T., Eck, T. F., Smirnov, A., Holben, B. N., and Thulasiraman, S.: Spectral discrimination of coarse and fine mode optical depth, J Geophys Res-Atmos, 108, 10.1029/2002jd002975, 2003.

O'rgill, M., and Sehmel, G.: Frequency and diurnal variation of dust storms in the contiguous U.S.A., Atmospheric Environment, 10, 813-825, 1976.

Painter, T. H., Deems, J. S., Belnap, J., Hamlet, A. F., Landry, C. C., and Udall, B.: Response of Colorado River runoff to dust radiative forcing in snow, P Natl Acad Sci USA, 107, 17125-17130, 10.1073/pnas.0913139107, 2010.

Painter, T. H., Skiles, S. M., Deems, J. S., Brandt, W. T., and Dozier, J.: Variation in Rising Limb of Colorado River Snowmelt Runoff Hydrograph Controlled by Dust Radiative Forcing in Snow, Geophys Res Lett, 45, 797-808, 10.1002/2017gl075826, 2018.

Pu, B., and Ginoux, P.: The impact of the Pacific Decadal Oscillation on springtime dust activity in Syria, Atmos Chem Phys, 16, 13431-13448, 10.5194/acp-16-13431-2016, 2016.

Pu, B., and Ginoux, P.: Projection of American dustiness in the late 21st century due to climate change, Scientific reports, 7, 10.1038/s41598-017-05431-9, 2017.

Pu, B., and Ginoux, P.: Climatic factors contributing to long-term variations in surface fine dust concentration in the United States, Atmos Chem Phys, 18, 4201-4215, 10.5194/acp-18-4201-2018, 2018a.

Pu, B., and Ginoux, P.: How reliable are CMIP5 models in simulating dust optical depth?, Atmos Chem Phys, 18, 12491-12510, 10.5194/acp-18-12491-2018, 2018b.

Putman, W. M., and Lin, S. H.: Finite-volume transport on various cubed-sphere grids, J Comput Phys, 227, 55-78, 10.1016/j.jcp.2007.07.022, 2007.

Raupach, M. R., Gillette, D. A., and Leys, J. F.: The Effect of Roughness Elements on Wind Erosion Threshold, J Geophys Res-Atmos, 98, 3023-3029, Doi 10.1029/92jd01922, 1993.

Rayner, N. A., Parker, D. E., Horton, E. B., Folland, C. K., Alexander, L. V., Rowell, D. P., Kent, E. C., and Kaplan, A.: Global analyses of sea surface temperature, sea ice, and night marine air temperature since the late nineteenth century, J Geophys Res-Atmos, 108, 10.1029/2002jd002670, 2003.

Reid, J. S., Hyer, E. J., Prins, E. M., Westphal, D. L., Zhang, J. L., Wang, J., Christopher, S. A., Curtis, C. A., Schmidt, C. C., Eleuterio, D. P., Richardson, K. A., and Hoffman, J. P.: Global Monitoring and Forecasting of Biomass-Burning Smoke:

Description of and Lessons From the Fire Locating and Modeling of Burning Emissions (FLAMBE) Program, Ieee J-Stars, 2, 144-162, 10.1109/Jstars.2009.2027443, 2009.

Reynolds, R. W., Rayner, N. A., Smith, T. M., Stokes, D. C., and Wang, W. Q.: An improved in situ and satellite SST analysis for climate, J Climate, 15, 1609-1625, Doi 10.1175/1520-0442(2002)015<1609:Aiisas>2.0.Co;2, 2002.

Rieger, D., Steiner, A., Bachmann, V., Gasch, P., Forstner, J., Deetz, K., Vogel, B., and Vogel, H.: Impact of the 4 April 2014 Saharan dust outbreak on the photovoltaic power generation in Germany, Atmos Chem Phys, 17, 13391-13415, 10.5194/acp-17-13391-2017, 2017.

Rienecker, M. M., Suarez, M. J., Todling, R., Bacmeister, J., Takacs, L., Liu, H.-C., Gu, W., Sienkiewicz, M., Koster, R. D., Gelaro, R., Stajner, I., and Nielsen, J. E.: The GEOS‐5 Data Assimilation System—Documentation of versions 5.0.1, 5.1.0, and 5.2.0, Technical Report Series on Global Modeling and Data Assimilation, 27 (available at http://gmao.gsfc.nasa.gov/pubs/docs/Rienecker369.pdf), 2008.

Rosenfield, J. E., Considine, D. B., Meade, P. E., Bacmeister, J. T., Jackman, C. H., and Schoeberl, M. R.: Stratospheric effects of Mount Pinatubo aerosol studied with a coupled two-dimensional model, J Geophys Res-Atmos, 102, 3649-3670, Doi 10.1029/96jd03820, 1997.

Savoie, D. L., and Prospero, J. M.: Comparison of Oceanic and Continental Sources of Non-Sea-Salt Sulfate over the Pacific-Ocean, Nature, 339, 685-687, DOI 10.1038/339685a0, 1989.

Sayer, A. M., Hsu, N. C., Bettenhausen, C., and Jeong, M. J.: Validation and uncertainty estimates for MODIS Collection 6 "Deep Blue" aerosol data, J Geophys Res-Atmos, 118, 7864-7872, 10.1002/jgrd.50600, 2013.

Schepanski, K., Tegen, I., Laurent, B., Heinold, B., and Macke, A.: A new Saharan dust source activation frequency map derived from MSG-SEVIRI IR-channels, Geophys Res Lett, 34, 10.1029/2007gl030168, 2007.

Schepanski, K., Tegen, I., Todd, M. C., Heinold, B., Bonisch, G., Laurent, B., and Macke, A.: Meteorological processes forcing Saharan dust emission inferred from MSG-SEVIRI observations of subdaily dust source activation and numerical models, J Geophys Res-Atmos, 114, 10.1029/2008jd010325, 2009.

Shao, Y.: A model for mineral dust emission, J Geophys Res-Atmos, 106, 20239-20254, Doi 10.1029/2001jd900171, 2001.

Shao, Y. P., Wyrwoll, K. H., Chappell, A., Huang, J. P., Lin, Z. H., McTainsh, G. H., Mikami, M., Tanaka, T. Y., Wang, X. L., and Yoon, S.: Dust cycle: An emerging core theme in Earth system science, Aeolian Res, 2, 181-204, 10.1016/j.aeolia.2011.02.001, 2011.

Sharma, D., and Miller, R. L.: Revisiting the observed correlation between weekly averaged Indian monsoon precipitation and Arabian Sea aerosol optical depth, Geophys Res Lett, 44, 10006-10016, 10.1002/2017gl074373, 2017.

Solmon, F., Nair, V. S., and Mallet, M.: Increasing Arabian dust activity and the Indian summer monsoon, Atmos Chem Phys, 15, 8051-8064, 10.5194/acp-15-8051-2015, 2015.

Strong, J. D., Vecchi, G. A., and Ginoux, P.: The Climatological Effect of Saharan Dust on Global Tropical Cyclones in a Fully Coupled GCM, Journal of Geophysical Research - Atmospheres, 123, https://doi.org/10.1029/2017JD027808, 2018.

Strong, J. D. O., Vecchi, G. A., and Ginoux, P.: The Response of the Tropical Atlantic and West African Climate to Saharan Dust in a Fully Coupled GCM, J Climate, 28, 7071-7092, 10.1175/Jcli-D-14-00797.1, 2015.

Takemura, T., Okamoto, H., Maruyama, Y., Numaguti, A., Higurashi, A., and Nakajima, T.: Global three-dimensional simulation of aerosol optical thickness distribution of various origins, J Geophys Res-Atmos, 105, 17853-17873, Doi 10.1029/2000jd900265, 2000.

Taylor, K., Williamson, D., and Zwiers, F.: The sea surface temperature and sea ice concentration boundary conditions for AMIP II simulations (PCMDI Rep. 60, pp. 1–25), Livermore, CA:Program for Climate Model Diagnosis and Intercomparison, Lawrence Livermore National Laboratory, 2000.

Tegen, I., and Fung, I.: Modeling of Mineral Dust in the Atmosphere - Sources, Transport, and Optical-Thickness, J Geophys Res-Atmos, 99, 22897-22914, Doi 10.1029/94jd01928, 1994.

Tong, D. Q., Wang, J. X. L., Gill, T. E., Lei, H., and Wang, B. Y.: Intensified dust storm activity and Valley fever infection in the southwestern United States, Geophys Res Lett, 44, 4304-4312, 10.1002/2017gl073524, 2017.

Uno, I., Amano, H., Emori, S., Kinoshita, K., Matsui, I., and Sugimoto, N.: Trans-Pacific yellow sand transport observed in April 1998: A numerical simulation, J Geophys Res-Atmos, 106, 18331-18344, Doi 10.1029/2000jd900748, 2001.

Vinoj, V., Rasch, P. J., Wang, H. L., Yoon, J. H., Ma, P. L., Landu, K., and Singh, B.: Short-term modulation of Indian summer monsoon rainfall by West Asian dust, Nat Geosci, 7, 308-313, 10.1038/ngeo2107, 2014.

Watanabe, S., Hajima, T., Sudo, K., Nagashima, T., Takemura, T., Okajima, H., Nozawa, T., Kawase, H., Abe, M., Yokohata, T., Ise, T., Sato, H., Kato, E., Takata, K., Emori, S., and Kawamiya, M.: MIROC-ESM 2010: model description and basic results of CMIP5-20c3m experiments, Geosci Model Dev, 4, 845-872, 10.5194/gmd-4-845-2011, 2011.

Westphal, D. L., Curtis, C. A., Liu, M., and Walker, A. L.: Operational aerosol and dust storm forecasting, in WMO/GEO Expert Meeting on an International Sand and Dust Storm Warning System, IOP Conference Series Earth and Environmental Science, 2009.

Winker, D. M., Hunt, W., and Hostetler, C.: Status and performance of the CALIOP lidar, Bba Lib, 5575, 8-15, 10.1117/12.571955, 2004.

Winker, D. M., Hunt, W. H., and McGill, M. J.: Initial performance assessment of CALIOP, Geophys Res Lett, 34, 10.1029/2007gl030135, 2007.

Witek, M. L., Flatau, P. J., Quinn, P. K., and Westphal, D. L.: Global sea-salt modeling: Results and validation against multicampaign shipboard measurements, J Geophys Res-Atmos, 112, 10.1029/2006jd007779, 2007.

Wong, S., and Dessler, A. E.: Suppression of deep convection over the tropical North Atlantic by the Saharan Air Layer, Geophys Res Lett, 32, 10.1029/2004gl022295, 2005.

Wurzler, S., Reisin, T. G., and Levin, Z.: Modification of mineral dust particles by cloud processing and subsequent effects on drop size distributions, J Geophys Res-Atmos, 105, 4501-4512, Doi 10.1029/1999jd900980, 2000.

Yan, K., Park, T., Yan, G. J., Chen, C., Yang, B., Liu, Z., Nemani, R. R., Knyazikhin, Y., and Myneni, R. B.: Evaluation of MODIS LAI/FPAR Product Collection 6. Part 1: Consistency and Improvements, Remote Sens-Basel, 8, 10.3390/rs8050359, 2016a.

Yan, K., Park, T., Yan, G. J., Liu, Z., Yang, B., Chen, C., Nemani, R. R., Knyazikhin, Y., and Myneni, R. B.: Evaluation of MODIS LAI/FPAR Product Collection 6. Part 2: Validation and Intercomparison, Remote Sens-Basel, 8, 10.3390/rs8060460, 2016b.

Yu, H. B., Chin, M., Yuan, T. L., Bian, H. S., Remer, L. A., Prospero, J. M., Omar, A., Winker, D., Yang, Y. K., Zhang, Y., Zhang, Z. B., and Zhao, C.: The fertilizing role of African dust in the Amazon rainforest: A first multiyear assessment based on data from Cloud-Aerosol Lidar and Infrared Pathfinder Satellite Observations, Geophys Res Lett, 42, 1984-1991, 10.1002/2015gl063040, 2015.

Zender, C. S., Bian, H. S., and Newman, D.: Mineral Dust Entrainment and Deposition (DEAD) model: Description and 1990s dust climatology, J Geophys Res-Atmos, 108, 10.1029/2002jd002775, 2003.

Zhao, M., Golaz, J. C., Held, I. M., Guo, H., Balaji, V., Benson, R., Chen, J. H., Chen, X., Donner, L. J., Dunne, J. P., Dunne, K., Durachta, J., Fan, S. M., Freidenreich, S. M., Garner, S. T., Ginoux, P., Harris, L. M., Horowitz, L. W., Krasting, J. P., Langenhorst, A. R., Liang, Z., Lin, P., Lin, S. J., Malyshev, S. L., Mason, E., Milly, P. C. D., Ming, Y., Naik, V., Paulot, F., Paynter, D., Phillipps, P., Radhakrishnan, A., Ramaswamy, V., Robinson, T., Schwarzkopf, D., Seman, C. J., Shevliakova, E., Shen, Z., Shin, H., Silvers, L. G., Wilson, J. R., Winton, M., Wittenberg, A. T., Wyman, B., and Xiang, B.: The GFDL Global Atmosphere and Land Model AM4.0/LM4.0:1. Simulation Characteristics With Prescribed SSTs, J Adv Model Earth Sy, 10, 691-734, 10.1002/2017ms001208, 2018a.

Zhao, M., Golaz, J. C., Held, I. M., Guo, H., Balaji, V., Benson, R., Chen, J. H., Chen, X., Donner, L. J., Dunne, J. P., Dunne, K., Durachta, J., Fan, S. M., Freidenreich, S. M., Garner, S. T., Ginoux, P., Harris, L. M., Horowitz, L. W., Krasting, J. P., Langenhorst, A. R., Liang, Z., Lin, P., Lin, S. J., Malyshev, S. L., Mason, E., Milly, P. C. D., Ming, Y., Naik, V., Paulot, F., Paynter, D., Phillipps, P., Radhakrishnan, A., Ramaswamy, V., Robinson, T., Schwarzkopf, D., Seman, C. J., Shevliakova, E., Shen, Z., Shin, H., Silvers, L. G., Wilson, J. R., Winton, M., Wittenberg, A. T., Wyman, B., and Xiang, B.: The GFDL Global Atmosphere and Land Model AM4.0/LM4.0:2. Model Description, Sensitivity Studies, and Tuning Strategies, J Adv Model Earth Sy, 10, 735-769, 10.1002/2017ms001209, 2018b.

Table 1 Major dust source~~y~~ regions shown in Figure 1. Note that region names such as India and northern China are not exactly the same as their geographical definitions but also cover some areas from nearby countries.

Table 2 Sensitivity of annual mean wind erosion threshold (m s^{-1}) to the selection of different retrieval criteria. Note the setting of the last column is the same as DOD_{thresh}=0.2 or 0.02, except surface DOD (sDOD) from Aqua is used over North Africa.

Table 3 Sensitivity of annual mean wind erosion threshold (m s^{-1}) to surface wind speeds from different reanalyses (DOD_{thresh}= 0.2 or 0.02).

Table 4~~2~~ Simulation design

Figure 1. (a)-(e) Frequencies of occurrence (FoO; unit: days per season) in each season and annual mean. (f)-(j) Threshold of wind erosion ($V_{threshold}$; unit: m s^{-1}) derived from satellite products and reanalyses for each season and annual mean using DOD_{thresh}=0.2 (or 0.02). Black boxes in (f) denote nine ~~dusty~~ dust source regions as listed in Table 1.

Figure 2. ~~(a) Cumulative frequency of $V_{threshold}$ over global land for each season (black, orange, blue, green, and grey lines denote annual, SON, JJA, MAM, and DJF averages, respectively). Color dashed lines correspond to the percentages of $V_{threshold}$ = 6 m s^{-1} for each season and annual mean. Color arrows point to the value of $V_{threhsold}$ at the 50% level in each season and annual mean.~~ (a~~b~~)-(i) Frequency distribution of annual mean $V_{threshold}$ (black bars) in each region (black boxes in Fig. 1) and for dusty seasons, i.e., MAM (green) and JJA (blue) for regions in the Northern Hemisphere and SON (orange) and DJF (grey) for regions in the Southern Hemisphere. The mean (averaged over all grid points in the region, without area weight) and ± one standard deviations of $V_{threshold}$ in each region are shown on the top right of each plot.

Figure 3. (a)-(e) Threshold of wind erosion ($V_{threshold}$; unit: m s^{-1}) derived from satellite products and reanalyses for each season and annual mean using DOD_{thresh}=0.5 (or 0.05). Black boxes in (a) denote nine dust source regions as listed in Table 1.

Figure 4~~3~~. Climatology of annual mean AERONET (a) AOD (550 nm) and (b) SDA COD (500 nm) averaged over 2003-2015.

Figure 5~~4~~. Scatter plot of simulated annual mean (a) AOD and (b) COD in the Control run versus AERONET AOD and COD (left), and the relative difference (in percentage) (c) between modeled AOD and AERONET AOD and (d) between modeled COD and AERONET COD (right). (e) The relative contribution of DOD to COD in the model.

Figure 6~~5~~. Same as Fig. 5~~4~~ but for the V_{thresh}12mn simulation.

Figure 7~~6~~. (a) Climatology (2003-2015) of AERONET DOD (550 nm) over major dusty regions and (b) scatter plot of modeled DOD in the V_{thresh}12mn simulation versus AERONET DOD, and (c) the relative difference (in percentage) between modeled DOD and AERONET DOD in the V_{thresh}12mn simulation.

Figure 8~~7~~. Regional averaged annual mean DOD (2003-2015) over nine regions from the Control (grey), V_{thresh}12mn (orange), and V_{thresh}Ann (yellow) simulations and MODIS (black).

Figure 9~~8~~. Scatter plots (left column) of model simulated (from top to bottom are the Control, V_{thresh}Ann, and V_{thresh}12mn simulations) surface dust concentration versus the climatology of observed surface dust concentration from RSMAS stations (Savoie and Prospero 1989), and spatial pattern of surface dust concentration from model output (shading; right column) and the ratio between modeled and RSMAS station observed surface dust concentration (color triangles, with upward triangles indicating overestimation and downward triangles indicating underestimation). 16 stations were used, and numbers in each triangle (right) and grey dots (left) indicate the stations. The one-one, one-two and one-five lines are plotted in solid, dashed and dash-dotted lines in the scatter plots. Statistics in the scatter plots are calculated in logarithmic space.

Figure 10~~9~~. Annual mean surface fine dust concentration (μg m^{-3}) from IMPROVE stations (left column) and three simulations (middle column) and the differences between model and observation (right column) for 2002-2015.

Figure 11~~0~~. Seasonal cycle of DOD from MODIS (black), the Control (grey), V_{thresh}12mn (orange), and V_{thresh}Ann (yellow) runs, and gridded AERONET SDA COD (blue) averaged over nine regions. The annual mean of each dataset in each region is listed on the top of the plot.

Figure 12~~1~~. Seasonal cycle of DOD over 12 AERONET SDA sites (see Fig. S7~~5~~ in the Supplement for locations) from the Control (grey), V_{thresh}12mn (orange), and V_{thresh}Ann (yellow) simulations, along with DOD from MODIS (blue), and COD from AERONET (black dotted line). All values are averaged over 2003-2015. The location (lat/long) and the name (due to space, only first seven characters are shown) of the sites are listed at the top of each plot.

Figure 13~~2~~. (a)-(c) Seasonal cycle of PM_{10} surface concentration (black) over three sites from the LISA project, along with PM_{10} surface dust concentration from the Control (grey), V_{thresh}12mn (orange), and V_{thresh}Ann (yellow) simulations. Error bars are ± one standard deviations of daily mean in each month averaged over 2006-2014. Unites: μg m^{-3}. (d)-(f) seasonal cycle of DOD (550 nm) from three AERONET sites co-located with LISA sites (blue) versus that modeled by the Control (grey), V_{thresh}12mn (orange), and V_{thresh}Ann (yellow) simulations.

Figure 14~~3~~. Daily DOD from MODIS (top panel), daily DOD simulated by the V_{thresh}12mn run along with anomalies (with reference to the 2000-2015 mean) of surface wind vectors (m s^{-1}; bottom panel) from Oct. 17th to Oct. 19th, 2012. Only DOD over land is shown. Missing values in MODIS DOD (top panel) are plotted in grey shading.

Figure 145. Frequency (%) distribution of regional averaged daily DOD from MODIS (black) versus that from the Control (light blue) and V_{thresh}12mn (orange) simulations for the Sahara, the Sahel, the Arabian Peninsula, northern China, India, western to central U.S., South America, South Africa, and Australia from 2003 to 2015. X-axis denotes the ranges of DOD (the bin spacing for dusty regions is 0.05 and for less dusty regions is 0.01), and y-axis is percentage of occurrence. The light green boxes denote the averaging areas. For regions in the Northern Hemisphere frequency in MAM is shown, while for regions in the Southern Hemisphere frequency in SON is shown.

Table 1 Major dust source~~y~~ regions shown in Figure 1. Note that region names such as India and northern China are not exactly the same as their geographical definitions but also cover some areas from nearby countries.

No.	**Regions**	**Lat/long**
1	Sahel	10°-20°N, 18°W-35°E
2	Sahara	20°-35°N, 15°W-25°E
3	Arabian Peninsula	15°-35°N, 35°-60°E
4	Northern China (N. China)	35°-45°N, 77°-103°E
5	India	20°-35°N, 60°-85°E
6	U.S.	25°-45°N, 102°-125°W
7	South Africa (S. Africa)	17°-35°S, 15°-30°E
8	South America (S. America)	18°-55°S, 65°-75°W
9	Australia	15°-35°S, 128-147°E

Table 2 Sensitivity of annual mean wind erosion threshold (m s^{-1}) to the selection of different retrieval criteria. Note the setting of the last column is the same as DOD_{thresh}=0.2 or 0.02, except surface DOD (sDOD) from Aqua is used over North Africa.

Regions	**Soil Moisture (cm^3 cm^{-3})**			**LAI (m^2m^{-2})**			**Snow coverage (%)**			**DOD_{thresh}**		
	<0.1	<0.15	None	<0.15	<0.3	<0.5	<=0.2	<=2	<=10	=0.2 (0.02)	=0.5 (0.05)	sDOD
Sahel	3.21	3.19	3.22	3.24	3.21	3.19	3.21	3.21	3.21	3.21	4.93	6.05
Sahara	4.61	4.56	4.49	4.54	4.61	4.59	4.61	4.61	4.61	4.61	7.59	7.66
AP	5.37	5.26	5.26	5.26	5.37	5.37	5.37	5.36	5.35	5.37	8.00	5.57
N. China	7.73	7.64	7.07	7.79	7.73	7.71	7.73	7.56	7.44	7.73	10.15	7.73
India	5.63	5.12	4.99	6.46	5.63	5.63	5.63	5.61	5.60	5.63	8.59	5.63
U.S.	5.71	5.23	4.98	6.53	5.71	5.56	5.71	5.60	5.41	5.71	7.04	5.71
S. Africa	5.41	5.23	5.20	6.72	5.41	5.10	5.41	5.40	5.40	5.41	6.46	5.41
S. America	6.46	6.32	6.20	6.88	6.46	6.39	6.46	6.39	6.35	6.46	8.20	6.46
Australia	5.19	5.16	5.14	5.66	5.19	5.22	5.19	5.19	5.19	5.19	6.49	5.19

Table 3 Sensitivity of annual mean wind erosion threshold (m s^{-1}) to surface wind speeds from different reanalyses (DOD_{thresh}= 0.2 or 0.02).

Regions	**Reanalysis**		
	NCEP	ERA-Interim	ERA5
Sahel	3.21	4.54	4.80
Sahara	4.61	5.56	5.63
AP	5.37	6.12	5.50
N. China	7.73	7.94	7.05
India	5.63	7.01	5.70
U.S.	5.71	6.82	6.18
S. Africa	5.41	7.17	6.26
S. America	6.46	7.51	6.36
Australia	5.19	7.36	6.68

Table 4~~2~~ Simulation design

Simulations	**Wind erosion threshold**	**Source function**
Control	6 m s^{-1}	*S*
V_{thresh}12mn	12-month $V_{threshold}$	*S'*
V_{thresh}Ann	Annual mean $V_{threshold}$	*S'*

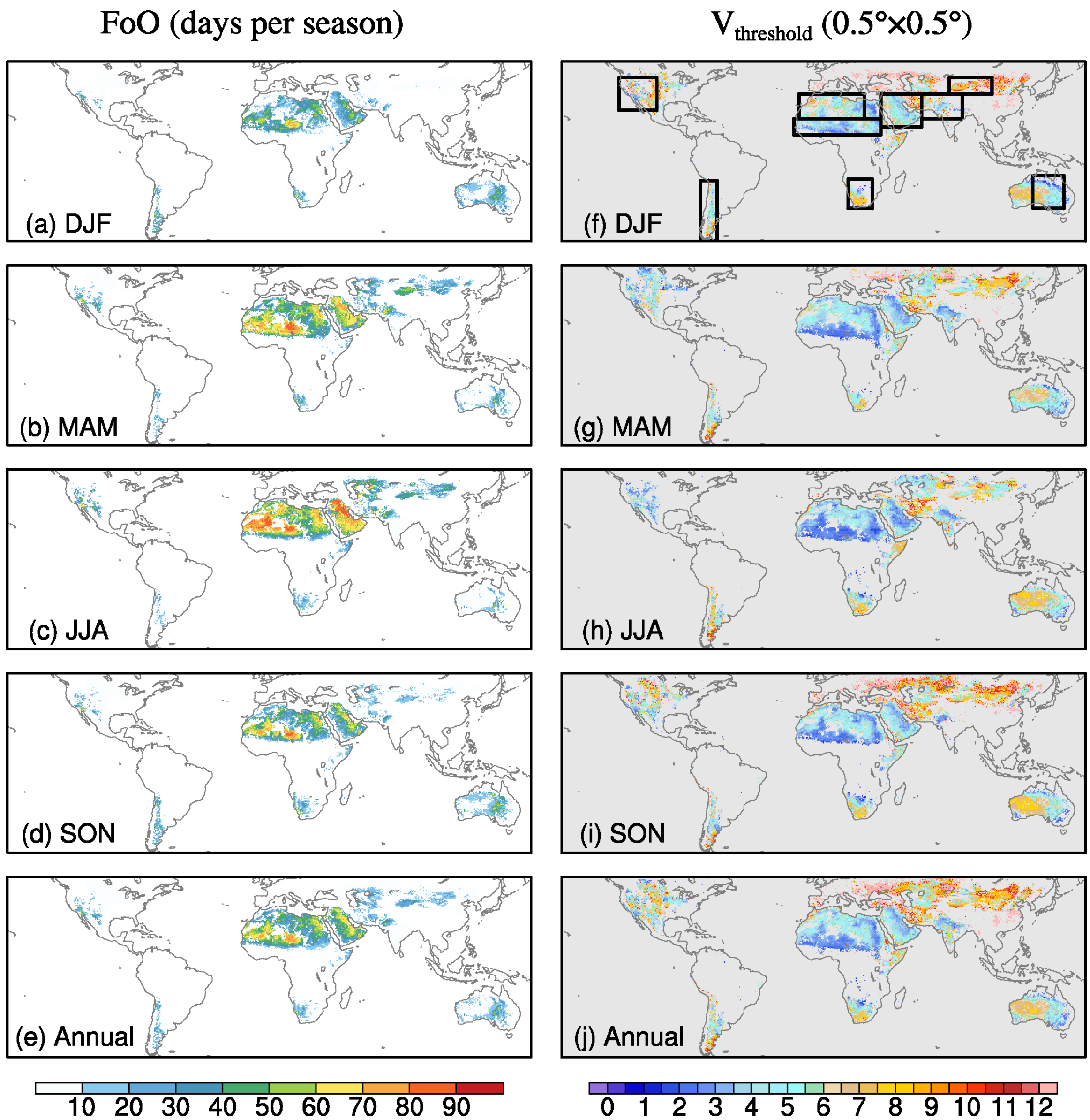

Figure 1. (a)-(e) Frequencies of occurrence (FoO; unit: days per season) in each season and annual mean. (f)-(j) Threshold of wind erosion ($V_{threshold}$; unit: m s^{-1}) derived from satellite products and reanalyses for each season and annual mean using DOD_{thresh} = 0.2 (or 0.02). Black boxes in (f) denote nine dust source ~~dusty~~ regions as listed in Table 1.

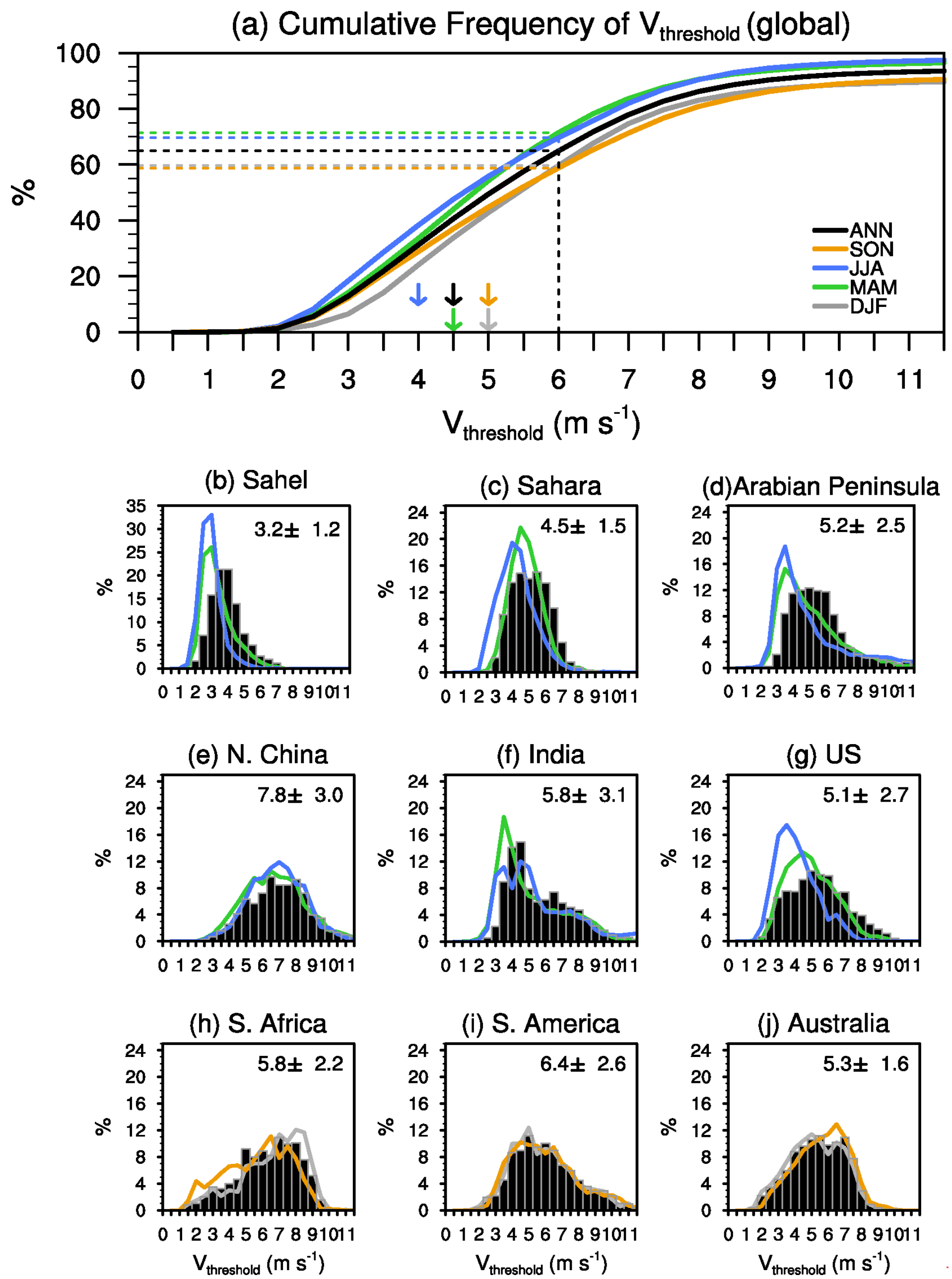

(a) Cumulative Frequency of $V_{threshold}$ (global)
%
ANN
SON
JJA
MAM
DJF
$V_{threshold}$ (m s^{-1})
(b) Sahel
3.2± 1.2
(c) Sahara
4.5± 1.5
(d)Arabian Peninsula
5.2± 2.5
(e) N. China
7.8± 3.0
(f) India
5.8± 3.1
(g) US
5.1± 2.7
(h) S. Africa
5.8± 2.2
(i) S. America
6.4± 2.6
(j) Australia
5.3± 1.6

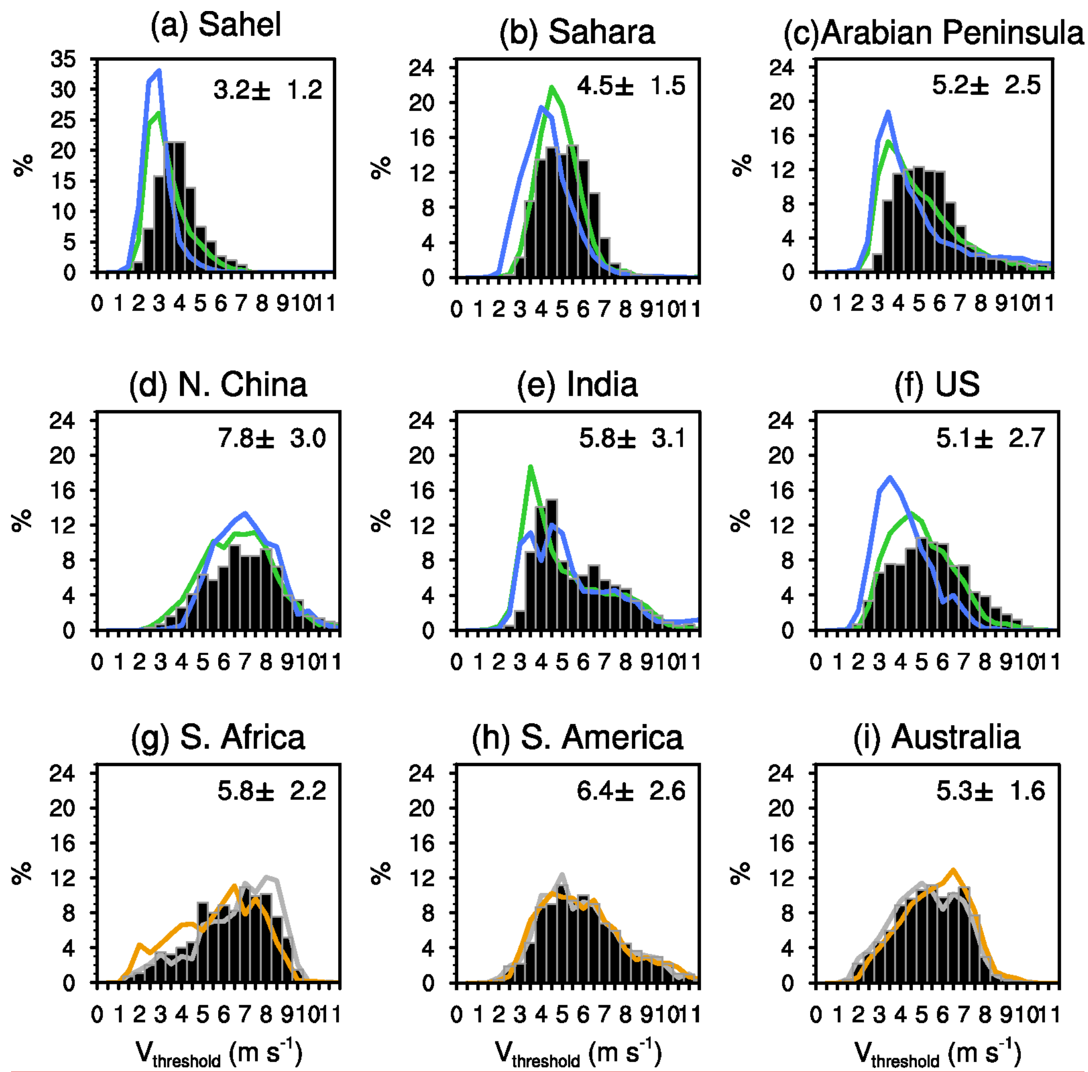

Figure 2. ~~(a) Cumulative frequency of $V_{threshold}$ over global land for each season (black, orange, blue, green, and grey lines denote annual, SON, JJA, MAM, and DJF averages, respectively). Color dashed lines correspond to the percentages of $V_{threshold}$ = 6 m s^{-1} for each season and annual mean. Color arrows point to the value of $V_{threhsold}$ at the 50% level in each season and annual mean.~~ (a~~b~~)-(i) Frequency distribution of annual mean $V_{threshold}$ (black bars) in each region (black boxes in Fig. 1) and for dusty seasons, i.e., MAM (green) and JJA (blue) for regions in the Northern Hemisphere and SON (orange) and DJF (grey) for regions in the Southern Hemisphere. The mean (averaged over all grid points in the region, without area weight) and ± one standard deviations of $V_{threshold}$ in each region are shown on the top right of each plot.

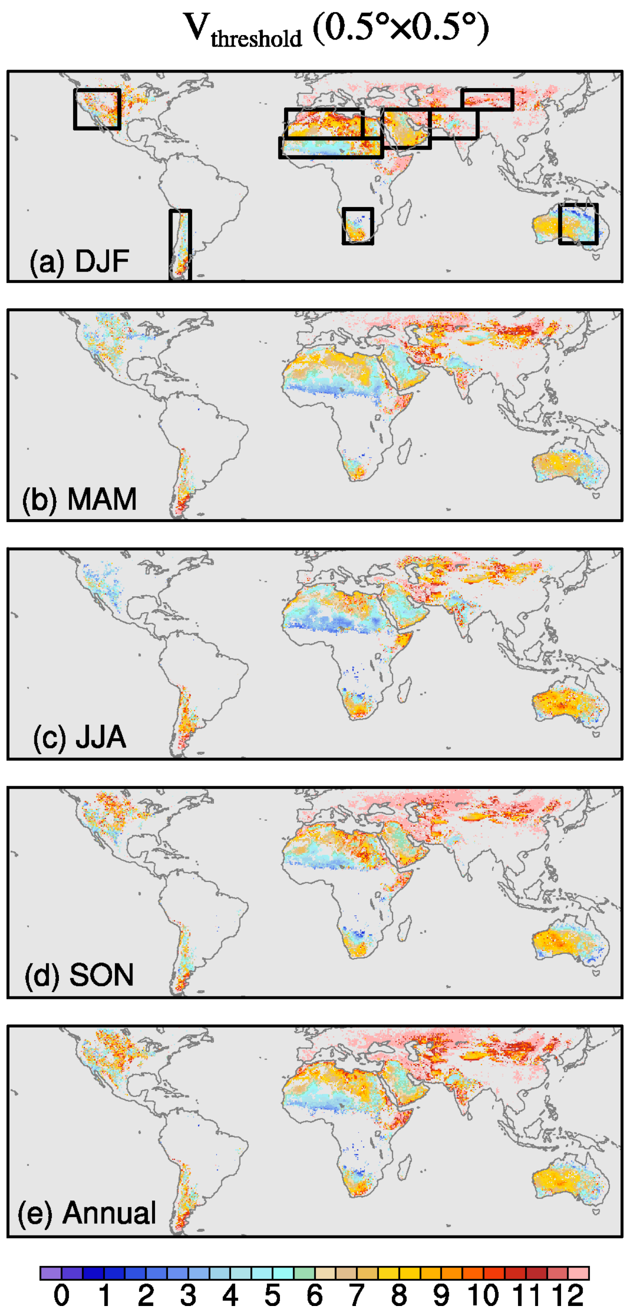

Figure 3. (a)-(e) Threshold of wind erosion ($V_{threshold;}$ unit: m s^{-1}) derived from satellite products and reanalyses for each season and annual mean using DOD_{thresh}=0.5 (or 0.05). Black boxes in (a) denote nine dust source regions as listed in Table 1.

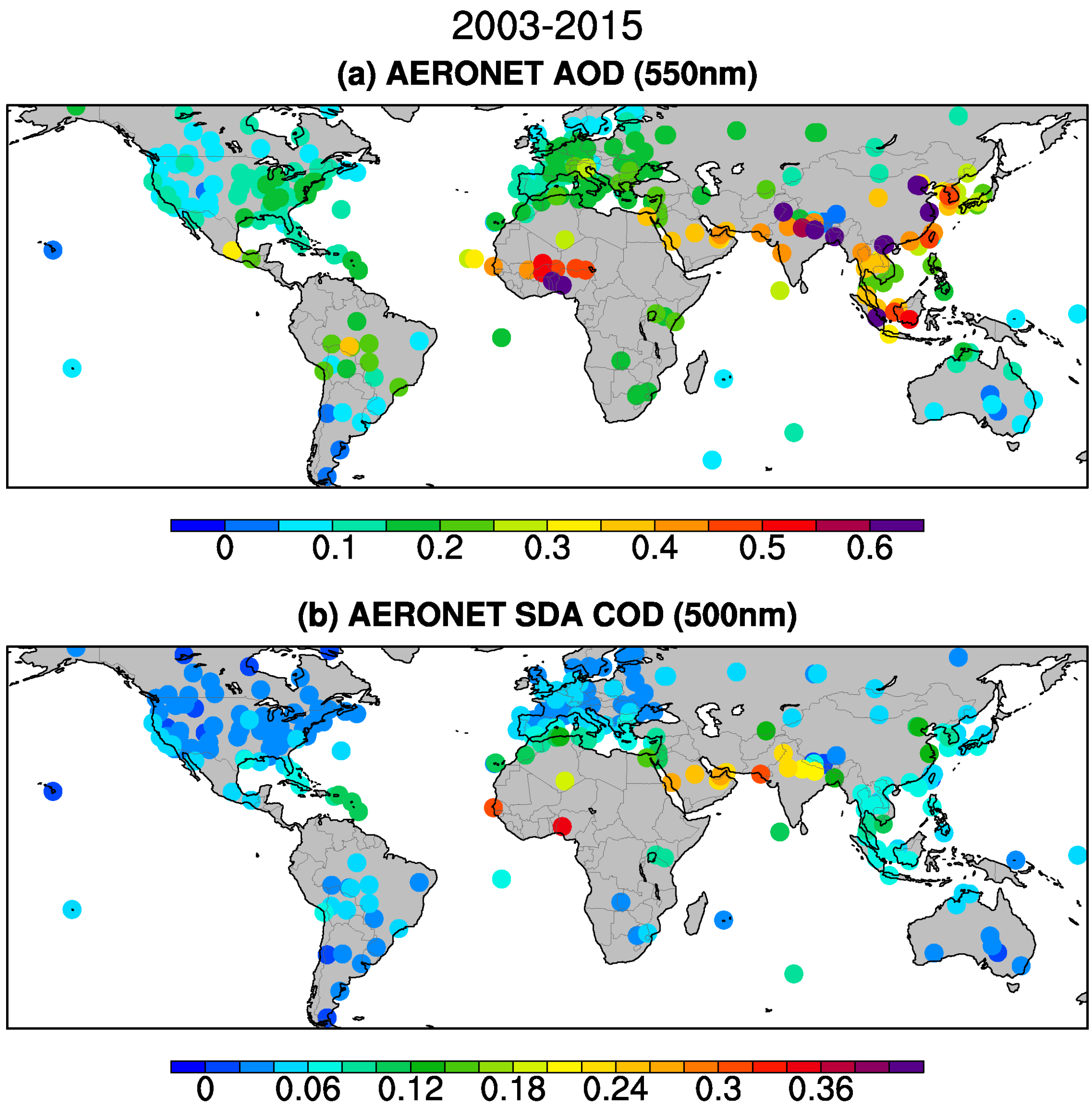

Figure 4~~3~~. Climatology of annual mean AERONET (a) AOD (550 nm) and (b) SDA COD (500 nm) averaged over 2003-2015.

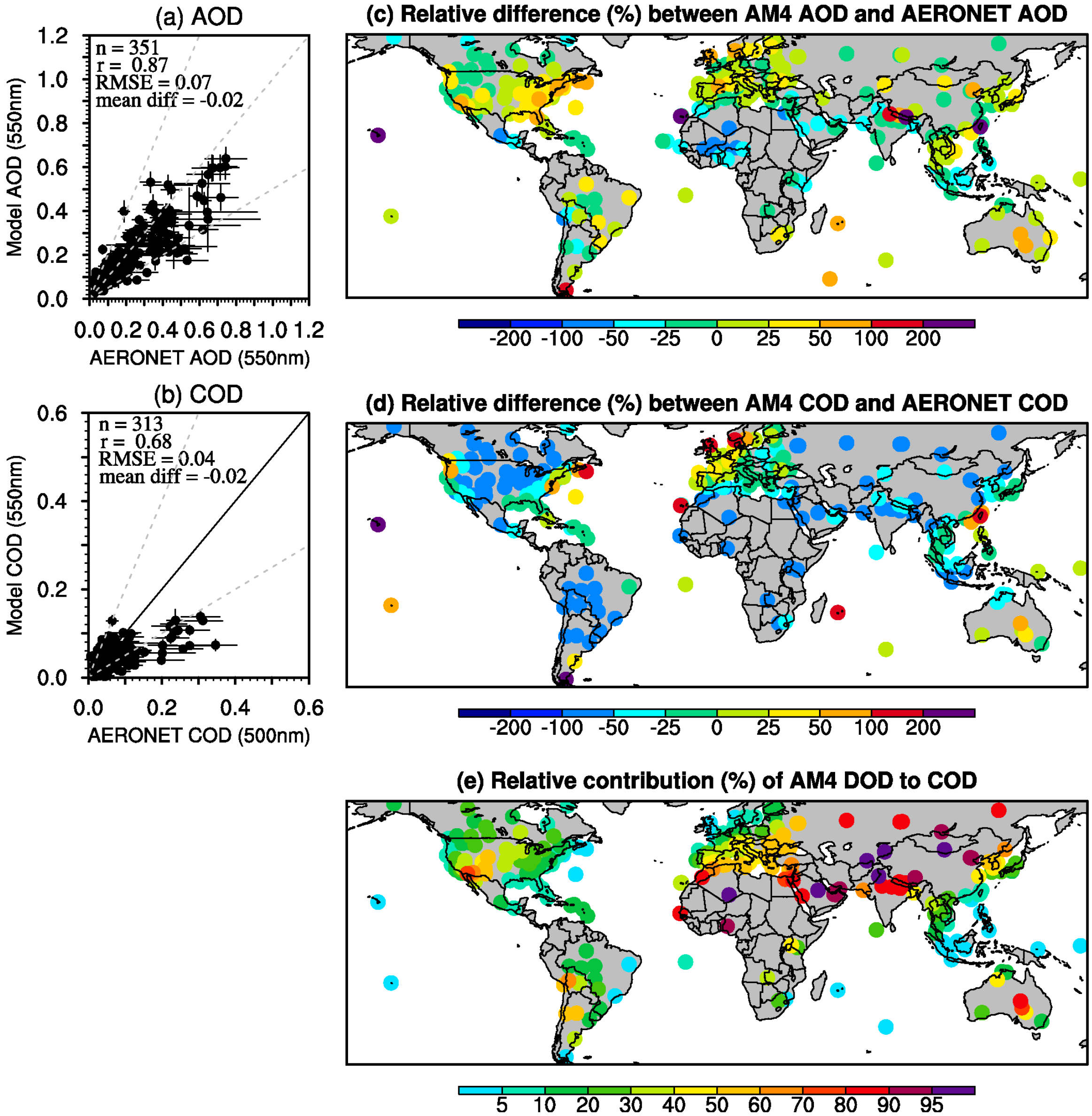

Figure 54. Scatter plot of simulated annual mean (a) AOD and (b) COD in the Control run versus AERONET AOD and COD (left), and the relative difference (in percentage) (c) between modeled AOD and AERONET AOD and (d) between modeled COD and AERONET COD (right). (e) The relative contribution of DOD to COD in the model.

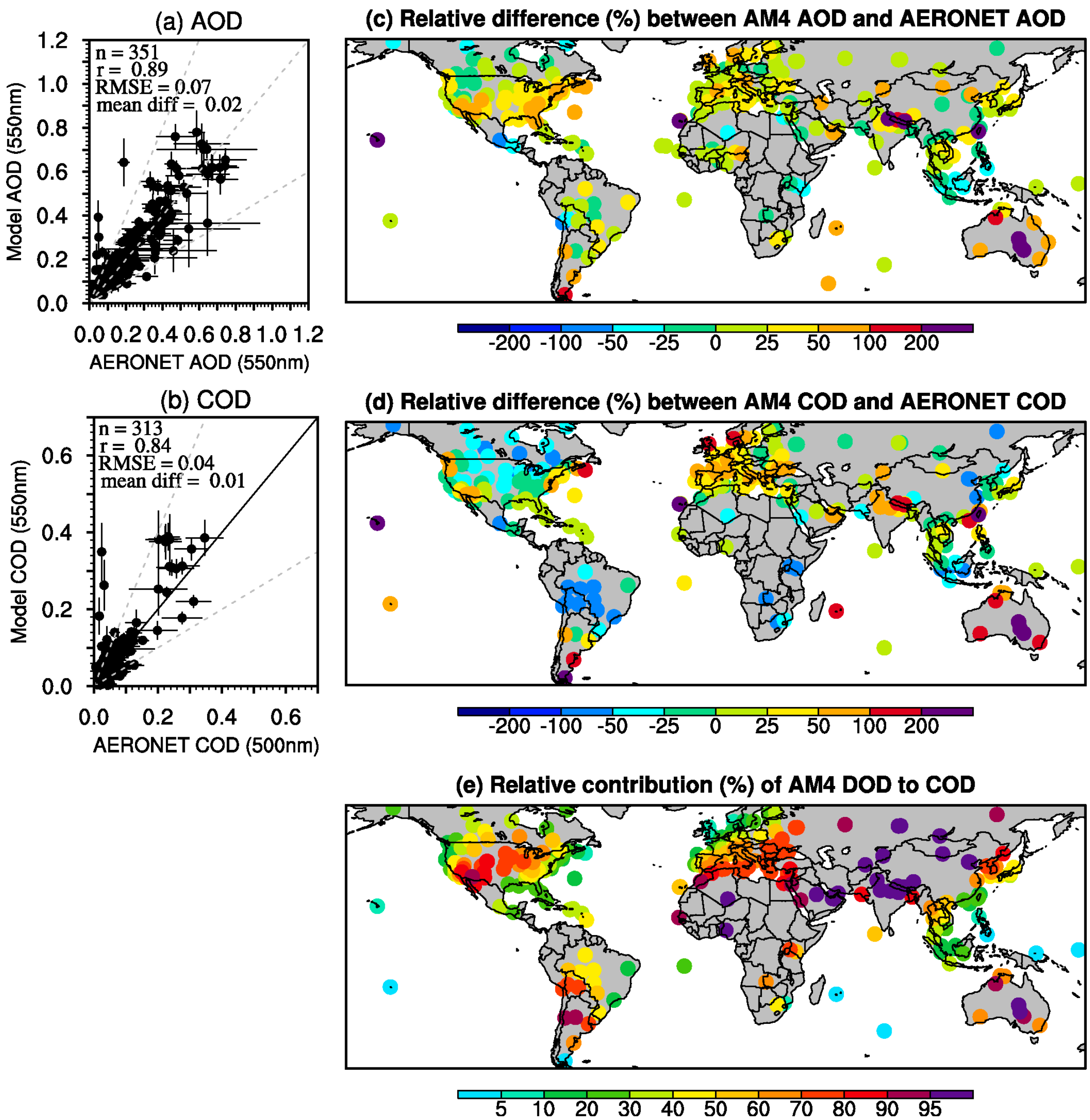

Figure 6~~5~~. Same as Fig. 5~~4~~ but for the V_{thresh}12mn simulation.

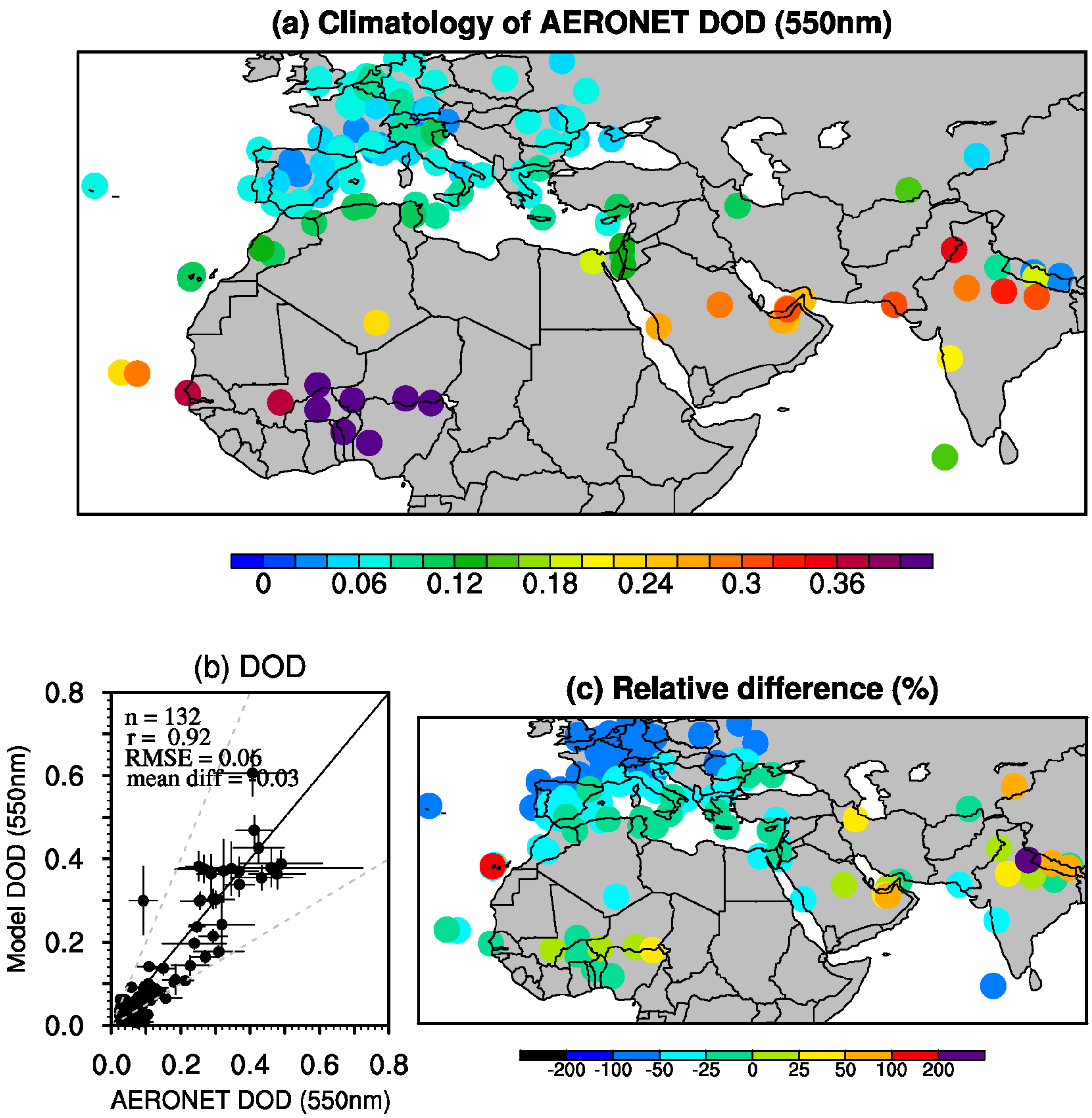

Figure 7~~6~~. (a) Climatology (2003-2015) of AERONET DOD (550 nm) over major dusty regions and (b) scatter plot of modeled DOD in the V_{thresh}12mn simulation versus AERONET DOD, and (c) the relative difference (in percentage) between modeled DOD and AERONET DOD in the V_{thresh}12mn simulation.

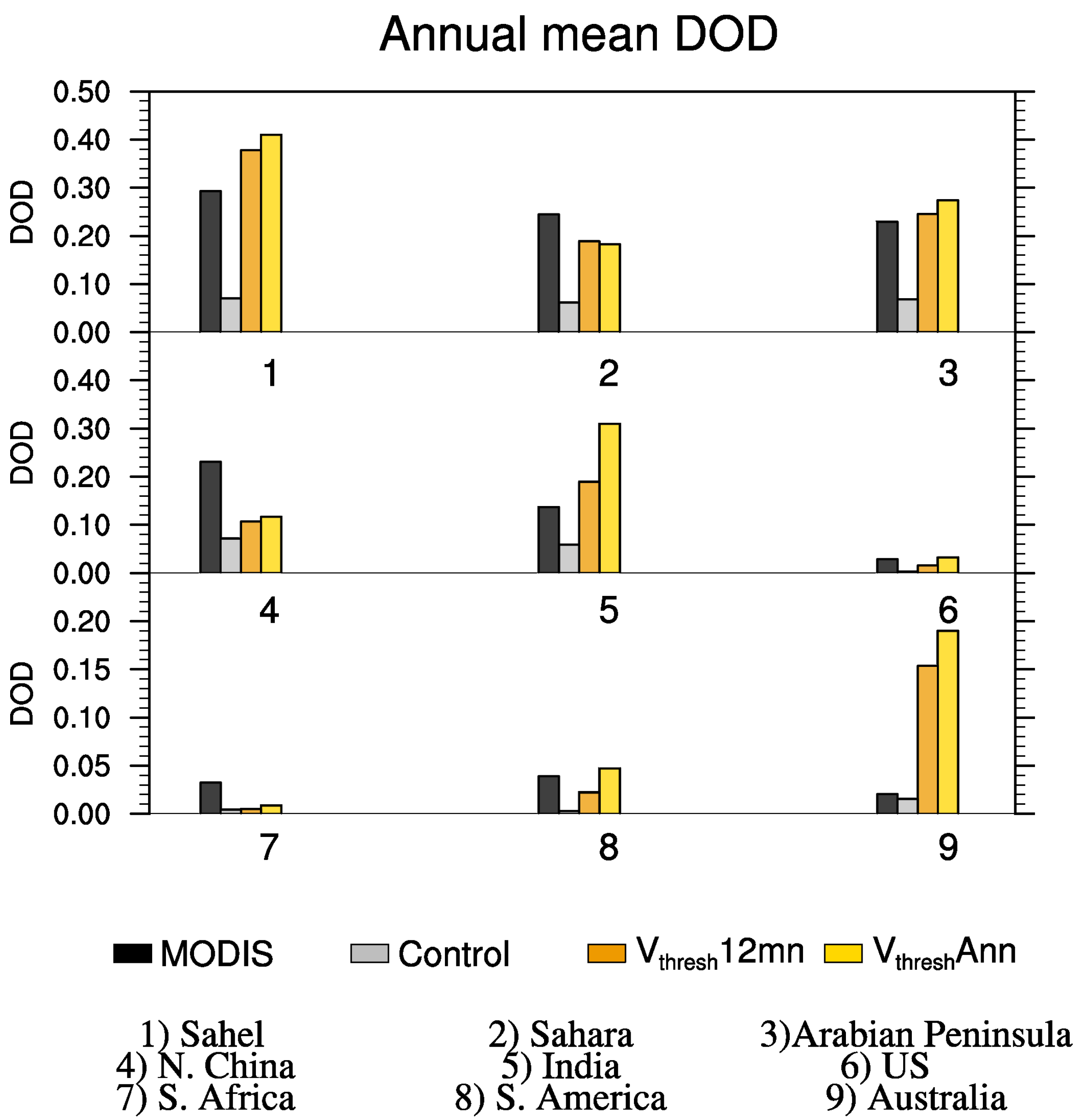

Figure 8~~7~~. Regional averaged annual mean DOD (2003-2015) over nine regions from the Control (grey), V_{thresh}12mn (orange), and V_{thresh}Ann (yellow) simulations and MODIS (black).

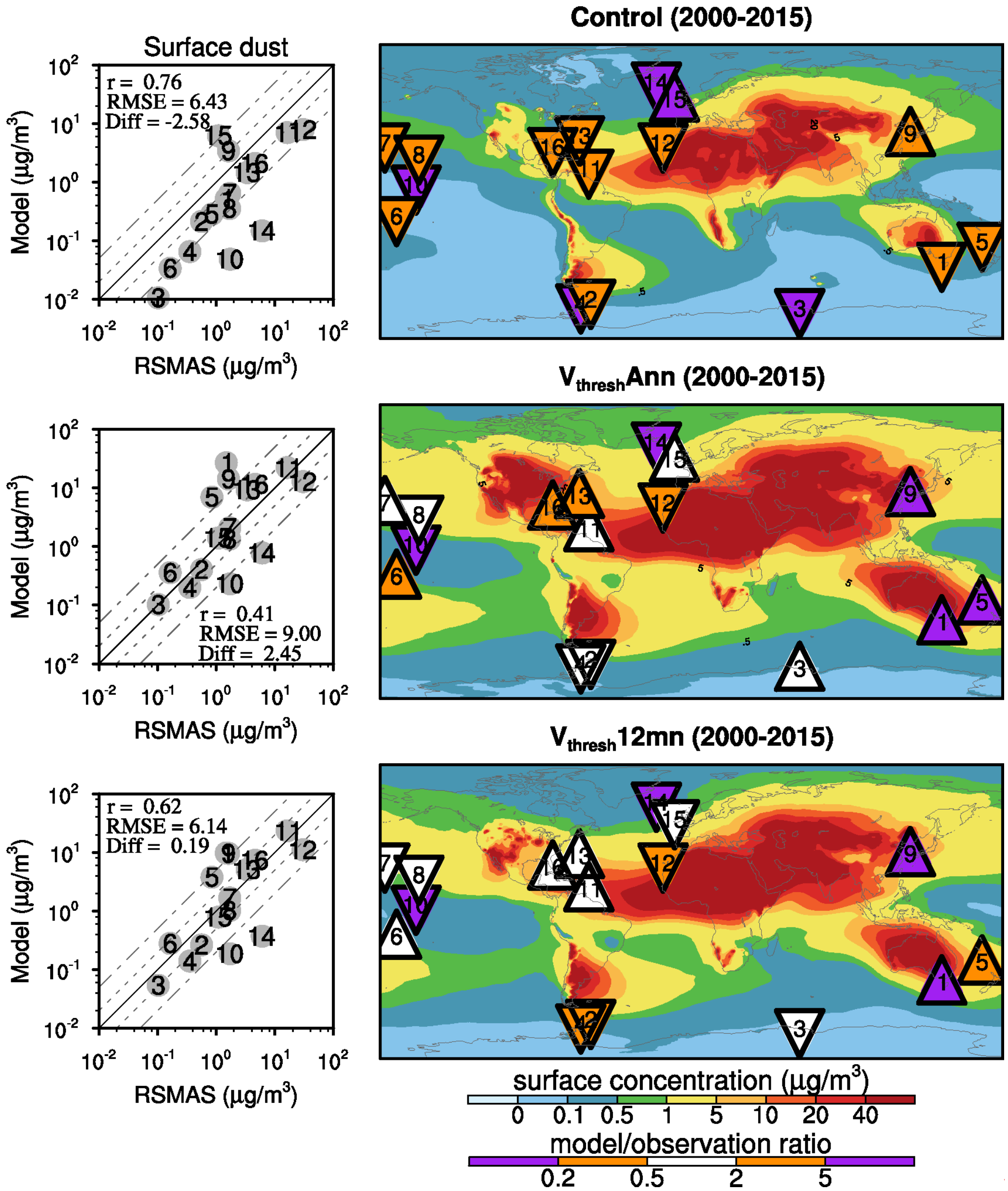
Surface dust
r = 0.76
RMSE = 6.43
Diff = -2.58
Model (µg/m³)
RSMAS (µg/m³)
Control (2000-2015)
r = 0.41
RMSE = 9.00
Diff = 2.45
V threshAnn (2000-2015)
r = 0.62
RMSE = 6.14
Diff = 0.19
V thresh12mn (2000-2015)
surface concentration (µg/m³)
0 0.1 0.5 1 5 10 20 40
model/observation ratio
0.2 0.5 2 5

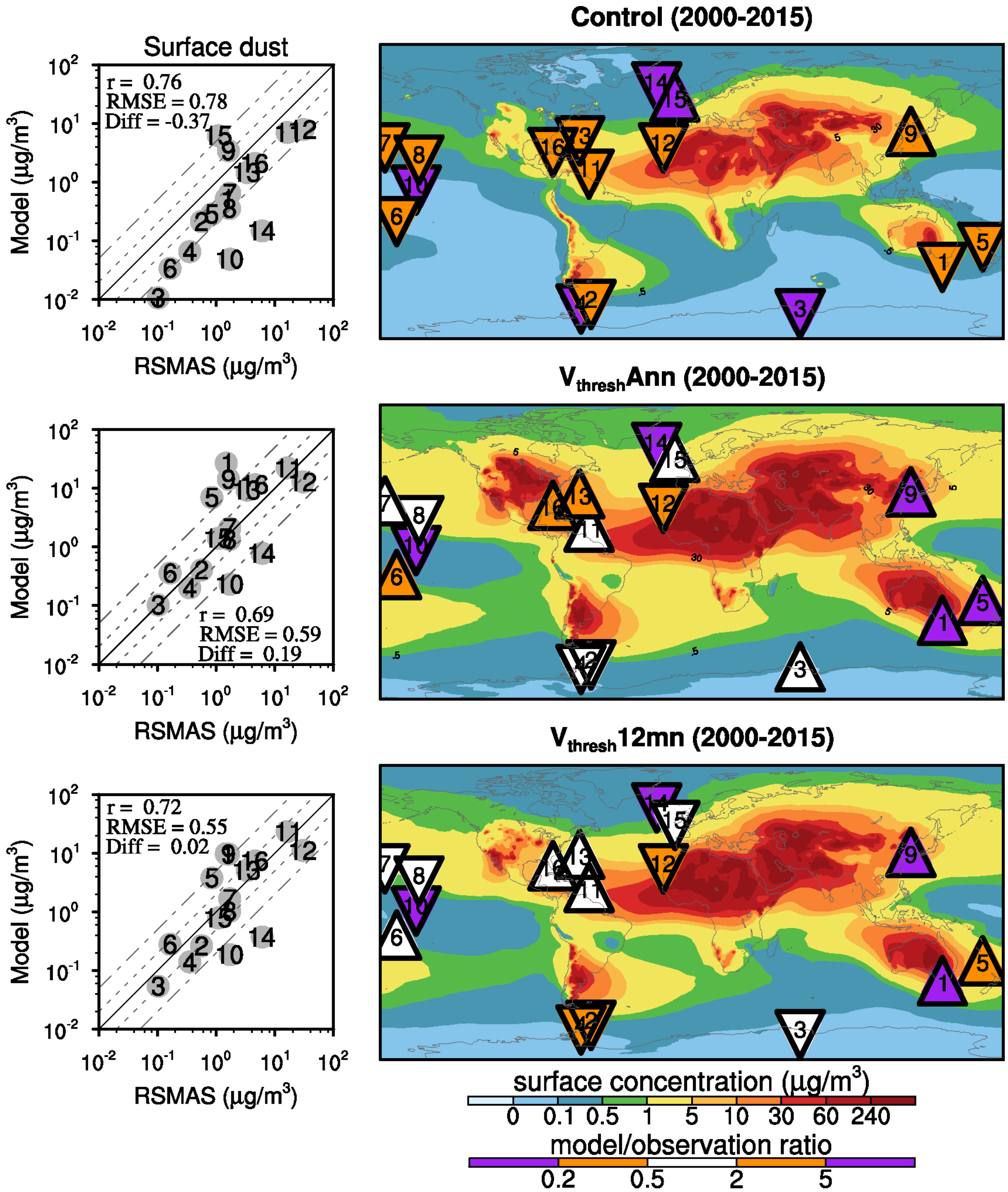

Figure 9~~8~~. Scatter plots (left column) of model simulated (from top to bottom are the Control, V_{thresh}Ann, and V_{thresh}12mn simulations) surface dust concentration (μg m^{-3}) versus the climatology of observed surface dust concentration from RSMAS stations (Savoie and Prospero 1989), and spatial pattern of surface dust concentration from model output (shading; right column) and the ratio between modeled and RSMAS station observed surface dust concentration (color triangles, with upward triangles indicating overestimation and downward triangles indicating underestimation). 16 stations were used, and numbers in each triangle (right) and grey dots (left) indicate the stations. The one-one, one-two and one-five lines are plotted in solid, dashed and dash-dotted lines in the scatter plots. Statistics in the scatter plots are calculated in logarithmic space.

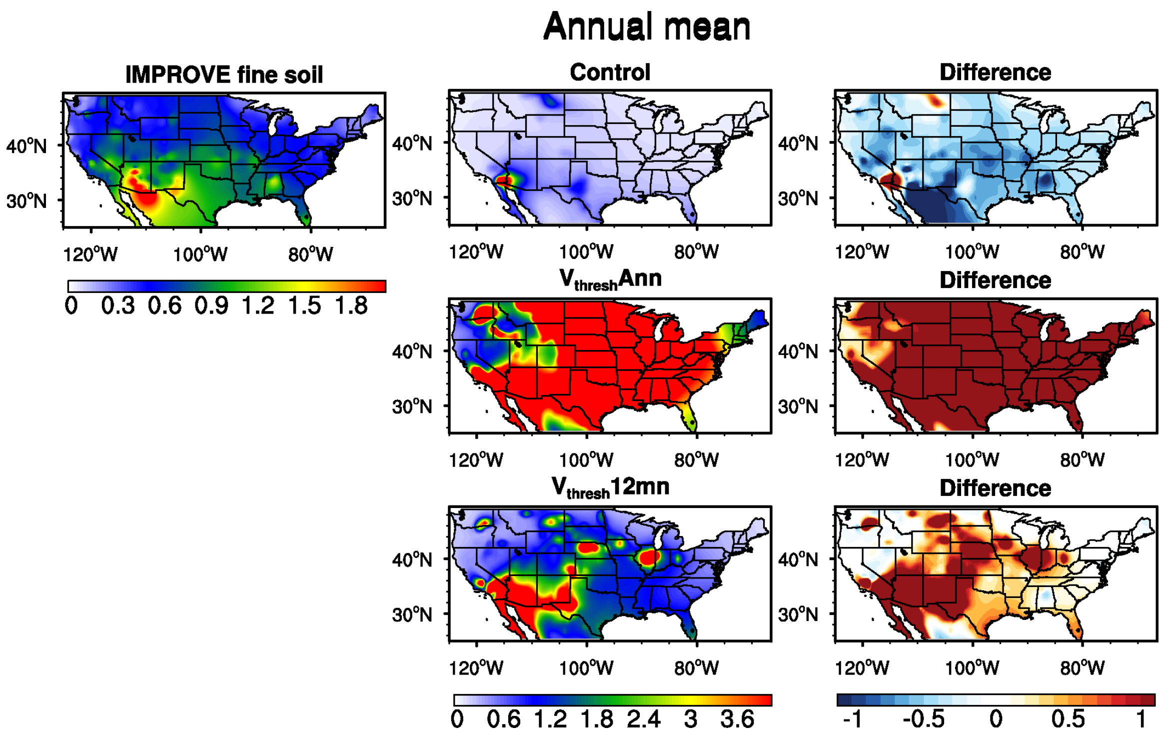

Figure 10~~9~~. Annual mean surface fine dust concentration (μg m^{-3}) from IMPROVE stations (left column) and three simulations (middle column) and the differences between model and observation (right column) for 2002-2015.

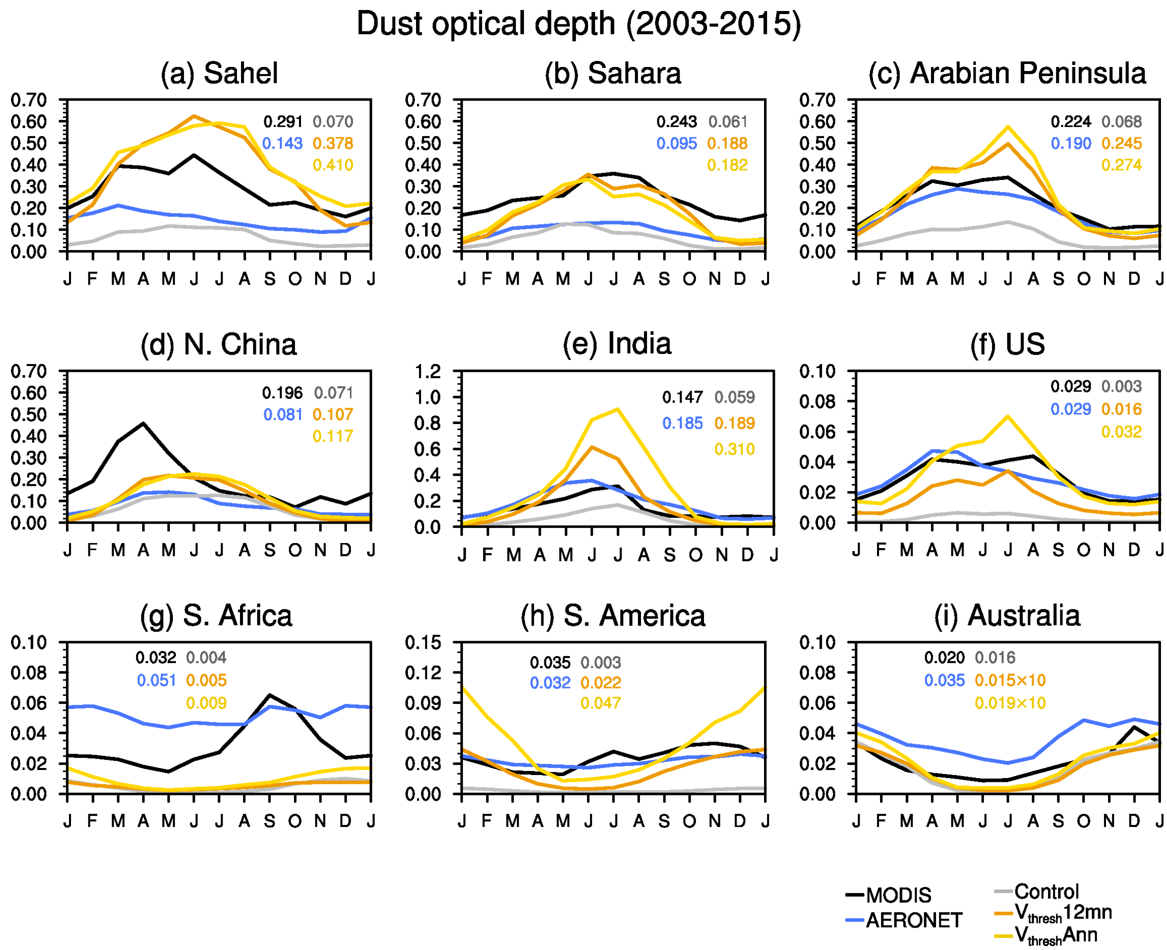

Figure 11~~0~~. Seasonal cycle of DOD from MODIS (black), the Control (grey), V_{thresh}12mn (orange), and V_{thresh}Ann (yellow) runs, and gridded AERONET SDA COD (blue) averaged over nine regions. The annual mean of each dataset in each region is listed on the top of the plot.

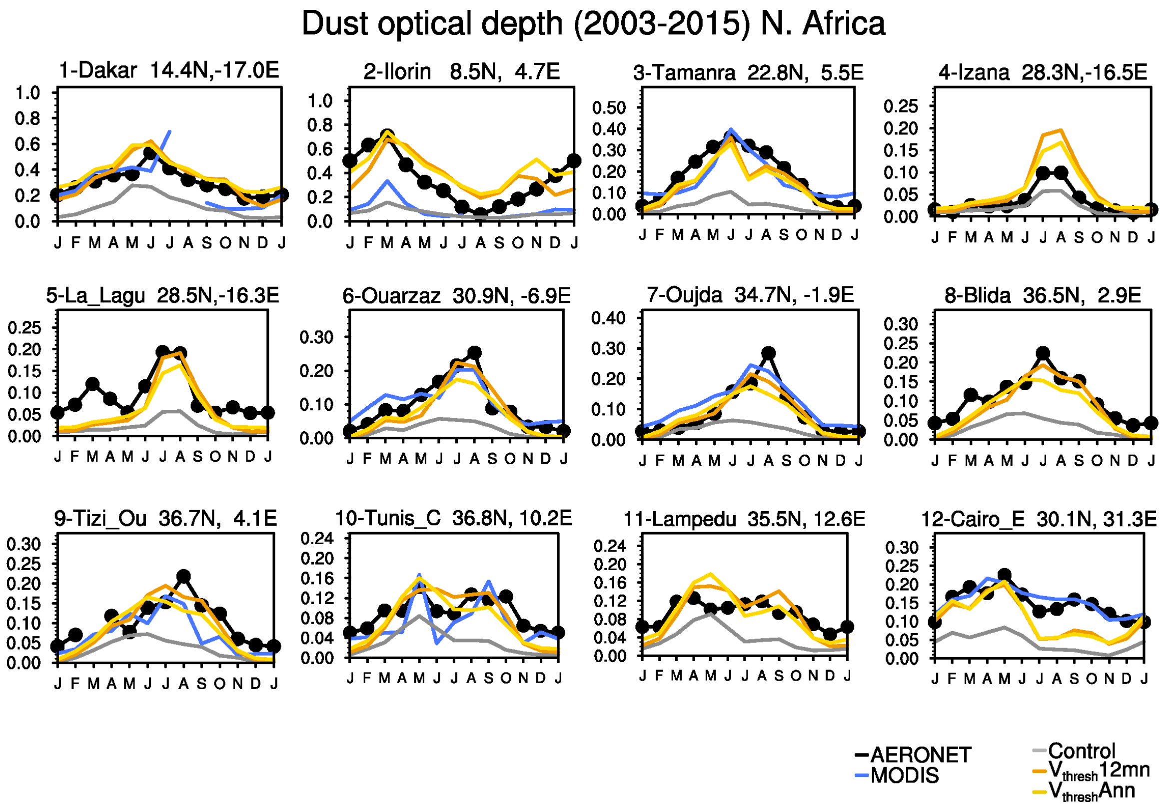

Figure 12~~1~~. Seasonal cycle of DOD over 12 AERONET SDA sites (see Fig. S7~~5~~ in the Supplement for locations) from the Control (grey), V_{thresh}12mn (orange), and V_{thresh}Ann (yellow) simulations, along with DOD from MODIS (blue), and COD from AERONET (black dotted line). All values are averaged over 2003-2015. The location (lat/long) and the name (due to space, only first seven characters are shown) of the sites are listed at the top of each plot.

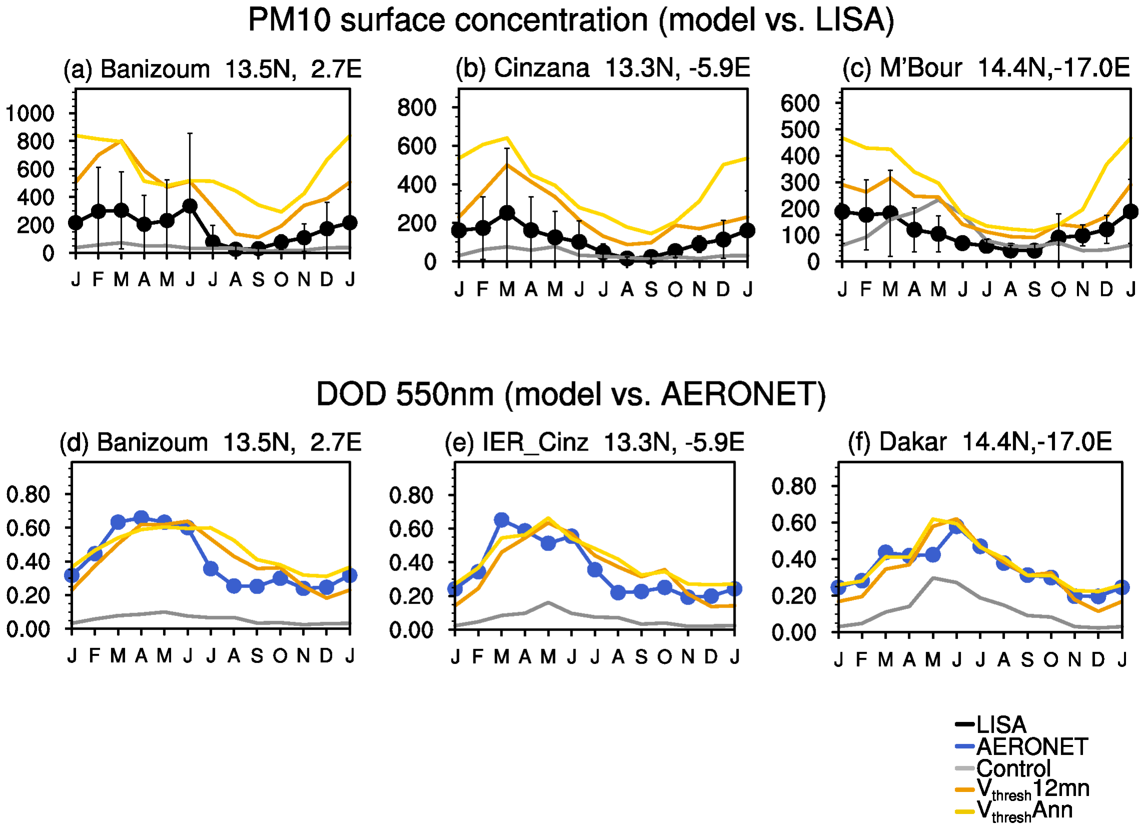

Figure 13~~2~~. (a)-(c) Seasonal cycle of PM_{10} surface concentration (black) over three sites from the LISA project, along with PM_{10} surface dust concentration from the Control (grey), V_{thresh}12mn (orange), and V_{thresh}Ann (yellow) simulations. Error bars are ± one standard deviations of daily mean in each month averaged over 2006-2014. Unites: µg m^{-3}. (d)-(f) seasonal cycle of DOD (550 nm) from three AERONET sites co-located with LISA sites (blue) versus that modeled by the Control (grey), V_{thresh}12mn (orange), and V_{thresh}Ann (yellow) simulations.

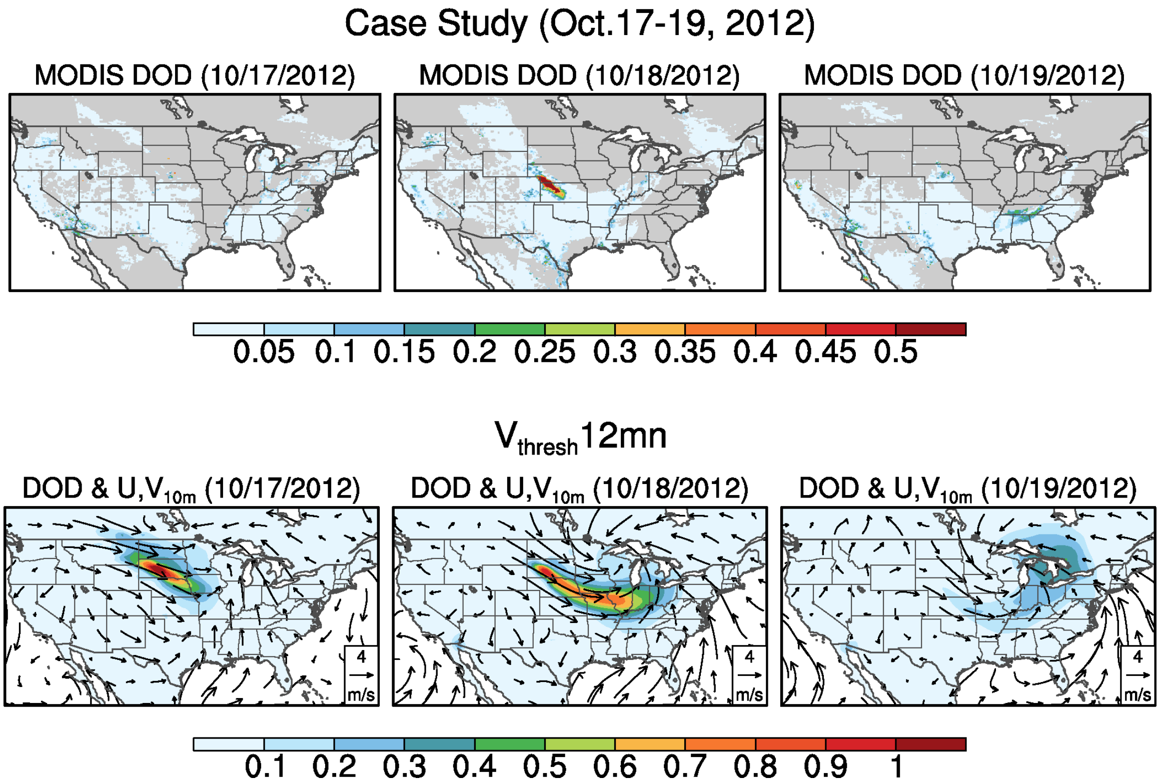

Figure 14~~3~~. Daily DOD from MODIS (top panel), daily DOD simulated by the V_{thresh}12mn run along with anomalies (with reference to the 2000-2015 mean) of surface wind vectors (m s^{-1}; bottom panel) from Oct. 17th to Oct. 19th, 2012. Only DOD over land is shown. Missing values in MODIS DOD (top panel) are plotted in grey shading.

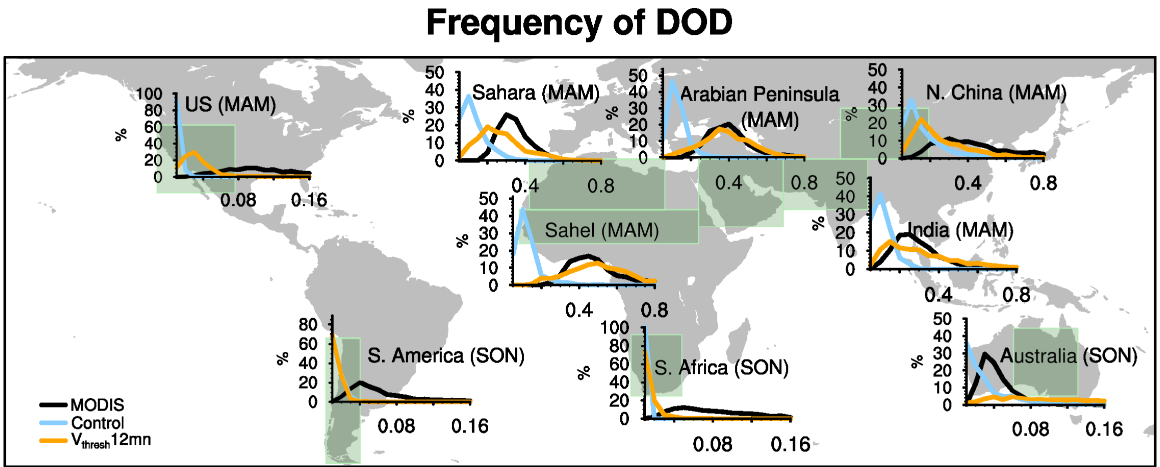

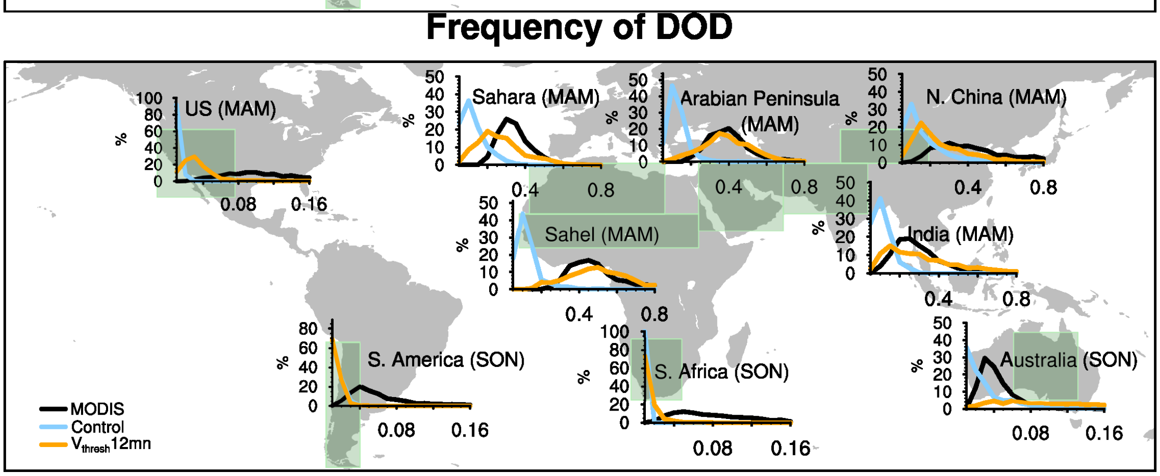

Figure 154. Frequency (%) distribution of regional averaged daily DOD from MODIS (black) versus that from the Control (light blue) and V_{thresh}12mn (orange) simulations for the Sahara, the Sahel, the Arabian Peninsula, northern China, India, western to central U.S., South America, South Africa, and Australia from 2003 to 2015. X-axis denotes the ranges of DOD (the bin spacing for dusty regions is 0.05 and for less dusty regions is 0.01), and y-axis is percentage of occurrence. The light green boxes denote the averaging areas. For regions in the Northern Hemisphere frequency in MAM is shown, while for regions in the Southern Hemisphere frequency in SON is shown.